# Durham E-Theses

## *Wind Turbine Generator Reliability: An Exploration of the Root Causes of Generator Bearing Failures*

### WHITTLE, MATTHEW

# Wind Turbine Generator Reliability: An Exploration of the Root Causes of Generator Bearing Failures

## Matthew W. G. Whittle

Thesis submitted towards the
degree of Doctor of Philosophy

Energy Group

School of Engineering and Computing Sciences

Durham University

United Kingdom

September 2013

# Wind Turbine Generator Reliability: An exploration of the root causes of generator bearing failures

Matthew W. G. Whittle

## Abstract

Increasing the availability of multi-megawatt wind turbines (WT) is necessary if the cost of energy generated by wind is to be reduced. Reliability surveys have shown that WT generator bearings have a relatively high failure rate, with failures happening too early to be due to classical rolling contact fatigue.

It has been the purpose of the present work to demonstrate the value of models which may help to explain some of the failure modes of wind turbine generators (and their root causes). The work has considered two potential root causes of wind turbine generator failure. Firstly, gearbox-generator misalignment caused by deflection of the compliant drivetrain under loading. Secondly, electrical discharge machining (EDM) of the generator bearings due to the common-mode voltage caused by pulse width modulation (PWM) of the power electronics.

Numerical simulations have been used to investigate these potential failure modes and to show how they bring about premature failure. It has been shown that there exists a mechanism by which gearbox-generator misalignment can exacerbate EDM. This demonstrates the importance of holistic analyses of WTs, which are complex electromechanical systems with non-trivial interactions between sub-assemblies. The need for further research has been shown.

# Declaration

The work in this thesis is based on research carried out in the Energy Group, School of Engineering and Computing Sciences, Durham University. No part of this report has been submitted elsewhere for any other degree or qualification and it is all my own work unless referenced to the contrary in the text.

Parts of this work have been published in the following:

## Journals

M. Whittle, J. Trevelyan, and P.J. Tavner. Bearing currents in wind turbine generators. *JRSE*, 2013. *In press.*

M. Whittle, J. Trevelyan, W. Shin and P.J. Tavner. Misalignment in wind turbine drivetrains: improving bearing reliability. *Wind Energy*, 2013. DOI: 10.1002/we.1629

P.J. Tavner, D.M. Greenwood, M. Whittle, R. Gindele, S. Faulstich, and B. Hahn. Study of weather and location effects on wind turbine failure rates. *Wind Energy*, 2012. DOI: 10.1002/we.538

## Conferences

M. Whittle, J. Trevelyan, L. Ran and J. Wu. Bearing Currents in Wind Turbine Generators. In *Proceedings of EWEA 2012*, pp. 165-167, Copenhagen: 16-19 April, 2012.

M. Whittle, W. Shin, J. Trevelyan and J. Wu. A parametric study of the effect of generator misalignment on bearing fatigue life in wind turbine generators. In *Proceedings of EWEA 2011*, pp. 24-27, Brussels: 14-17 March, 2011.

P.J. Tavner, R. Gindele, S. Faulstich, B. Hahn, M. Whittle and D.M. Greenwood. Study of Effects of Weather and Location on Wind Turbine Failure Rates. In *Proceedings of EWEC 2010*, pp. 255-258 Warsaw: 20-23, April, 2010.

# Acknowledgements

I would like to thank my doctoral supervisor, Jon Trevelyan, for his guidance and his probing questions. I am also grateful to the many other Durham scholars, particularly Peter Tavner, Li Ran, Junjie Wu and Hui Long, with whom I have had many enlightening conversations over the last four years. I have been encouraged by their advice and by their commitment to research. This commitment was demonstrated in many ways, not least by those who drove over a thousand miles to reach a conference rather than let an erupting icelandic volcano interrupt the pursuit of learning! I remember with fondness the camaraderie of that trip.

I would like to thank the students of the Energy group, in particular Peter Wyllie. Without the technical staff the testing would not have been possible. I would especially like to thank Colin Wintrip, Scott Ramsey and Ian Hutchinson; their contribution was invaluable.

I am indebted to Won Shin, Xiaoqin Ma and John Coultate at Romax Technology Ltd. Much of the work was only possible because Romax provided me with their drivetrain numerical simulation software *gratis*. Also, despite pressure on their time, they have been very helpful in providing critical analyses of the research.

I would also like to thank my parents. My Dad gave me his love of applied science and his gift for analytical reasoning. My Mum gave me boundless support and encouragement. I would like to express gratitude to my sister, Sarah, and Matthew King for proof reading the manuscript, and to my wife, Tarsila, for her patience and support.

*In memory of my dear Mum and in offering to the Creator whom she loved.*


*Compassionate Lord, breathe in*
*this offering and look more favorably on it*
*than upon a more sumptuous sacrifice*
*offered with rich smoke. Please find*
*this simple string of words acceptable.*
- St. Grigor Narekatsi


Matthew Whittle
Durham, September 2013

*The proper operation (working or function) is not in existence for the sake of being, but being for the sake of operation.*

    - Dante Alighieri, De Monarchia, I, iii

*Those who wish to succeed must ask the right preliminary questions.*

    - Aristotle, Metaphysics, II, (III), i

# Contents

# List of Figures

# List of Tables

# Nomenclature & Glossary

| Symbol | Definition |
|---|---|
| $A$ | area |
| $A$ | dimensionless constant |
| $A_{mn}$ | plate area for capacitance between component $m$ and $n$ |
| $A_{Hz}$ | Hertzian contact area |
| $a$ | radius of Hertzian contact |
| $a_{iso}$ | dimensionless factor used in ISO 2810:2007 |
| $B$ | dimensionless constant |
| $b_m$ | bearing rating factor |
| $b_0$ | slot opening width |
| $C$ | bearing dynamic loading capacity |
| $C_b$ | bearing capacitance |
| $C_p$ | power coefficient |
| $C_u$ | fatigue load limit |
| $C_{wr}$ | winding-rotor capacitance |
| $C_{wrr}$ | winding-rotor capacitance for rotor-fed case |
| $C_{wrs}$ | winding-rotor capacitance for stator-fed case |
| $C_{rf}$ | rotor-frame capacitance |
| $C_{wf}$ | winding-frame capacitance |
| $D_i$ | inner raceway diameter |
| $D_o$ | outer raceway diameter |
| $D_w$ | nominal ball diameter |
| $D_y$ | contact ellipse diameter (along the y axis) |
| $d$ | rolling element diameter |
| $d$ | rotor bar depth |
| $d$ | plate separation |
| $d$ | stator slot width |
| $d_m$ | bearing mean diameter |
| $d_{re}$ | rotor outer diameter |
| $E$ | e.m.f |
| $E_i$ | Young's modulus of material i |
| $e$ | dimensionless exponent used in ISO 2810:2007 |
| $F$ | force |
| $F_a$ | actual axial bearing load |
| $f_c$ | dimensionless bearing geometry factor |
| $F_e$ | equivalent bearing load |
| $F_r$ | actual radial bearing load |
| $F_{rm}$ | minimum radial load requirement |
| $f_{cage}$ | cage angular speed |
| $f_{ri}$ | rolling element relative frequency with respect to inner raceway |

| Symbol | Definition |
|---|---|
| $f_{ro}$ | rolling element relative frequency with respect to outer raceway |
| $f_{bpfi}$ | inner raceway ball pass frequency |
| $f_{bpfo}$ | outer raceway ball pass frequency |
| $f$ | electrical frequency |
| $G$ | dimensionless material parameter |
| $H$ | dimensionless film thickness |
| $H_{min}$ | Hamrock-Dowson minimum film thickness |
| $h$ | film thickness |
| $h_0$ | eight of the slot opening |
| $h_{wedge+ins}$ | Combined thickness of the slot wedge and slot insulation |
| $I$ | rms current |
| $i$ | number of rows of rolling elements |
| $i$ | bearing current |
| $i_{a,b,c}$ | line currents a, b and c |
| $J$ | number of stress cycles |
| $J_b$ | apparent current density |
| $k$ | dimensionless constant |
| $k$ | dimensionless ellipticity parameter |
| $k_c$ | Carter's coefficient |
| $k_r$ | minimum load factor |
| $L$ | insulation life |
| $L_l$ | line inductance |
| $l_{fe}$ | core length |
| $l_v$ | length of stressed volume |
| $L_{we}$ | effective roller length |
| $L_{10}$ | bearing fatigue life (90 % survival rate) |
| $M$ | probability of failure |
| $N$ | 2 number of rotor bars |
| $n$ | number of shaft revolutions per second |
| $P$ | power |
| $P$ | applied load |
| $p$ | number of pole pairs |
| $p_{iv,as}$ | asymptotic isoviscous pressure |
| $R$ | radius of contacting sphere |
| $R_b$ | bearing resistance |
| $R_m$ | machine resistance |
| $R_x$ | relative radius of curvature |
| $r_t$ | rotor tooth width |
| $S$ | probability of survival |
| $t$ | time |
| $t_g$ | rotor groundwall insulation thickness |
| $U$ | wind speed |
| $U$ | dimensionless speed parameter |
| $u$ | surface velocity |

| Symbol | Definition |
|---|---|
| $V$ | volume |
| $V_i$ | inner raceway speed |
| $V_o$ | outer raceway speed |
| $V_{cage}$ | cage speed |
| $v_{a,b,c}$ | pahse voltages a, b and c |
| $v_n$ | common-mode voltage |
| $W$ | dimensionless load parameter |
| $X$ | dimensionless constant used in ISO 281:2007 calculations |
| $Y$ | dimensionless constant used in ISO 281:2007 calculations |
| $y$ | instantaneous fundamental voltage target value |
| $Z$ | number of rolling elements per row |
| $Z_b$ | bearing impedance |
| $Z_0$ | depth to point of maximum shear stress |
| $\alpha$ | coefficient of thermal expansion |
| $\beta$ | pulse duration |
| $\delta$ | air gap |
| $\delta_e$ | equivalent air gap |
| $\epsilon$ | thermoelastic strain state |
| $\epsilon^e$ | elastic strain vector |
| $\epsilon_{lb}$ | dielectric strength |
| $\epsilon_0$ | permittivity of air |
| $\epsilon_g$ | relative permittivity of groundwall insulation |
| $\eta$ | dynamic viscosity |
| $\eta_0$ | atmospheric viscosity |
| $\nu$ | oil kinematic viscosity |
| $\nu_i$ | Poisson's ratio of material i |
| $\rho$ | fluid density |
| $\sigma$ | actual stress |
| $\sigma_u$ | fatigue stress limit |
| $\Phi$ | magnetic flux |
| $\omega$ | electrical frequency |
| $\omega_s$ | synchronous speed |

| Abbreviation | Meaning |
|---|---|
| AC | Alternating current |
| BVR | Bearing voltage ratio |
| CFD | Computational fluid dynamics |
| COE | Cost of energy |

| Abbreviations | Meaning |
| --- | --- |
| CVT | Continuously variable transmission |
| DC | Direct current |
| DE | Drive end |
| DFIG | Doubly fed induction generator |
| DWD | Deutscher Wetterdienst |
| EDM | Electrostatic discharge machining |
| EHL | Elastohydrodynamic lubrication |
| FE | Finite element |
| HF | High frequency |
| HSS | High speed stage |
| HV | High voltage |
| HVRT | High voltage ride–through |
| IGBT | Insulate–gate bipolar transistor |
| IWES | Institut für Windenergie und Energiesystemtechnik |
| LCR | Inductor-capacitor-resistor |
| LVRT | Low voltage ride–through |
| LWK | Landwirtschaftskammer |
| MDOF | Multi-degree of freedom |
| NDE | Non-drive end |
| OPEX | Operating expenditure |
| O&M | Operation and maintenance |
| PD | Partial discharge |
| PWM | Pulse-width modulation |
| RCF | Rolling contact fatigue |
| SCADA | Supervisory control and data acquisition |
| TEFC | Totally enclosed fan cooled |
| UMP | Unbalanced magnetic pull |
| VPI | Vacuum pressure impregnation |
| WEI | Wind energy index |
| WMEP | Wissenschaftliches Mess und Evaluierungsprogramm |
| WSD | Windstats Germany |
| WSDK | Windstats Denmark |
| WT | Wind turbine |

# Chapter 1

# Introduction

## 1.1 Historical Context

The wind has been used by human societies for over 3000 years to provide mechanical work for a variety of purposes. However, the industrial revolution led to a relative decline in the use of wind energy, favouring, instead, the energy dense and reliable fossil fuelled combustion. Nevertheless, wind technology continued to develop and in 1888 the first wind turbine used to generate electricity was constructed in Ohio (Figure 1.1). Two years later, in Denmark, it was followed by Poul LaCour's wind turbine (Figure 1.2). By 1918, there was approximately 3 $MW$ of installed capacity in Denmark - about 3 % of national electricity consumption [1]. Throughout much of the 20th century interest in using the wind to generate electricity was largely restricted to off-grid applications in remote areas.

## 1.2 The Return to Renewable Energy

The discovery of large reserves of energy dense material underground, in the form of coal, oil and gas, has enabled rapid economic development over the last three hundred years. It has, however, brought with it a heavy dependence upon a finite resource and a whole host of environmental and ecological problems. Prosperous societies have been built on the wealth derived from fossil fuels, but now our dependence upon fossil fuels is being challenged.

In the 1970s there were unprecedented rises in the price of oil due to the restriction of the supply by OPEC, and subsequent fears over energy security led to renewed interest in
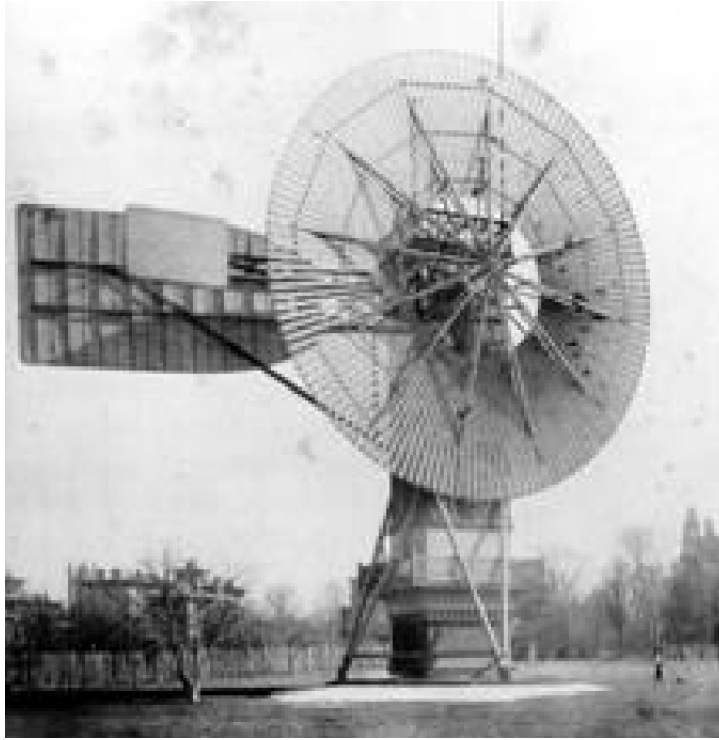
Figure 1.1:  The world's first wind turbine used to generate electricity (Ohio, 1888), reproduced from [1].

renewable sources such as wind energy. Since then there has been increased appreciation of the finitude of fossil fuels with recent debate surrounding whether oil extraction has already peaked (see Figure 1.3). The situation is complex and contentious. The data show that for a quarter of a century production has outstripped new discoveries of oil. Advances in technology are making it possible to exploit hitherto inaccessible fossil fuel resources. Improved deep sea drilling techniques have enabled production in fields previously considered commercially infeasible, though the recent disaster in the Gulf of Mexico has shown that there are significant risks involved. Hydraulic fracturing is praised by some as the solution to the growing energy gap as demand increases and new discoveries fail to keep pace, but by others it is criticised as an environmental menace.

As well as the short/medium term economic concerns regarding dependence upon finite fossil fuels there is also increasing concern regarding the environmental effects of anthropic greenhouse gas emissions. Although this remains a politically charged subject the last thirty years have seen, in broad terms, growing support for renewable technologies as a

Figure 1.2: Poul LaCour's turbine: the beginning of the wind energy industry in Denmark (Askov Laboratory, 1891), reproduced from [1].

means of mitigating anthropic greenhouse gas emissions.

Thus, in the last decades wind energy has undergone rapid technological development and commercial growth with turbine power ratings increasing and prices falling (see Figures 1.4 and 1.5).

Today's wind industry is becoming one in which large arrays of multi-MW wind turbines may be seen as industrial wind energy power plants, rather than as an 'intermediate technology' solution to rural energy scarcity. For example phase one of the London Array, which is about to begin production, will have a capacity of 630 $MW$; there are plans to expand this with a second phase of development.

## 1.3   The Cost of Wind Energy

Despite the rapid growth seen by the wind energy industry over the last few decades, its contribution to global electricity generation remains small compared to traditional sources. The primary reason for this is that the markets are disinterested. Despite the
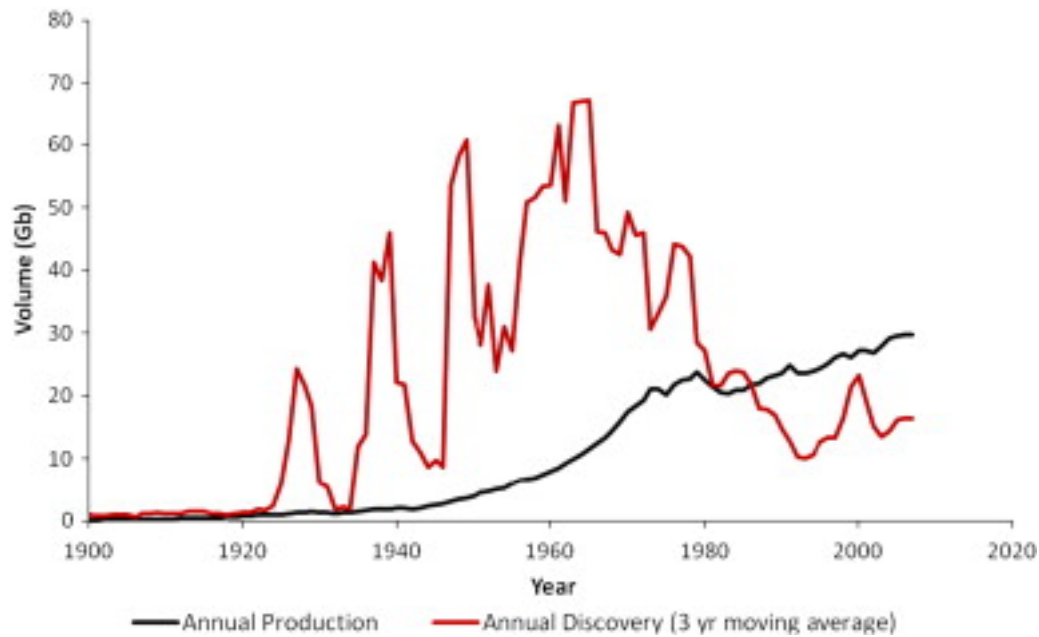
Figure 1.3: Oil discoveries and production [2]

reduction in the capital cost of wind energy noted in Section 1.1 it remains expensive. In 2008, the House of Lords Economic Affairs Committee reported that the cost of onshore wind was 7 pence per kWh, whilst coal, gas and nuclear cost approximately 4 pence per kWh [28]. It has been argued by the European Wind Energy Association (EWEA) that exposure to fuel price volatility (in other words, risk) has not been factored into most economic analyses of energy generation and that, therefore, most of these analyses neglect an important economic advantage of wind energy [6]. However, the EWEA analysis makes no reference to the cost of supply intermittency which becomes increasingly significant as wind energy market penetration increases.

The IMechE acknowledges that the cost of wind energy - along with other green energy sources - is a barrier to its widespread adoption. Nevertheless, in its Energy Plan for the UK, the IMechE suggests that the UK's wind energy capacity should be increased to 40 *GW* by 2050 [29]; this is a fivefold increase from current levels. Such an increase in wind energy capacity will be a major component in the UK's bid to reduce its dependence on fossil fuels. As a nascent industry, wind energy has been highly dependent upon legislative support. This support has been most forthcoming in Western European countries and in some states of the USA, particularly in California and Texas, although in recent years
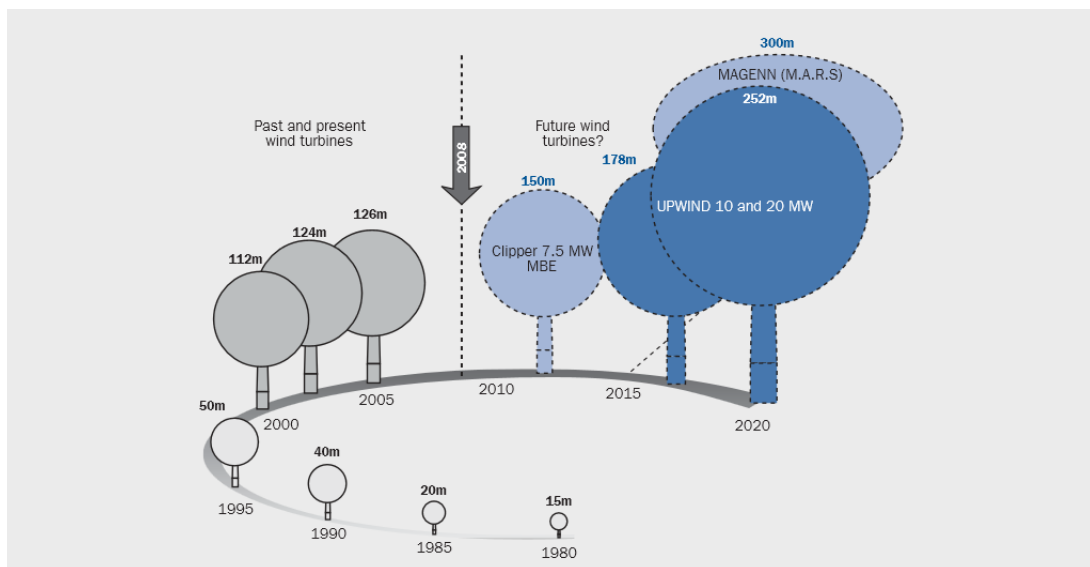
Figure 1.4: Commercially available turbine ratings, reproduced from [3]

wind energy has grown very rapidly in many other countries as legislation has been passed to stimulate its growth. In China, for example, the wind industry has grown very rapidly since legislation was passed in 2006 granting the industry significant tax breaks [30]. By 2012 global installed wind capacity stood at 282 $GW$ (see Figure 1.6) [4]. The rapid growth of the industry has, however, in some cases resulted in very poor performance of wind farms due to poor reliability, poor operational practices and constraints in the supply chain.

Wind turbines are capital intensive (typically 75% of the total cost of onshore wind energy is capital), see Figure 1.7 [6]. The largest component of operating expenditure (OPEX) is due to service and maintenance, although land rent and insurance are also important OPEX costs, see Figure 1.8. Poor reliability of drivetrain components is responsible for a large proportion of OPEX. Often failures in the gearbox or generator cannot be repaired in situ and a new gearbox or generator must be installed. This requires the use of a crane, which is costly. Offshore OPEX costs are considerably higher because a barge must be brought in. These are in high demand in the offshore industry so operators often have to wait many months until a barge becomes available before they can carry out essential operations and maintenance (O&M). In addition, poor weather can prevent access to the turbines for many days, or even weeks, at a time. There is an
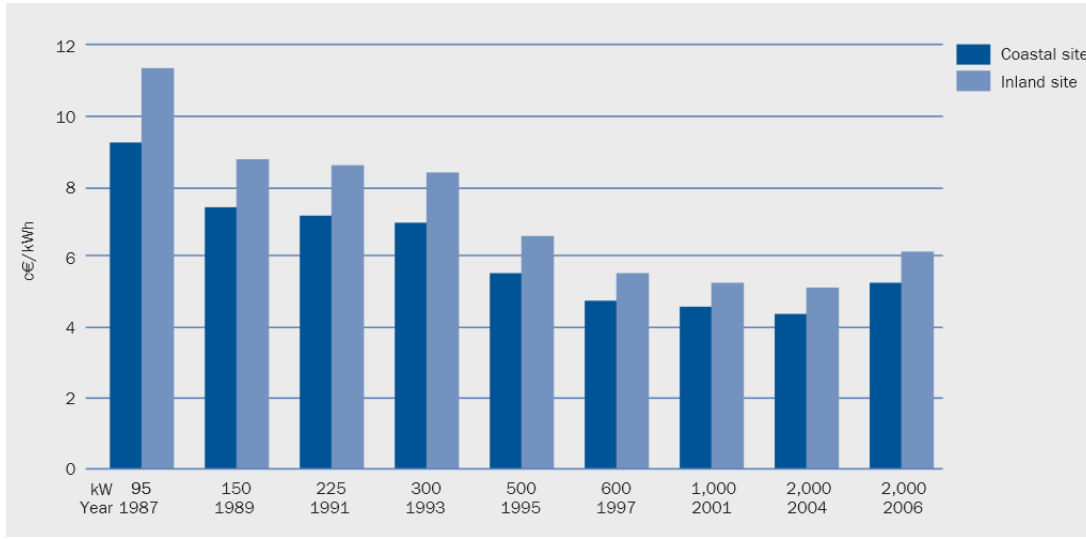
Figure 1.5: Onshore wind energy cost per kWh [3]
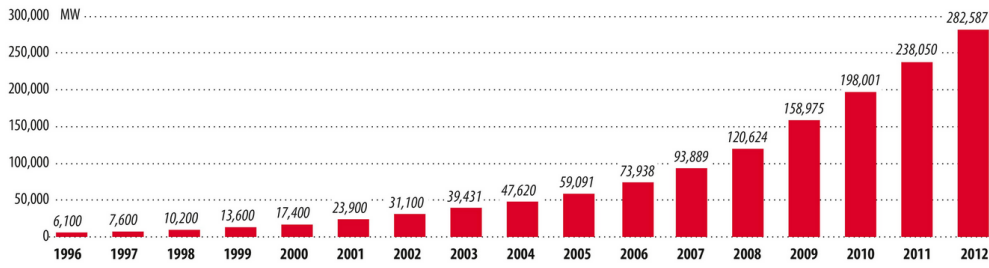


Figure 1.6: Cumulative installed wind capacity [4]

urgent need to improve the reliability of wind turbines. Offshore this must be combined with a pro-active condition based maintenance strategy to optimise O&M resources if wind energy is to be competitive with fossil fuelled generation.

## 1.4   This Thesis

Wind energy must become economically competitive if it is to achieve sustainable significant market penetration. If it is not able to do so the long term viability of the industry will be threatened. The energy source is freely available and so the operating costs of wind turbines should be quite low. However, the published data show that the reliability of multi-$MW$ wind turbines is quite poor with many drivetrain and power take-off components failing before their design life [31]. This poor reliability results in lost power production and increased O&M costs, which increases the cost of energy. This research
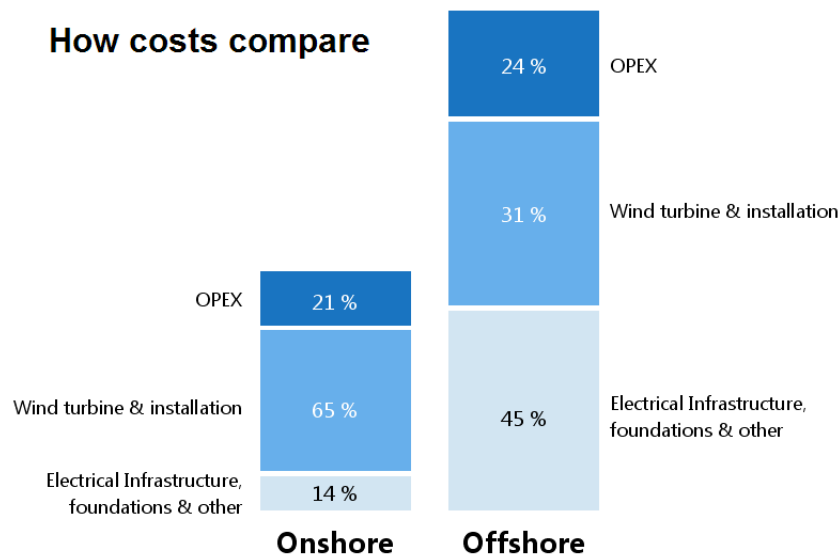
Figure 1.7: Relative CAPEX and OPEX costs for wind energy onshore and offshore, reproduced from [5]

was motivated by published reliability data which showed that generator failure rates in wind turbines were unacceptably high. Electrical machines are mature technology used in a range of other industrial applications in which much lower failure rates are observed [32]; however it should be noted that DFIGs which are so common in wind turbines, are not widespread elsewhere.

Chapter 2 presents a survey of the technology; there is an overview of the most important multi-$MW$ wind turbine topologies, and the basic principles of operation of wind turbines are outlined. The chapter continues with a discussion of the drivetrain and power take-off assemblies of wind turbines. Having introduced the subject of analysis, the published reliability data for wind turbines are presented and discussed in Chapter 3, which seeks to explain why research effort should be expended upon understanding the root causes for the reliability data of wind turbine generators. Chapter 4 explains the construction of electrical machines as a basis for the subsequent description of their reliability data and failure modes. One important differentiating factor between the wind industry and other applications in which medium sized electrical machines are used is the mission profile. The mission profile of wind turbines tends to be highly variable; this is a consequence of the highly stochastic nature of the wind itself. This is in con-
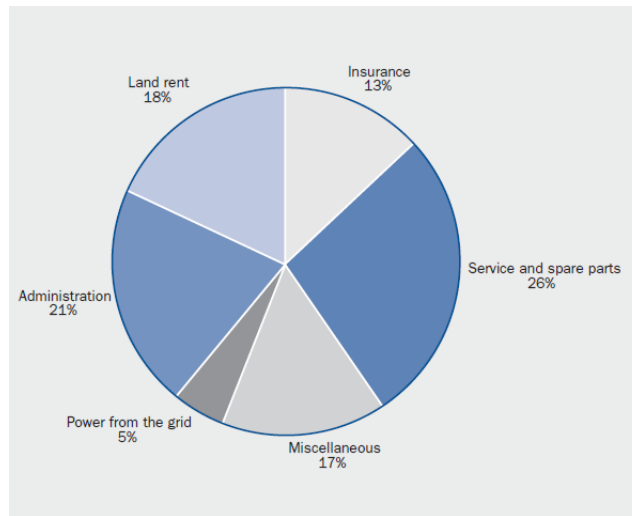
Figure 1.8: OPEX costs by category, reproduced from [6]

trast to many industrial applications of medium and large electrical machines, which tend to operate with long periods of steady-state operation and carefully controlled ramp-up/down. Chapter 5 presents new research; it describes a statistical analysis of weather data and failure data which, motivated by the observation that the mission profile of wind turbines contrasts with many other applications, explored whether there might be a correlation between the turbine operational state and failure rates. The resulting analysis indicated that there may indeed be a correlation, but this 'top-down' statistical approach has limitations. The next three chapters present the majority of the original research. In these chapters numerical simulations, which were used to investigate two important possible root causes of wind turbine generator failure, are presented. This work seeks to go beyond the statistical analysis presented in Chapter 5, which cannot imply causality, and cannot elucidate root causes. Chapter 6 gives the theoretical basis of the analyses. Chapter 7 presents the computational investigation into gearbox-generator misalignment; Chapter 8 discusses the model developed to investigate bearing currents in wind turbine generators. Finally the thesis is summarised, and areas are identified for further work, in Chapter 9.

# Chapter 2

# Wind Turbines: An Overview of the Technology

Wind turbines have changed significantly in the last thirty years. Those pioneering wind technology thirty years ago were typically building turbines rated for 150 $kW$ using technologies borrowed from other applications. Today's turbines are typically rated at 2-5 $MW$ and are much more sophisticated than their predecessors. A number of different concepts have been proposed, and it remains the case that differences of opinion exist within the industry regarding the best conceptual approach. An overview of the technology is here presented, with a particular focus on the drivetrain and its reliability.

## 2.1   Clash of the Concepts

The main wind turbine architectures are outlined in Figure 2.1. Types A and B represent versions of the 'Danish concept' wind turbine. These turbines were essentially fixed speed (although Type B introduced limited speed variability by the simple means of variable resistance). Many of these turbines are still in operation but they are no longer installed in significant numbers. To achieve variable speed operation it is now common to utilise power electronic converters to decouple the turbine generator from the grid frequency. Type C, the dominant technology currently, employs a doubly fed induction generator (DFIG) so that a partially rated converter may be used. Multi-MW power electronic

converters are costly, (typically more than 5 % of the total cost of the wind turbine), and the use of a partially rated converter results in considerable savings, at the cost of increased complexity of the generator and a reduced variable speed range.

The gearless version of the Type D architecture has, in recent years, grown in popularity and it is noted that Enercon (the third largest wind turbine manufacturer with a global market share of 9%) has ceased manufacture of geared systems. The major motivation for this is that by eliminating the gearbox, a costly assembly (approximately 13 % of the system cost according to Morthorst and Awerbuch [6]), the part count is significantly reduced and the reliability may be increased. It may be seen from Figure 3.1 that wind turbine failure rates are not dominated by the gearbox, but it is true that gearbox (and generator) failures are costly due to their long downtimes [33] and the requirement for heavy lifting equipment. Although some in the industry predict a gradual move away from geared turbines in favour of direct drive systems, there is still much disagreement about the relative merits of the different systems.

Certainly the direct-drive concept eliminates an expensive assembly with a significant failure rate and long downtime. However, a price is paid for this. In order to eliminate the requirement for a gearbox the generator synchronous speed must be reduced to match that of the wind turbine rotor (usually below 20 rpm). Recall that the synchronous speed is governed by

$$\omega_s = \frac{60f}{p} \tag{2.1}$$

where $\omega_s$ is synchronous speed, $f$ is electrical frequency, and $p$ is the number of pole pairs.

It may be seen that a large number of poles is required for a low speed generator. In order to accommodate the large number of poles the machine radius must be increased.

Therefore, the synchronous machines used in direct-drive wind turbines are large, heavy, and more expensive than the smaller radius induction machines used in geared turbines. Furthermore, the manufacture of these unusual machines is likely to be less

standardised than that of high volume, high speed induction machines, raising quality concerns.

**Type A**
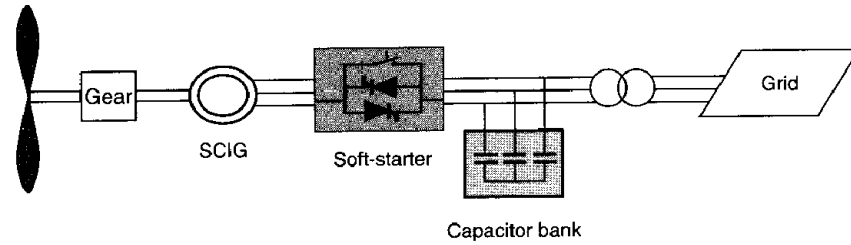
**Type B**
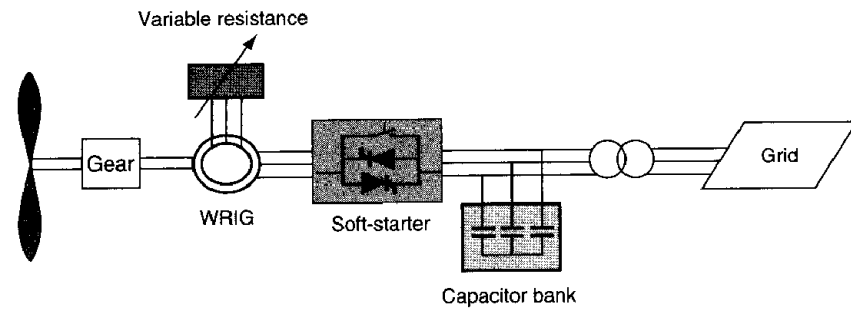
**Type C**
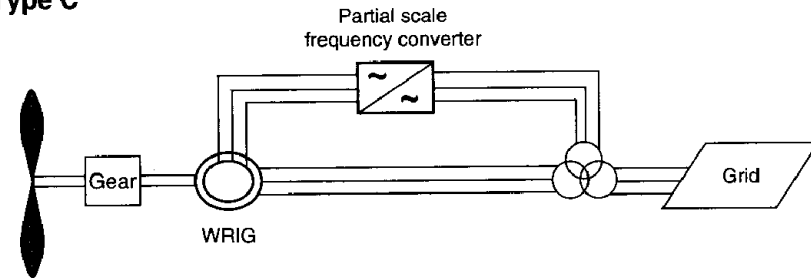
**Type D**
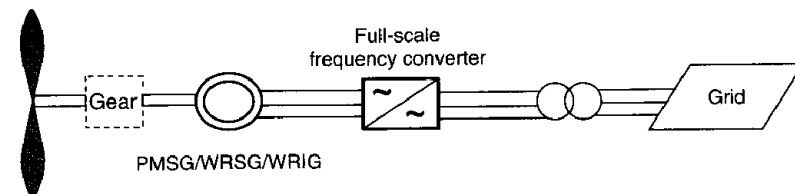
Figure 2.1: Wind turbine architectures (reproduced from [7])

Some investigators have noted that generator failure rates in direct-drive wind turbines are higher than in geared wind turbines. It is not known why this may be, but the following possible explanations have been advanced [32]:

- The gearbox sacrificially protects the generator from the worst of the transient loading derived from turbulence in the wind. Thus, when the gearbox is removed the generator is exposed to more arduous loading.

- Synchronous machines are mechanically more complex than induction machines.

- The manufacture of the direct-drive synchronous generators is less standardised.

- Wound rotor synchronous machines have very long windings, and so may suffer from a higher rate of insulation system failures.

After years of predictions that the future of wind turbines was the gearless design, there is now a developing awareness in the industry of the limitations of these designs - particularly for machines rated above 6 $MW$. The latest cost models suggest that a medium speed drivetrain may be a better solution than either conventional geared designs or gearless direct drive [9, 34]. These medium speed designs [1] typically have a two stage gearbox, yielding a gear ratio of 30 to 40, with a 5 or 6 pole pair machine (corresponding to a synchronous speed of 500 or 600 rpm for a 50 $Hz$ grid frequency). These machines eliminate one of the stages of the gearbox, and along with it its capital cost and the OPEX cost associated with failures, at the cost of a slightly larger and more expensive electrical machine. This trade-off is attractive for large turbines. It is expected that these turbines will dominate the future market offshore, where very large turbines reduce the number of expensive piled foundations required per installed $MW$. Onshore, however, where transport and installation of very large turbines presents logistical difficulties it is likely that 2 to 4 $MW$ turbines will continue to dominate new installations. It is, therefore, likely that onshore the traditional high speed generator (with a three stage gearbox) and direct drive turbines will remain the standard choice for new installations in years to come.

---

[1]Sometimes medium speed turbine drivetrains are known as 'hybrid designs', though the author does not consider this an appropriate name as these designs reside in a continuum; they are not a combination of qualitatively different forms or functions.

## 2.2 Wind Turbine Performance

The power output of a wind turbine is given by

$$P = \frac{1}{2}C_p\rho A U^3 \qquad (2.2)$$

where $C_p$ is the dimensionless power coefficient, $\rho$ is the fluid density (in this case the fluid is air so $\rho = 1.225 kg/m^3$), $A$ is the rotor swept area and $U$ is the wind speed. $C_p$ is defined as the proportion of power in the wind which is extracted by the wind turbine and it has a theoretical limit, found by Betz, of 0.59.

The performance of a wind turbine is often characterised by the $C_p$-$\lambda$ curve, where $\lambda$ is the dimensionless tip speed ratio (the ratio between the tangential velocity of the blade tip and the free stream wind velocity). They are typically of the form shown in Figure 2.2.
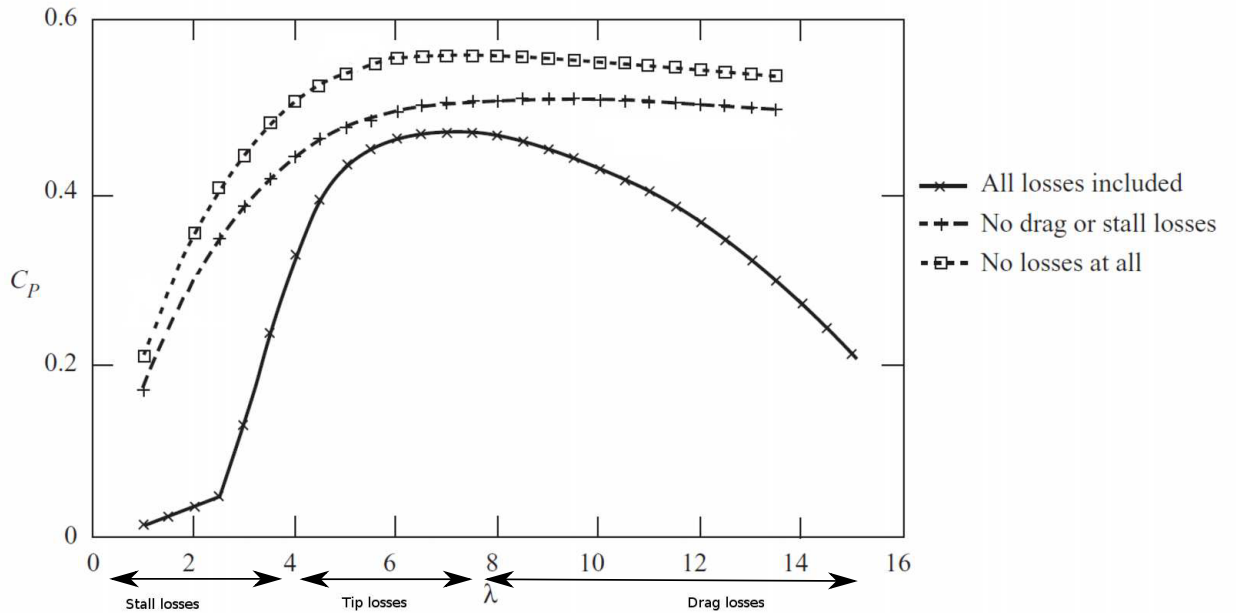


Figure 2.2: Typical $C_p$-$\lambda$ showing the effect of stall and drag losses on the turbine performance (reproduced from [8])

As can be seen from Figure 2.2 there is a rapid decline in $C_p$ either side of the optimum tip speed ratio. At low tip speed ratios the angle of attack is too high and stall occurs,

whereas at high tip speed ratios the angle of attack is too low resulting in significant drag. Given the highly variable nature of the wind it is, therefore, only possible to achieve high aerodynamic performance of the turbine with variable speed operation. However given that the synchronous speed of an AC generator is fixed, for a given number of pole pairs, by the grid frequency (see Equation 2.2) the only way of achieving this variable speed is by (a) continuously variable transmission (CVT) or (b) use of a power electronic converter to decouple the machine frequency from the grid frequency.

Hydraulic CVTs have been used in wind turbines, but they have suffered from low efficiencies when compared with geared transmissions [35]. They also have a larger number of parts which has caused concern about reliability, particularly because of the number of seals which are prone to perish. Nonetheless, development of hydraulic CVTs continues and these technologies may play a role in the future of the wind industries if efficiencies can be improved and reliability concerns allayed.

Another approach is to use a differential planetary gearbox in which a servo motor, or motor-generator, is used to drive one of the gears thus varying the speed ratio in order to keep the output speed constant (see for example [36]). These differential gearing CVTs still require power electronics because the motor/motor-generator is required to be variable speed in order to change the differential ratio, but this can be rated at only 5 to 15% of the primary generator rating. However, at present almost all wind turbines operating in the field use fixed ratio geared transmission, or else they are direct drive, and achieve speed control via power electronic converters.

## 2.3   Wind Turbine Gearboxes

In a typical multi-$MW$ wind turbine, which is the focus of the present work, the turbine rotor has a nominal speed in the range of 15 to 18 rpm. In order to enable the use of a standard 'off the shelf' two pole pair induction machine a speed ratio of around 83 to 100 is demanded of the gearbox. This equates to having three stages, the first stage of which is always planetary in order to achieve a sufficiently high ratio and share the high torque load across multiple contacts. The second stage may be planetary, or parallel, whilst the

third stage is almost always parallel.

As discussed above, there is a growing number of so called medium speed gearboxes for larger WTs (rated above 5 $MW$). These gearboxes are usually two stage, often planetary-planetary, and have an overall speed ratio of 30 to 40. They are also often integrated with the generator in one housing. One consequence of this is to mitigate misalignment between the gearbox and the generator which, as will be seen in Chapter 7, can be the cause of coupling and generator bearing failure. There are different philosophies with regards to the drivetrain mounting. The three most common arrangements are:

- three point mounted (one main bearing, two compliant torque arm mounts, see Figure 2.3a),

- four point mounted (two main bearings and two compliant torque arm mounts, see Figure 2.3b),

- integrated design, see Figure 2.3c.

The three point and four point mount designs are very different to the integrated design. In the three point and four point mount designs the bending loads from the blades are, in theory, taken by the main bearing not by the gearbox directly. In the integrated design the gearbox housing is directly bolted to the nacelle bedplate, the main bearing is incorporated in the gearbox, and the gearbox housing must transmit the bending loads from the blades to the nacelle bedplate.

The gearbox has been much scrutinised in the wind industry and widely blamed for the poor overall reliability and availability of many multi-$MW$ wind turbines. Whilst the reliability of WT gearboxes has not always been high enough, the available failure data indicate that some of the charges leveled against the gearbox are exaggerated, see Chapter 3. Nonetheless, gearbox failures have been too common in WTs in large part because of the arduous loading regime they experience due to fluctuations in the wind, the consequences of which are transient off-axis loads, as well as often extreme ambient
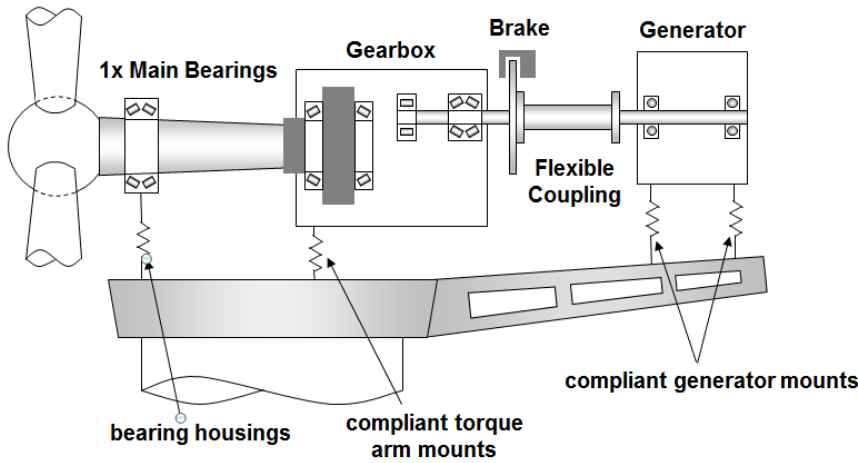
(a) Three point mounted gearbox
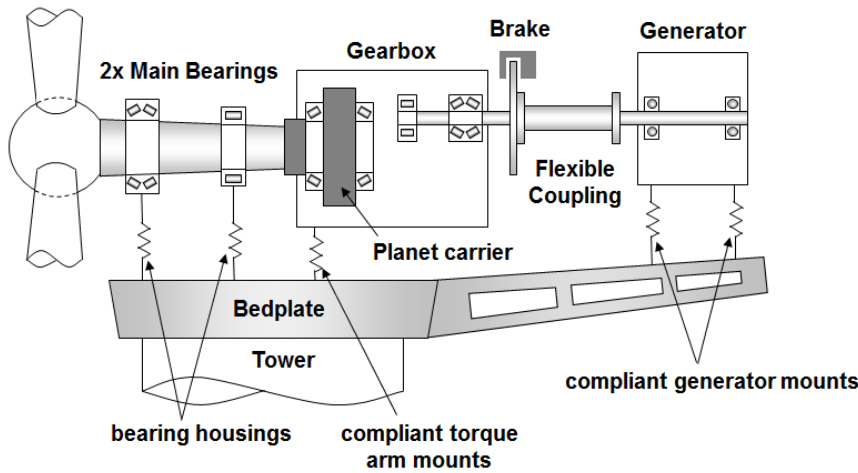
(b) Four point mounted gearbox, probably the most common mounting arrangement at present for multi-$MW$ gearboxes
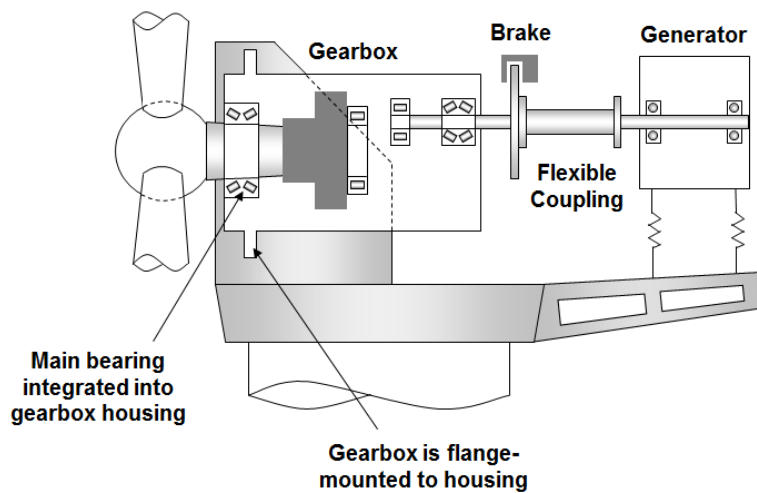
(c) Integrated gearbox, this mounting arrangement is less common, but it saves weight and space

Figure 2.3: Standard mounting arrangement for multi-$MW$ wind turbine drivetrains (figures reproduced from [9])

conditions, which may include large temperature variation and ingress of dust, water or snow depending on location.

The gear design codes used in the wind industry assume that the contact patch of the gear teeth is centred in the contacting teeth, i.e. that edge effects can be neglected [37]. If, however, there are significant off-axis loads caused by transient events such as gusts, grid faults or emergency shutdown then there may be misalignment between the gear teeth, and the contact patch may move away from the centre resulting in higher than expected edge stresses. This will only be accommodated in the gearbox design if the loading, and the structural flexibilities, are accurately characterised [10]. Figure 2.4 shows the effect of compliance of the drivetrain, under load, upon the gear contact patch.
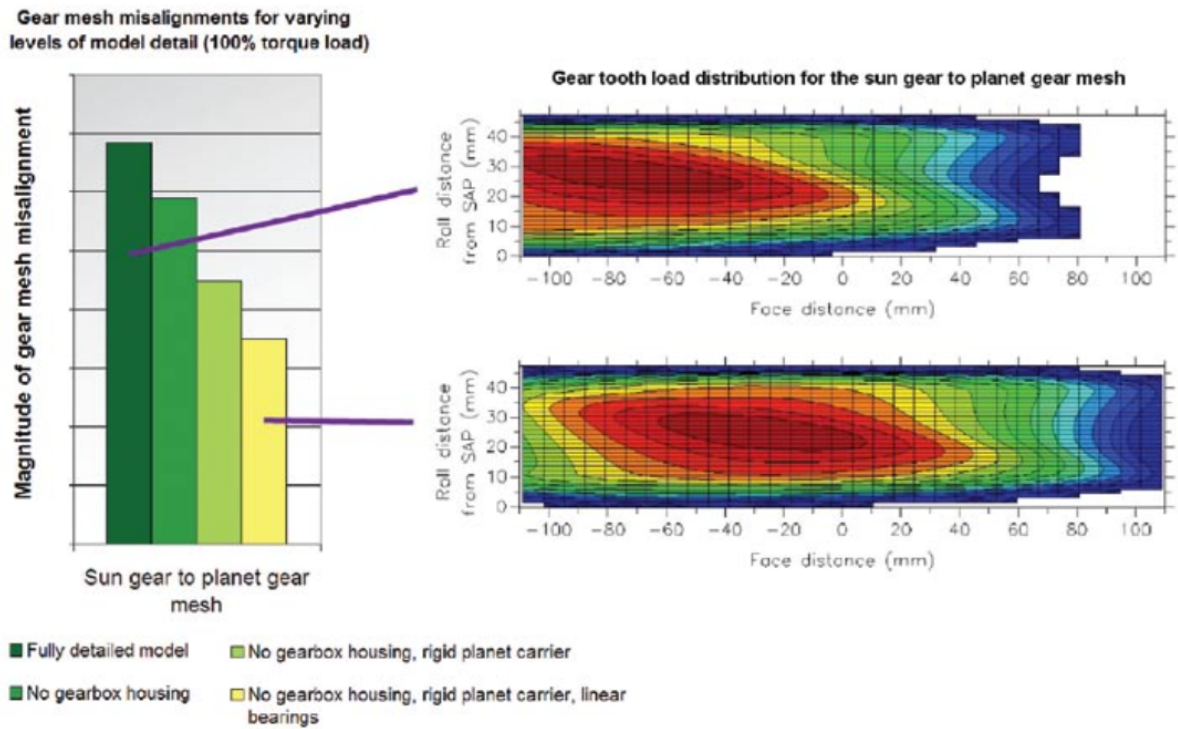


Figure 2.4: The effect of drivetrain compliance upon gear contact patches in wind turbines (reproduced from [10])

Considerable research effort has been expended on understanding the loads that drive the failure of WT gearboxes and it is becoming increasingly clear that established design practices are not appropriate [38–40]. Gearboxes that are designed and built to specification are failing in service long before the calculated design life because the load data to which they are designed do not reflect the loading that they experience in service.

A major challenge for the industry is to understand better the dynamics of the whole system and take these into account in the design process. This is not easy because to do so will require inter-disciplinary and inter-organisational collaboration. To understand the dynamic loads on the wind turbine gearbox requires, in addition to the complexities of the gearbox itself, an understanding of the wind resource, the aerodynamics, the electrical assemblies (the generator and the power electronics) and the control system. It is in developing an holistic understanding of the system, which accurately characterises its dynamic response to the volatile wind input, that the wind industry must build intellectual capability in years to come.

## 2.4   Generators

Wind turbine generators are, at present, almost all low voltage machines, typically 690 $V$. The generated electricity is then stepped up to distribution level, 3.3 $kV$, by a transformer which is usually located in the nacelle, but may also be located at the base of the tower. As turbines get larger, however, the case for medium voltage becomes stronger. Losses are reduced and nacelle size and weight may also be reduced by eliminating the large, and heavy, transformer. For large offshore turbines medium voltage machines are likely to become the standard in the future.

Currently most turbines are either Type C or Type D (see Figure 2.1). Type C turbines have wound rotor induction machines in which the stator is directly grid connected (via a step-up transformer) and the rotor is isolated from the grid frequency by a back-to-back power electronic converter. The power electronic converter is typically only rated for approximately 20% of the machine rating. This is to minimise cost because, whereas the cost of electrical machines is a function of torque, for power electronics it is principally a function of power. The use of partially rated power electronics gives only limited speed control, but the cost paid in terms of lower efficiency is small.

Induction machines are mass produced and they have a proven track record of robust performance in a wide range of industrial applications, though outside of the renewable energy industry it is not usual to use them as generators. One drawback to using induc-

tion machines as generators is that, because they rely on the grid to provide their field excitation, they tend to weaken the grid. Unfortunately the best wind resources are often in more remote locations which have weak grids and this has led to grid compliance issues. In the early days of the wind industry this was of little importance, but as wind turbines start to achieve significant penetration in the electricity generation market their influence on power quality is becoming greater and operators have started to require wind farms to meet stringent grid compliance criteria. Consequently low voltage ridethrough (LVRT) and high voltage ridethrough (HVRT) have posed challenging control problems for the wind industry, and this is an area where there has been considerable research effort over the last decade.

Type D turbines usually use synchronous machines with a fully rated converter connected to the stator windings. The use of a fully rated converter fully decouples the machine from the grid frequency allowing full speed control. These turbines do not suffer the same grid compliance challenges as Type C turbines because the synchronous machine provides its own excitation. They are usually gearless, though this is not necessarily the case, and consequently are said to be more reliable, but as has already been discussed the situation here is not as clear as their proponents may suggest.

The field excitation may be provided by permanent magnets, or field windings. Many wind turbine manufacturers in the last decade favoured permanent magnet excitation because of its higher efficiency, lower weight and, potentially, higher reliability. However there are serious concerns about the security of supply of the rare earth metals which are required to manufacture these magnets. Currently China accounts for about 97% of the rare earth metal industry and, in 2009, it began restricting exports which prompted price increases. Rare earth metals find many applications including automotive, military technology and consumer electronics. Other countries, in particular the USA, Japan and Australia, have now started to fund research and exploration of rare earth metal; indeed, in March 2013 researchers in Japan announced discoveries of significant deposits in Japanese territorial waters. These discoveries may well decrease the price of rare earth

metals in the future, but given the high level of demand from a range of industries and the highly politicised nature of the supply chain some wind turbine manufacturers have preferred to opt for wound rotor machines as the perceived risk is lower.

From Faraday's law

$$E = -\frac{d\Phi}{dt} \tag{2.3}$$

it is known that it is the rate of change of magnetic flux, $\Phi$, with respect to time, $t$, which produces the e.m.f, $E$, and, therefore, it does not matter whether the field excitation is provided by the stator or the rotor windings. It is, however, usual for the generator to be provided by a rotating field because it simplifies removal of the power from the armature windings; in the case of a permanent magnet machine it eliminates the need for sliprings and brushgear altogether.

Electrical machines, rated between 1 and 5 $MW$ typically achieve efficiencies in the region of 97 to 98 % [41], but even 2% losses for a 5 $MW$ machine equates to 100 $kW$ of heat output. This heat is generated in the middle of the machine and its removal is critical, otherwise the generator will overheat and failure will follow shortly. Cooling in wind turbine generators is usually achieved by means of a large fan on the rotor which blows air over the rotor and stator. The housing is designed with ribs to increase the surface area and shrouding to maximise the convective exchange of heat. It is also common in the generators to have water cooling circuits which pass through the stator to further increase the heat transfer. In some generators pins are used to separate the stator laminations which further improves the heat exchange.

Electrical machines are usually reliable compared to other drivetrain components such as gearboxes, but it is interesting to note that in the wind industry generators have proven to be the cause of significant downtime. This is because both their failure rate, and the downtime per failure, is unacceptably high as shall be seen in Chapter 3.

## 2.5 Power Electronics

Power electronic converters provide the interface between the generator and the grid and allow the optimum tip speed ratio to be maintained across a wide range of wind speeds, which improves energy capture and also mitigates the harsh transient loading that may be caused by aerodynamic stalling. By increasing the level of control over the turbine power electronic converters also help to ensure grid compliance which is applied more stringently now that wind energy generation on some networks accounts for a significant proportion of generating capacity. In the event of a low voltage fault the turbine is required to ride through (i.e. not disconnect) within certain prescribed limits. The power electronic converter increases the extent to which the turbine may be controlled and, therefore, makes ride-through possible without the turbine suffering excessive damaging transient loads.

Fundamental to the power electronic converter, which decouples wind turbines from the grid frequency allowing for variable speed operation, is the insulated-gate bipolar transistor (IGBT). IGBTs were introduced in the early 1980s and the technology has continued to improve with increased current rise time and fall time rates being achieved as well as higher voltage and current ratings.

Three phase back-to-back converters, with bridge coupled IGBTs, are used in wind turbines with a capacitor bank across the DC link to decouple the rotor-side and grid-side inverters allowing for separate control of the two inverters.

Many switching strategies exist, but pulse-width modulation (PWM) is the most commonly used in wind turbine power electronic converters. The switching frequency must be considerably higher than the desired fundamental frequency. The IGBTs are switched to generate a series of voltage pulses whose duration is modulated sinusoidally such that

$$\frac{\beta_1}{y_1} = \frac{\beta_2}{y_2} \tag{2.4}$$

where $\beta_i$ is the $ith$ pulse duration, $y_i$ is the $ith$ instantaneous target fundamental value

(see Figure 2.5).
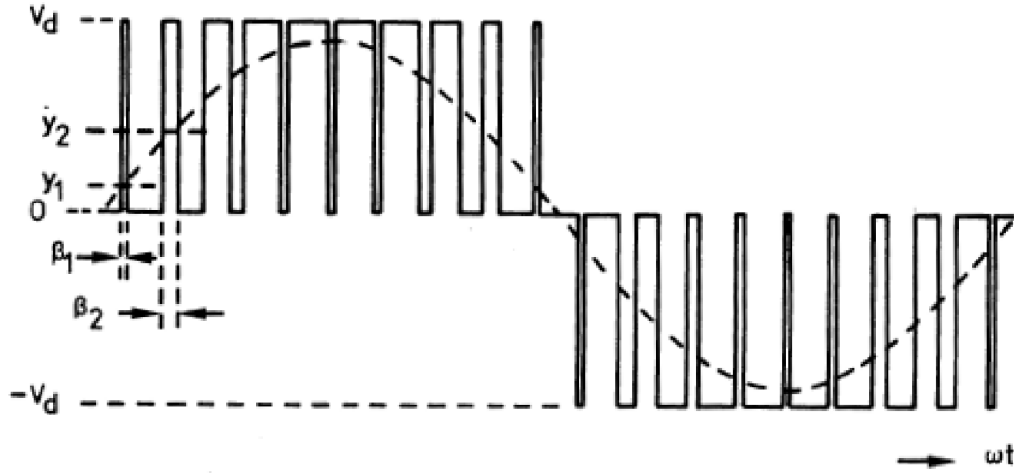


Figure 2.5: Sinusoidal PWM (single phase), reproduced from [11]

As long as the ratio of the switching frequency to the fundamental frequency is sufficiently high, the average, or steady-state, effect will be close to that of the fundamental. The definition of 'sufficient' in this context depends upon the quality of the signal required and this is application specific. For wind turbines a switching frequency of 1-8 $kHz$ is typical.

The high $dV/dt$ (where $V$ is voltage) can, however, adversely affect the winding insulation and bearings of the generator due to parasitic effects, which for most purposes can be neglected. This will be explored in Chapter 8.

## 2.6 Control

Although there are still many fixed speed turbines in operation in the field they have now been superseded by variable speed, pitch regulated, turbines for new farms. Variable speed, pitch controlled, wind turbines allow the speed to vary below rated wind speed (usually 12.5 $m/s$) in order to track peak $C_p$. This also reduces the noise emissions at low wind speeds, which is particularly important in European countries where noise emissions from wind turbines are tightly regulated. By allowing the speed to change, torque variations are reduced which is beneficial for the gearbox and the generator.

Above rated wind speed the turbine is operated in constant speed mode[2] and pitched to feather in order to limit the power generated. Large wind turbines shut down above 25 $m/s$.

The different regions of the turbine control are shown in Figure 2.6, which graphs operational data from the SCADA (Supervisory Control and Data Acquisition) system of a 2 $MW$ wind turbine.
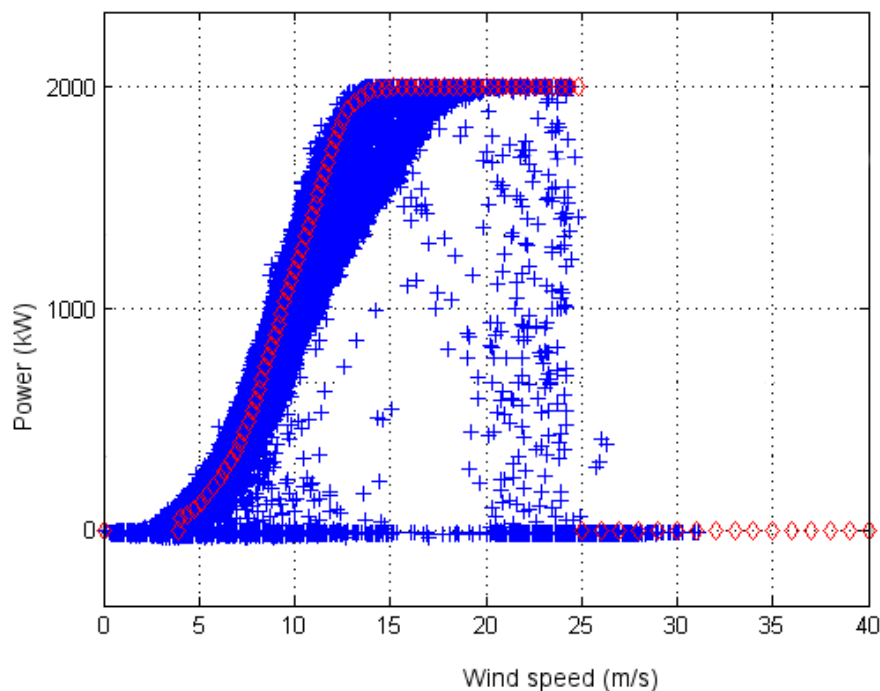


Figure 2.6: The power curve of a 2 $MW$ wind turbine. The red diamonds denote the datasheet curve, the blue crosses the data measured by the SCADA system.

## 2.7 Summary

In this chapter an overview of the technology in modern multi-$MW$ wind turbines has been presented. This overview of the technology has presented the current state of the art in wind turbine drivetrains, and has also discussed likely developments in the future. The present chapter has introduced the technology with particular emphasis upon the drive-train – the gearbox and generator – and with not infrequent references to reliability. In

---

[2]This is broadly true, although many wind turbine controllers now have sophisticated logic which allows the turbine to operate outside of its usual regime in specific circumstances to preserve the health of the turbine. So, for example, some turbines will allow overspeed for a short time if there is a significant gust in order to limit the torque.

the next chapter a systematic overview of the published reliability data for wind turbines is presented.

# Chapter 3

# Wind Turbine Reliability

Modern wind turbines usually have a design life of 20 years, while traditional steam turbine generator systems have a design life of 40 years. Furthermore, wind turbine generator failure rates are about three times those of conventional generation technologies [26, 31]. There are fundamental differences between wind energy and conventional energy sources:

- wind energy generation is decentralised

- the ambient environment in which the plant operates can be inhospitable

- the energy source fluctuates. Wind turbines must operate with a highly variable mission profile, whereas convention fossil fired generation plant operates with very carefully controlled mission profiles.

Over the last two decades there has been a drive to understand how fluctuations in the wind give rise to fatigue loading in wind turbine blades, see for example [42–45]. Indeed, with this increased understanding, blade failure rates have been reduced (though they remain significant).

Wind turbine failure data have been categorised by subassembly, see Figure 3.1. Though generators fail less frequently than some other subassemblies, their contribution to the overall wind turbine failure rate is significant. In addition, generator failures are particularly costly because of the large downtime incurred.
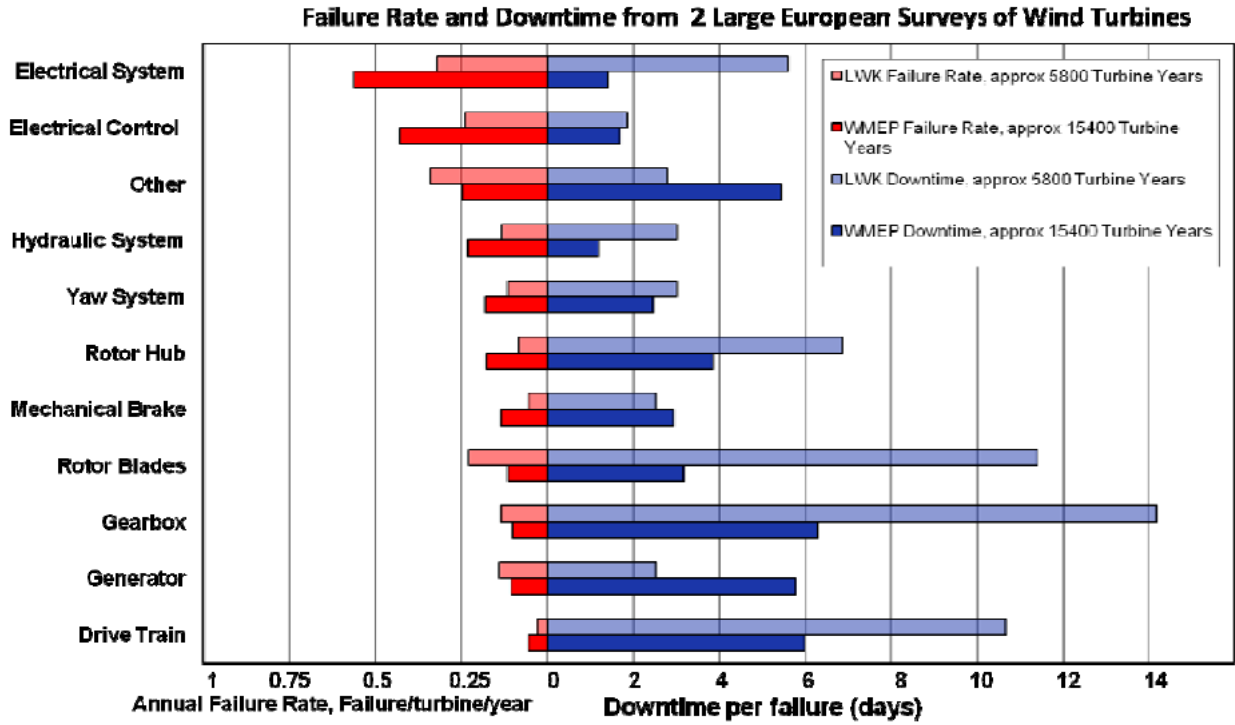
Figure 3.1: Distribution of failure rate and downtime by subassembly from the two publicly available datesets: WMEP (approximately 15400 turbine years) and LWK (approximately 5800 turbine years), reproduced from [12]

The *Wissenschaftliches Mess und Evaluierungsprogramm* (WMEP) [33] and *Landwirtschaftskammer* (LWK) [46] surveys provide large datasets of failure rate and downtime data which are give valuable insights into the reliability of the various subassemblies of wind turbines. These datasets have some important limitations. Many of the turbines are old, and some of the turbines may be in the wear out phase of the bath tub curve. It must also be recognised that the majority of turbines will be much lower power than modern turbines, and of redundant technologies. Also many of the turbines, particularly in the WMEP survey are owned by farmers and small cooperatives. The quality of O&M carried out is likely to be highly variable, given the diversity of owner/operators. The Reliawind study [12] attempted to address these limitations by considering only turbines that met the following requirements:

- The farm must have at least 15 turbines

- The turbines should have been operating for a minimum of two years

- The turbines must be variable speed and pitch regulated

- Rated greater than or equal to 850 $kW$.

It is interesting to note that the findings of the Reliawind survey are broadly comparable to the WMEP and LWK surveys; see Figure 3.2 for the failure rates found in Reliawind, and Figure 3.3 for the downtimes. Note that the Reliawind survey categorises the data by assembly, but also by subsystem; i.e the data are shown for the individual assemblies, but also for the subsystems such as, for example, power take-off or drivetrain. In spite of the diverse technologies and power ratings, the same trends emerge. Electrical faults, relating to the power electronics and control system, are quite common, but these faults have quite low downtime. It is likely that these faults are often caused by the system tripping and can often be reset remotely. Even when components need to be replaced it can often be done in-situ. Gearbox and generator faults are less common, but the associated downtime is greater as these faults often involve major O&M activity and replacement of the whole assembly. In 2009 Faulstich *et al.* showed that, onshore, 75% of failures accounted for only 5% of downtime with the remaining 25% of failures being responsible for 95% of downtime (Figure 3.4) [13]. These 25% of failures did come from all subassemblies, but were predominantly from the gearbox, drivetrain and generator, see Figure 3.5.

In 2006 Tavner *et al.* performed statistical analyses on wind turbine failure and meteorological data from Denmark [47]. A positive correlation between the wind energy index (WEI), closely related to wind speed, and wind turbine failures was identified. Furthermore, the correlation between failure and WEI showed significant variation for the different wind turbine subassemblies. The subassembly with the maximum correlation between failure and WEI was the generator. Tavner *et al.* suggested that this correlation may be a consequence of the fact that most wind turbine electrical systems have been adopted from conventional drive technology without due consideration of the fundamentally different operating environment.

It has been found that generator failure rates in the wind energy industry compare unfavourably with other industries. Outside of the wind energy industry, a failure rate
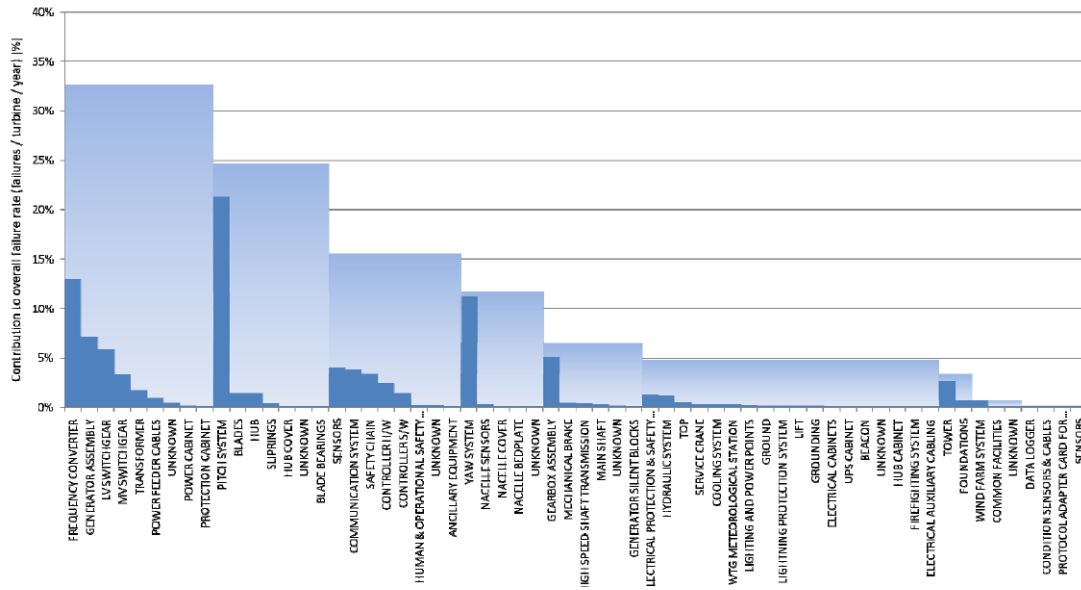
Figure 3.2: Distribution of normalised failure rate by subassembly from the Reliawind survey, reproduced from [12]

of 0.0315 to 0.0707 failures per generator per year is typical [15]. However, in the wind turbine industry generator failure rates of greater than 0.1 failures per generator per year or greater are typical [31, 32, 48, 49]. In the next chapter generator reliability is discussed with particular reference to the wind industry. The construction of electrical machines is described, and their failure data and failure modes are discussed.
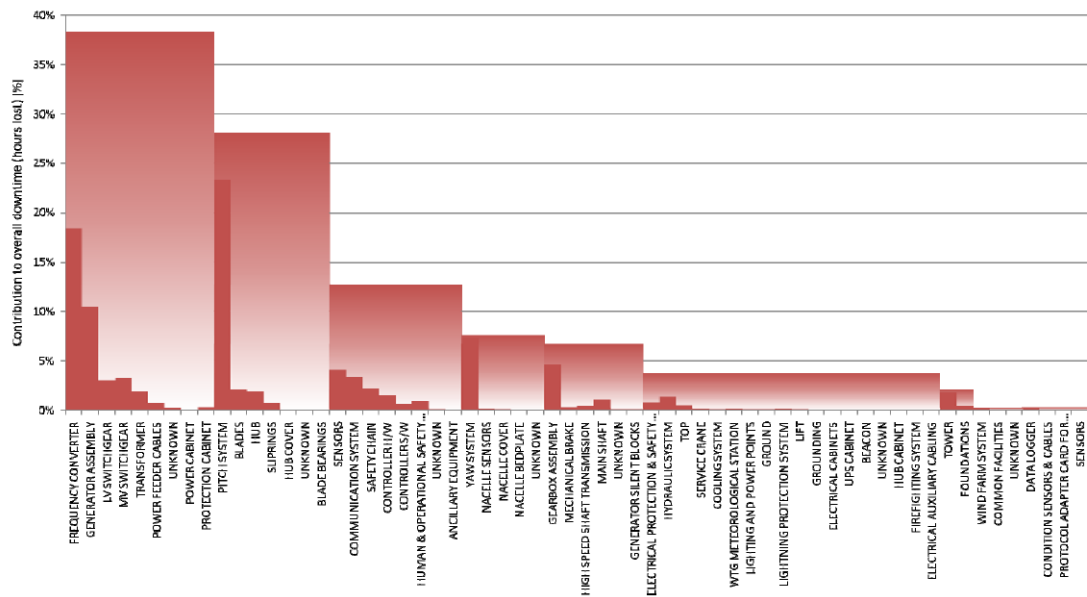
Figure 3.3: Distribution of normalised downtime by subassembly from the Reliawind survey, reproduced from [12]
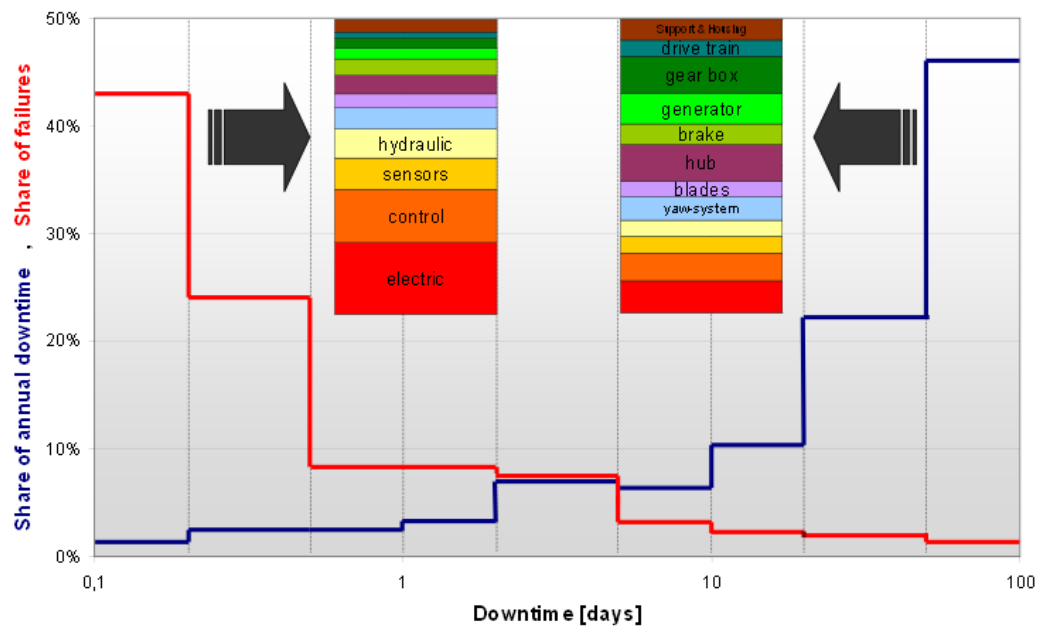


Figure 3.4: 25% of failures are responsible for 95% of downtime onshore, reproduced from [13]
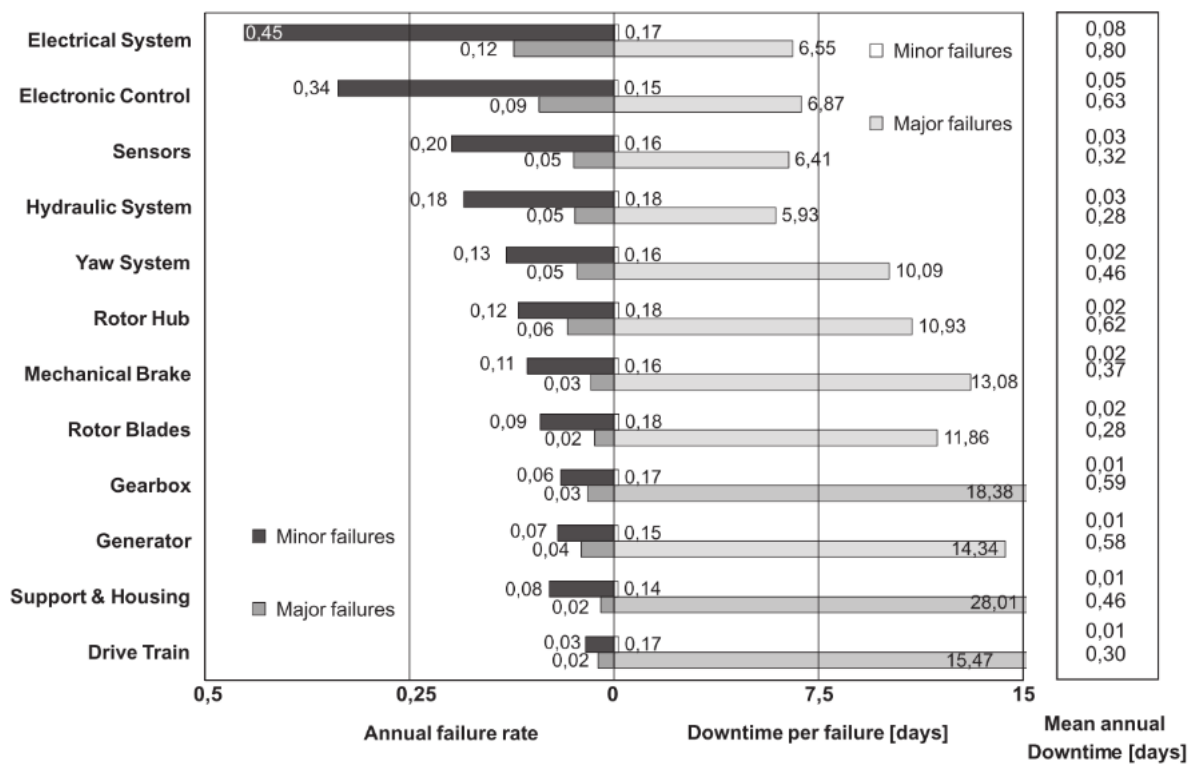
Figure 3.5: Distribution of failures by subassembly and categorised as either major or minor failures, reproduced from [14]

# Chapter 4

# Electrical machines: their construction, their reliability and their failure modes

In this chapter, data from the wind industry are supported with data from other industries for increased statistical robustness. Firstly, an overview of the construction of electric machines is presented.

## 4.1 Construction of rotating electrical machines

Electrical requirements mean that the design of electrical machines must be suboptimal from a mechanical point of view. Good conductors tend to have poor mechanical properties, while insulating materials are even weaker mechanically. Furthermore, insulating materials, which must be located very close to major heat sources in electrical machines (ohmic losses in the conductors), suffer thermal deterioration at relatively modest temperatures, see Table 4.1. Wind turbine generators typically have class F insulation which is rated to 155 °C. Additionally, electromagnetic considerations result in geometric stress raisers. Compromise is inherent in the design of electric machines.

Figure 4.1 shows a cutaway view of a 4 kW totally enclosed fan cooled (TEFC) squirrel cage induction machine (many of the features are similar to other types of machines). The

| Thermal class (°C) | Letter designation |
|:---:|:---:|
| 90 | Y |
| 105 | A |
| 120 | E |
| 130 | B |
| 155 | F |
| 180 | H |
| 200 | N |
| 220 | R |
| 250 | - |

Table 4.1: Thermal classification of electrical insulation [23]

stator and rotor cores are laminated to reduce iron losses, with laminations separated by a thin layer of varnish. Recently, at least one manufacturer has improved cooling by separating stator core laminations by welded short steel pins in order to provide radial cooling ducts [50].

The stator core is compressed before being clamped between end plates in the fabricated stator housing, whereas the rotor core is shrunk onto the shaft while clamped under pressure to ensure that it will withstand the large forces it is subjected to in operation.

The lined stator slots are tightly packed with copper conductors, typically insulated with mica paper and held in place with epoxy-glass wedges. In order to minimise the presence of voids in the windings the stator winding insulation system is consolidated with epoxy resin by the vacuum pressure impregnation (VPI) process. Note that in Figure 4.1 the stator conductors are random wound (sometimes also called mush wound), however in a wind turbine generator, rated at perhaps 2 MW, the stator windings would usually be form wound as in Figure 4.2. The reasons for this are discussed in Section 4.1.1.

Rotor construction depends upon the type of generator used. The traditional 'Danish concept' wind turbine (Type A in Figure 2.1) uses a squirrel cage induction machine. The squirrel cage rotor has uninsulated copper bars which are brazed to end rings to form a short circuit. However, the squirrel cage induction machine is no longer the main generator used in wind turbines. It has largely been replaced by the DFIG, which allows economic variable speed operation. The main difference between the DFIG and squirrel
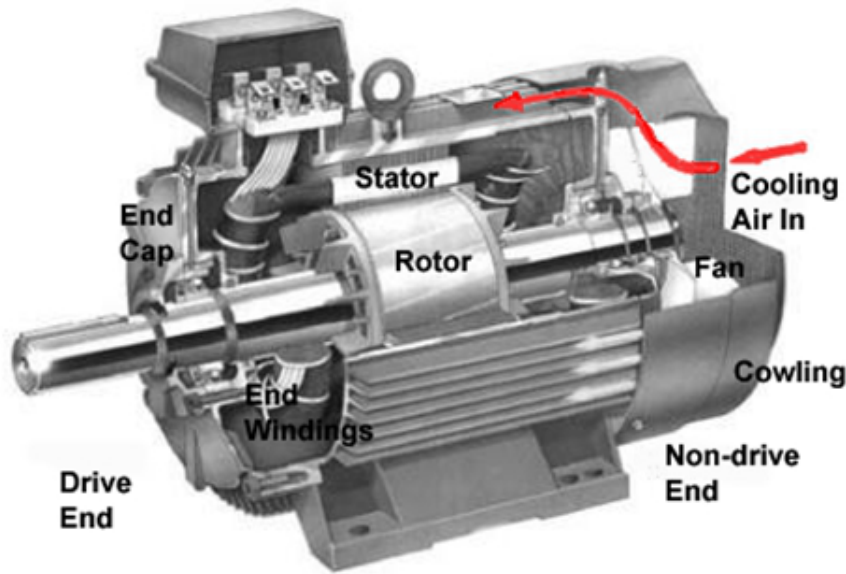
Figure 4.1: Cutaway of a squirrel cage induction machine showing salient features (reproduced from [15])

cage machines is that DFIG has a wound rotor, with slip rings and brushgear.

Another important generator technology is the synchronous machine. In wind turbines these are used in low speed direct drive architectures. They are very large radius machines, and consequently they are very heavy. The rotors are generally of salient pole design because of the large number of poles required to achieve slow speed operation. The field excitation may be provided by either windings or rare earth metal permanent magnets.

The shaft must be stiff because a small air gap is required. Any eccentricity would increase the air gap on one side, and decrease it on the other, leading to unbalanced magnetic pull (UMP) which exacerbates the problem. This is a particular issue in long machines. In wind turbine generators it is usual to employ rolling element bearings to ensure that the rotor is accurately centred. More details are now presented concerning the key subassemblies of electrical machines.

### 4.1.1 Stator winding construction

*The content of Section 4.1.1 is largely taken from Stone et al. [16]. Where material is drawn from other authors it is cited locally.*

There are three types of stator winding construction, the choice of which depends on the rating of the generator:

- Random-wound (also called mush wound), $< 600\ kW$

- Form-wound with multi-turn coils, $600\ kW$ - $100\ MW$

- Form-wound with Roebel bars, $> 100\ MW$

Form-wound stator windings are made from insulated coils that have been preformed prior to insertion in the stator core slots. Each coil has multiple turns, and several coils are connected in series to achieve the correct number of turns per phase. The coil usually has a twisted turn in the end winding, see Figure 4.2. This transposes the position of the conducting strands in the bar in order to reduce circulating currents. The magnetic flux in the slot is not constant; it is at a maximum nearest to the rotor and decreases with slot depth. If the strands in the bar were always at the same depth in the slot the strands nearest to the rotor would have the greatest induced voltage leading to significant circulating currents and increased Ohmic losses. So this transposition of the conducting strands is necessary. However, unfortunately, this feature acts as a stress concentrator in the end windings. In addition, extra insulation is needed to preclude air pockets from the transposition regions and thus prevent partial discharge (PD).

Wind turbine generators, typically rated between 2 and 5 $MW$, are form-wound. Most electrical machines with multi-megawatt ratings (and form-wound stator windings) operate at 1 $kV$ or greater but, unusually, wind turbine generators are typically operated at 690 $V$. There has been some interest in using high voltage (HV) systems in wind turbines [7]; this would increase the efficiency of the system, reducing the amount of heat that must be dissipated, leading to a reduction in machine size and weight. It would also be possible to eliminate the need for a transformer. However, the cost associated with HV systems, not least because of the retraining required for O&M staff, has deterred many in the industry.

Figure 4.2: Form-wound stator winding, reproduced from [16]

There are three components to stator winding insulation (see Figure 4.3):

- Strand insulation

- Turn insulation

- Groundwall insulation

**Strand insulation**

There are two reasons for splitting the conductor into separately insulated strands. Firstly, in order to carry the required current the conductor may need to be quite thick which makes it difficult to bend the endwinding region of the coil. The current density of a conductor is limited by thermal requirements. Ohmic losses are related to the square of current, so as current density is increased the heat loss per unit volume increases sharply and more effective cooling is required.

Secondly, the conductor must be subdivided because of a phenomenon known as the skin effect. If a conductor has a large enough cross-sectional area the current will tend to flow only around the periphery of the conductor. For 60 *Hz* AC the skin depth is
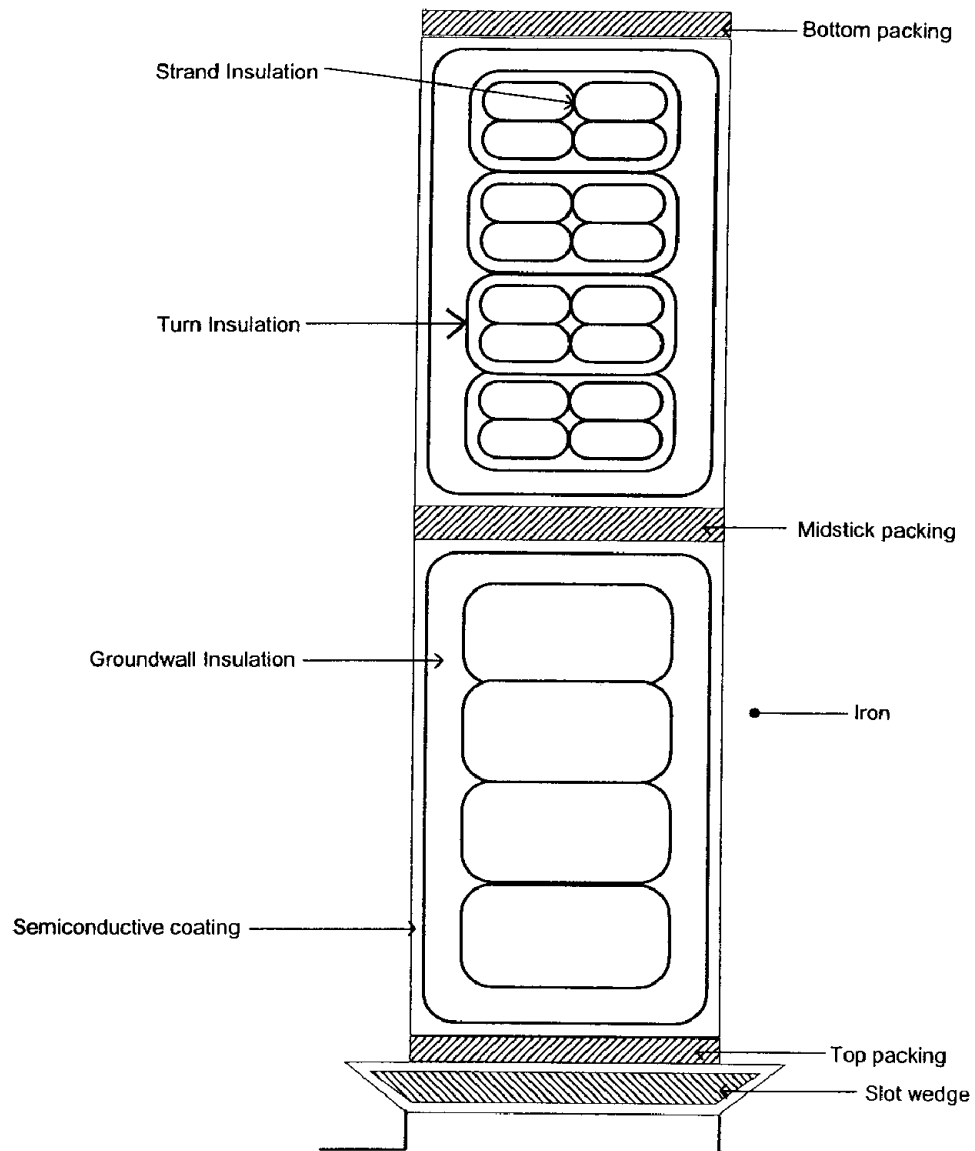
Figure 4.3: Winding section, reproduced from [16]

8.5 $mm$; if the depth of the conductor is greater than 8.5 $mm$ the current will tend not to flow through the centre of the conductor. Clearly, such an effect is not desirable as it represents an inefficient use of space and material. So by having separately insulated strands, each of small cross-sectional area, the total cross-sectional area of the conductor is used to carry current rather than only the peripheral area.

Typically electrical machines are designed to operate around 2.5 $A/mm^2$, at higher current densities the insulation may be damaged or the copper may even melt. For a wind turbine rated at 2 $MW$ the phase power is 0.66 $MW$, therefore phase currents of approximately 1 $kA$ will be experienced. If a current density of 2.5 $A/mm^2$ is assumed then a 20 $mm$ by 20 $mm$ conductor is required. This would be difficult to bend in the form winding process, so it is helpful to divide this into parallel strands. Furthermore, a 20 $mm$ by 20 $mm$ conductor would experience the skin effect.

The electrical stress[1] across strand insulation is very small, so the insulation can be thin. However, because of the winding forming process the strand insulation must have good mechanical properties so as not to fracture during manufacturing.

**Turn insulation**

It is necessary, in order to prevent shorts between adjacent turns in a coil, to employ turn insulation. Turn-to-turn shorts result in very large circulating currents flowing in the shorted region due to the transformer effect. This quickly results in overheating which damages the groundwall insulation, consequently causing a ground fault.

In a random-wound machine the voltage between adjacent turns could be anything up to a maximum of the phase-to-phase voltage (this is why random-wound windings are rarely used above 600 $V$). In the case of form-wound systems the voltage across the turn insulation is largely known, and kept to a minimum by careful design of the winding arrangement. Nevertheless, form-wound arrangements suffer significant electrical stresses arising from large transient voltages associated with machine startup, lightning strikes, and the use of power electronic converters. It should be noted that all of these are

---

[1]Electrical stress is defined, in parallel plate geometry, as the voltage across the conducting plates, divided by the distance between the plates. It is a measure of the strength of the electric field.

important transient events in the case of wind turbine generators.

**Groundwall insulation**

Groundwall insulation provides separation between the core (which is grounded) and the stator windings. Should the groundwall insulation fail, a protective relay is tripped to protect the stator core. It is important for groundwall insulation to have low thermal resistance, particularly, if the windings are not directly cooled.

In addition, there are significant electromagnetic forces acting on the conductors (see Section 4.2.1). This radial force has an high frequency component (twice the electrical frequency) superimposed on a 'DC' force. There is also a component of the force in the circumferential direction, though this is typically an order of magnitude smaller than the radial component. These forces cause high frequency cyclic loading of the winding arrangement, and can result in damage of the groundwall insulation, particularly given the laminated construction of the stator core. Groundwall insulation is, therefore, required to be resistant to abrasion. To the author's knowledge the potential for fretting fatigue as a result of this vibration is not widely considered in the literature.

**Slot wedges**

In order to reduce the impact of the electromagnetic forces upon the winding arrangement wedges are used to hold firmly the winding arrangement in the slot. The slot wedges are made of an electrical insulant and are held in place by grooves.

**Endwinding bracing**

Form wound stator windings extend beyond the core. The windings are subject to electromagnetic forces and they are prone to vibration. During high transient loading the forces can be very large, and significant deflections are observed. Endwinding bracing is, therefore, very important in order to minimise fatigue loading and fretting.

Form-wound stators, such as those used in modern wind turbine generators, have a large endwinding region. To reduce vibration in the radial direction a stiff ring is laced to the endwindings. In addition, insulating blocks are placed between adjacent coils in

order to reduce vibration in the circumferential direction.

Electrical connections are made between series connected coils in the endwinding region. It is interesting to note that the Enercon E40 wind turbine suffers from high generator failure rates [31]. Though the available data set is small it seems that failure rates have been significantly reduced in the newer Enercon E66 by changing the manufacturing process to eliminate winding connections.

### 4.1.2   Rotor winding construction

DFIGs have a wound cylindrical rotor. The insulation system is similar to the stator windings. Slot wedges are used to counter the high centripetal force exerted on the windings.

Synchronous machine rotors do not usually have strand insulation in the rotor windings. This is because the current flowing in the rotor windings is DC and therefore does not experience the skin effect. The rotor insulation must be able to withstand high centrifugal forces as well as high temperatures which lead to thermal decomposition (described by the Arrhenius relationship) and thermal stresses (arising due to differing thermal expansion coefficients).

The rotor windings for wound pole synchronous machines are formed onto "pole bricks", fabricated from punched electrical steel laminations. The rotor pole bricks carry wire windings insulated in a similar manner to the stator windings.

### 4.1.3   Bearings

In wind turbine generators the rotor is usually supported by two grease lubricated ball bearings incorporated into the machine enclosure. The alignment of the rotor is very important because the air gap in the machine must be small. Furthermore, any eccentricity in the rotor results in unbalanced magnetic pull (UMP) which increases vibration and may lead to premature failure.

| Electrical | Mechanical |
| --- | --- |
| Core insulation failure | Bearing failure |
| Stator winding insulation failure | Rotor mechanical integrity failure |
| Rotor winding insulation failure | Stator mechanical integrity failure |
| Brushgear failure | |
| Slip ring failure | |
| Commutator failure | |

Table 4.2: Known failure modes for rotating electric machinery

| | MOD survey | IEEE large motor survey | Utility applications | Offshore and petrochemical |
| --- | --- | --- | --- | --- |
| Rating | $< 750\ kW$ | $> 150\ kW$ | $> 75\ kW$ | $> 11\ kW$ |
| Type | SCIM | IM | IM | IM |
| Voltage | Low | MV/HV | MV/HV | MV/HV |
| Bearings | 95% | 41% | 41% | 42% |
| Stator | 2% | 37% | 36% | 13% |
| Rotor | 1% | 10% | 9% | 8% |
| Other | 2% | 12% | 14% | 38% |

Table 4.3: Location of failures in four reliability surveys (SCIM - squirrel cage induction machine; IM - induction machine; MV - medium voltage; HV - high voltage) [15, 24–26]

## 4.2   Machine failure modes

The known failure modes of rotating electrical machines are summarised in Table 4.2.

The relative distribution of failures, in rotating electric machines, by subassembly has been the focus of a number of industrial surveys. The findings of these surveys were collated by Tavner *et al.* [15] for comparison, and the data are reproduced in Table 4.3. A recent survey of field data, from the US wind industry, generally shows a similar distribution of failures by component to the low voltage small/medium machines in the data collated by Tavner *et al.*, see Figure 4.4.

The largest of these surveys was that undertaken by the IEEE in 1985. It should be noted that the survey undertaken by the petrochemical industry included parts of the drivetrain, this probably explains the large number of faults classified as 'other'.

It may be seen that there is a contrast between smaller (low voltage) machines, where bearing failures dominate, and larger (higher voltage) machines where the frequency of 'stator-related' failures becomes comparable to that of bearing failures. The EPRI reli-
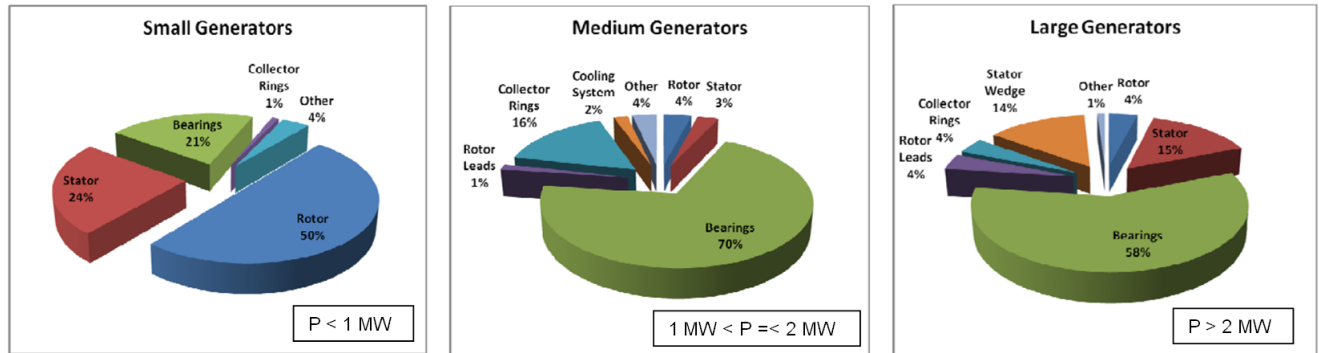
Figure 4.4: Survey of 800 failed wind turbine generators, reproduced from [17]

ability study [24, 25] categorises the data more finely by location than any other study, and in doing so reveals that stator failures are dominated by ground insulation failures (see Table 4.4).

Although some wind turbines have 1 $kV$ or 3.3 $kV$ generators, most wind turbine generators are rated at 690 $V$. Despite significant increases in wind turbine rating over the last few decades, such that wind turbines currently being installed are typically rated between 2 and 5 $MW$, there has been reluctance to move to higher voltages because this would require retraining of O&M staff with significant cost implications. It may be anticipated that this low operating voltage (690 $V$) would imply few stator winding problems. However, with wind turbine generators the case is not so simple. The mission profile and environment are particularly arduous, and furthermore the presence of the power electronic converter to decouple the generator from the grid frequency is known to produce high frequency harmonics in the voltage signal as a consequence of pulse-width-modulation (PWM) [51]. These harmonics increase the electrical stress experienced by the insulation system.

### 4.2.1 Stator windings

Stator winding failure mechanisms can be considered to fall into four categories [16]:

- Thermal

- Electrical

| Component |                    | % Failures |
|-----------|--------------------|------------|
| Bearings  |                    | 41         |
|           | Sleeve             | 16         |
|           | Antifriction       | 8          |
|           | Seals failure      | 6          |
|           | Thrust             | 5          |
|           | Oil leakage        | 3          |
|           | Other              | 3          |
| Stator    |                    | 37         |
|           | Ground insulation  | 23         |
|           | Turn insulation    | 4          |
|           | Bracing            | 3          |
|           | Wedges             | 1          |
|           | Frame              | 1          |
|           | Core               | 1          |
|           | Other              | 4          |
| Rotor     |                    | 10         |
|           | Cage               | 5          |
|           | Shaft              | 2          |
|           | Core               | 1          |
|           | Other              | 2          |

Table 4.4: Failures by component in EPRI study

- Ambient

- Mechanical

It will, however, become apparent that the different failure mechanisms cannot so easily be separated into the above categories. It would be incorrect to consider them as distinct and unrelated. Nevertheless, with due caution the above categories are helpful; each is now considered in turn.

**Thermal**

Insulation systems are only permitted to operate at relatively low temperatures (see Table 4.1). This is because of two important thermal ageing mechanisms:

1. Oxidation of insulation

2. Thermal stress

The first of these, oxidation of the insulation, is encouraged by high temperatures. This oxidation leads to increased brittleness and tends to result in delamination of the groundwall insulation. This can be approximated quite well as an Arrhenius rate reaction. The life of the insulation, $L$, is given by

$$L = Ae^{B/T} \tag{4.1}$$

where $A$ and $B$ are constants and $T$ is the temperature in Kelvin [16].

When the temperature of most materials is raised they expand, conversely when cooled they contract. This is the phenomenon which gives rise to the second thermal ageing mechanism.

Over a wide range of temperatures it has been demonstrated that the change in size is proportional to the temperature change [52]. Under free expansion or contraction no stresses are developed.

However, non-uniform changes in temperature are likely to result in different rates of expansion or contraction throughout a homogeneous body. Because of the mutual restraints different parts of a body place upon each other these differing rates of expansion and/or contraction induce thermal stresses to enforce bodily continuity. Similarly, the rigid fixing of dissimilar materials and external restraints both prevent expansion in an elevated temperature field, causing thermal stresses to be developed [52]. Therefore, assuming that no plastic strains are developed, the thermoelastic strain state, $\{\epsilon\}$, is the sum of two parts; one part comes from stresses arising from mechanical loads and the other derives from free thermal expansion, i.e.

$$\{\epsilon\} = \{\alpha\}\Delta T + \{\epsilon^e\} \tag{4.2}$$

where $\alpha$ is the coefficient of thermal expansion, $\Delta T$ is the temperature difference, $\{\epsilon^e\}$ is the elastic strain vector arising from mechanical loads.

**Electrical**

Electrical stress is generally not considered to be very important in machines rated below 1 $kV$. The dielectric strength of the insulation materials used in electrical machine winding arrangements is very high, typically in the range of 100 $kV/mm$ to 1 $MV/mm$ [16]. This is greater than anything the insulation would be likely to experience. This would suggest that electrical stress should pose no threat to the integrity of the winding system. However the presence of air pockets in the winding arrangement is a source of vulnerability to electrical stress. Figure 4.5 shows, in exaggerated form, the presence of an air pocket within the insulation system.

Gases typically have a dielectric strength of approximately 3 $kV/mm$. Electrons are torn from gaseous molecules which may be seen as sparking. This scorches the surface encouraging void growth and increasing the surface roughness of the insulation. This is known as partial discharge (PD); discharge is not complete, the insulation itself is not broken down by the electric stress, only the air pockets within the insulation system. This may be understood by reference to the electric circuit shown in Figure 4.6 where the insulation and air pocket are acting as capacitances in series. Repeated PD can eventually lead to failure of the winding insulation [16].

Wind turbine generators operate at the relatively low voltage of 690 $V$, therefore it may reasonably be expected that electrical stresses are unimportant. However, the situation is not quite so simple. To enable variable speed operation power electronic converters operating pulse width modulation (PWM) are used to interface with the grid. The very high slew rate ($dV/dt$) of the switching has been shown to result in significant transient voltage spikes in the generator. The use of power electronic converters operating PWM has been found to lead to partial discharge even in low voltage machines. This is an area of current interest in the literature [53], [54].

**Ambient**

Winding insulation systems can suffer damage as a consequence of their environment. Important factors are:

- Moisture

- Oil

- Aggressive chemicals, such as salt sea water

- Wear particles (for example, from brushgear)

- Dirt and debris entering from the external environment via ducts.

When moisture or dust are present on the insulation surface a phenomenon known as surface tracking may occur. Surface tracking occurs because the surface contaminant, which is never uniformly distributed, is conductive. The region of the surface with the highest resistivity is dried by the surface currents, which increases the resistivity yet further until a dry band is formed over which most of the surface voltage is developed. This can lead to decomposition of the air near to the track which, similarly to PD, scorches the insulation surface. This has been known to cause insulation failure at electrical stresses as low as 0.02-0.04 $kV/mm$ [15].

**Mechanical**

The rotor winding system is subject to centripetal force. In addition, the stator and rotor windings have significant applied electromagnetic forces. In 1931 Calvert [55] showed that the radial force acting on a coil in a slot is:

$$F = \frac{kI^2}{d} \tag{4.3}$$

where $I$ is the rms current through the conductor, $d$ is the width of the stator slot in metres, and $k$ is a constant.

So with an alternating current expressed by:

$$I = A\sin(\omega t) \tag{4.4}$$

where $\omega$ is the electrical frequency in radians per second, $t$ is time in seconds, and $A$ is the amplitude in Amps.

The force is found to be:

$$F = \frac{kA^2(1 - \cos(2\omega t))}{2d} \tag{4.5}$$

There are two important observations to make regarding Equation (4.5):

- The force is the superposition of a constant and an oscillating component

- The oscillating component of the force has a very high frequency, twice the electrical frequency, in the order of 60 to 120 $Hz$.

Calvert also considered the circumferential forces on the conductors. Though not insignificant, these were found to be approximately 10 % of the radial force.

It should be noted that the force experienced is proportional to the square of the current. During startup of induction generators there is a very large transient inrush current that may typically be five times the normal operating current. This, therefore, induces very significant transient cyclic loading every startup. Wind turbine generators, unlike industrial machinery in many other sectors, will experience startup often due to variation in the wind.

Equation (4.5) assumes a sinusoidal current with a constant amplitude and frequency. The case for a wind turbine generator will be much more complex. The frequency will vary, because of the implementation of a power electronic converter, and the amplitude will vary as a consequence of turbulence in the wind (see van der Hoven's spectrum, Figure 4.8) [56].

Significantly, the fatigue potential of these transients is not usually considered by manufacturers, rather it is ensured that the system can withstand one large transient load [16].

**Fatigue life predictions of windings**

The analyst attempting to predict the fatigue life of windings faces many difficulties as the problem is very complex. There are multiple ageing mechanisms with non-linear interactions. In addition, unpredictable transient loading events, such as lightning strikes, may
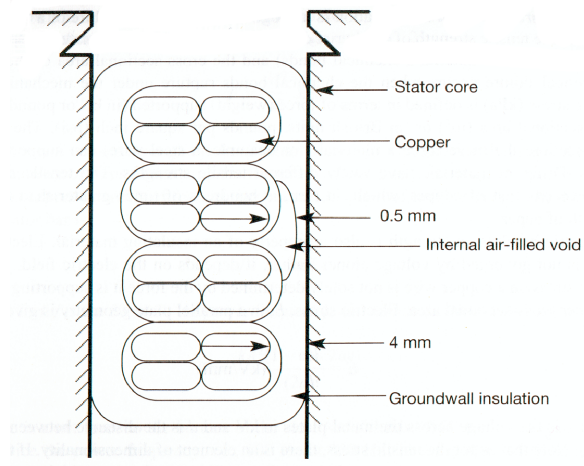
Figure 4.5: Partial discharge mechanism, reproduced from [16]
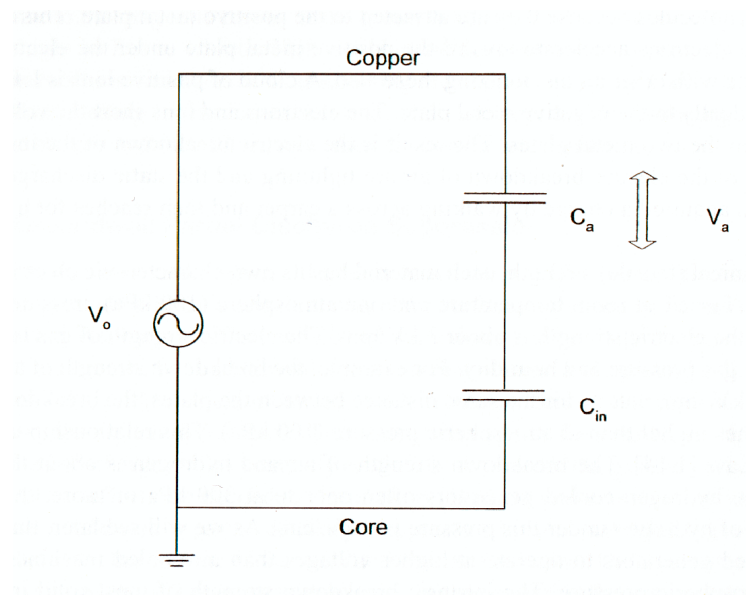


Figure 4.6: Partial discharge circuit, reproduced from [16]

combine with the ageing mechanisms outlined above to bring about failure. Fatigue may weaken the system, but the failure is often only brought about when some unpredictable transient load occurs.

Therefore accelerated ageing tests are normally used by industry to compare a new material or system of materials with a tried and tested benchmark for the purpose of trend analysis, rather than absolute life estimates. Standards have been developed for various tests.

## 4.2.2   Rolling element bearings

Bearing failures are important. Failure surveys suggest that they may be the dominant source of failures in wind turbine generators. There is a combination of factors which creates a demanding operating condition for bearings in the drivetrain of a wind turbine.

The purpose of bearings is to allow constrained relative motion between loaded surfaces. Bearings are, therefore, inherently vulnerable to fatigue and wear mechanisms. In fact the often quoted $L_{10}$ life of a rolling element bearing, defined as the time in operation after which 10 % of bearings would be expected to have failed, is calculated on the predicate that rolling element bearings will fail due to rolling contact fatigue [57].

Because of the ubiquitous nature of bearings and their contribution to machine failure there is a considerable volume of literature dedicated to improving the understanding of bearing loading. Historically, this took the form of experimental work and analytical Hertzian contact models [58]. More recently, significant advances in computing power have made possible advanced numerical modelling of bearings [59–64]. Bearings are not easily modelled using finite element (FE) ,or other numerical methods, as the point contact still proves problematic. In addition, the influence of the lubricant cannot be neglected, and so it becomes necessary to couple FE models with computational fluid dynamic (CFD) models.

An important observation with regard to bearing failure is that there is an undesirable positive feedback effect with bearing deterioration in rotating electrical machines. The deterioration of bearing contact surfaces leads to increased bearing vibration and higher

temperature (these phenomena are used for condition monitoring of bearings [15, 20]), both of which accelerate the rate of deterioration. In addition, bearing deterioration can lead to rotor eccentricity, which in turn results in UMP. Unfortunately, this places more load on the bearings, thereby aggravating the problem.

**Bearing currents**

It has been known for many years that currents flowing through the bearing are a source of bearing failure in rotating electrical machines. High voltages arise due to the capactive effect of the lubricant; eventually discharge may occur which leads to erosion damage known as electrostatic discharge machining (EDM) which can advance the onset of fatigue failure. Historically bearing currents were caused by electrostatic charging and magnetic flux asymmetries [18]. The first of these mechanisms, electrostatic charging, is due to friction which leads to a build up of charge, and therefore a DC voltage along the shaft, followed by discharge through the bearings. Magnetic flux asymmetries, on the other hand, lead to an AC voltage along the shaft at frequencies of the same order as the electrical supply frequency (under $100 \ Hz$). To prevent such bearing currents it is common practice to fit an insulated bearing on the nondrive end in order to break the circuit.

With the advent of widespread adoption of power electronic converters in wind turbine architectures (see Section 2.1) another source of bearing currents became important. The three phase electrical system should, ideally, be balanced with the neutral point at zero potential. However, the use of PWM in power electronic converters means that perfect instantaneous balance between the phases is not possible. This results in a common-mode voltage (sometimes called a zero sequence voltage) with a frequency equal to that of the switching frequency of the power electronics (typically around 10 kHz). Crucially, harmonics in the frequency range $50 \ kHz$ to $5 \ MHz$ are excited, and these are thought to be very damaging [65]. The currents arising from these high frequency voltage pulses are often termed '$dV/dt$ currents'.

Bearing currents cause damage to the surface of the bearing races by delivering energy to the contact area. Because the contact area is small, the energy density delivered by

| Bearing current Regime | Accumulated Energy ($kJ$) | Mean Power ($W$) | Peak Power ($W$) |
|---|---|---|---|
| Without (WO) | 0 | - | - |
| DC : 3 $A$ continuous (DC) | 233 | 2.7 | 2.7 |
| AC: 3 $A$ (rms) at 50 $Hz$ (AC) | 181 | 2.1 | 3.5 |
| Pulse 1: 1.5 A peak (10 $kHz$) (HFPC_1) | 0.778 | 0.009 | 8 |
| Pulse 2: 20 A peak (10 $kHz$) (HFPC_2) | 58 | 0.68 | 50 |

Table 4.5: Bearing current regimes applied by Zika *et al.* in [18]

the bearing currents can be quite high. In a study undertaken by Zika *et al.* the effects of the different types of bearing currents were considered [18]. In the study five bearing current regimes were applied to a thrust ball bearing (type 51305), see Table 4.5.

Bearing housing vibration was monitored using a piezoelectric accelerometer. The root-mean-square of the acceleration signals in the time domain were normalised with respect to their initial values to allow for comparison. The findings of the study are shown in Figure 4.7.
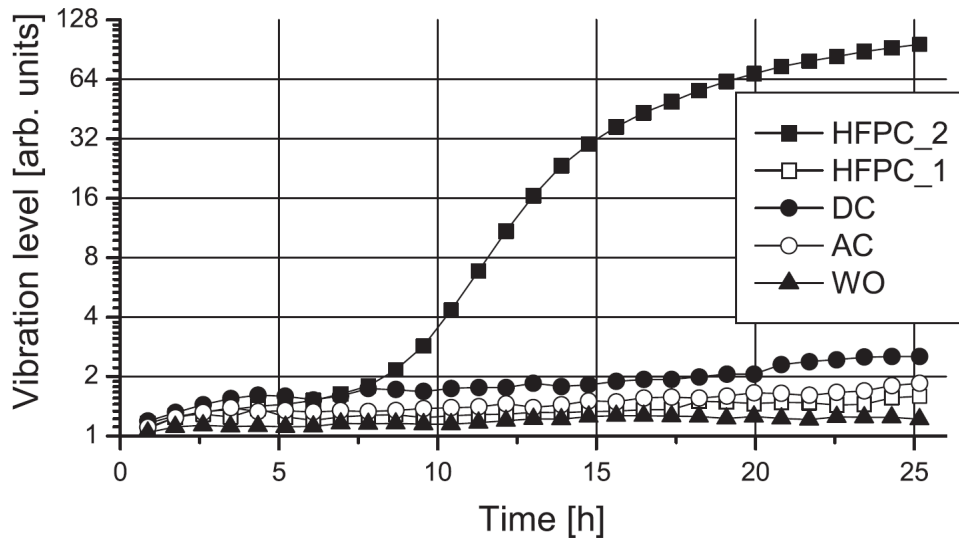


Figure 4.7: Bearing vibration in the time domain under different electrical stresses, reproduced from [18]

The following observations may be made in relation to Figure 4.7:

- After approximately 7 hours the bearing under the high frequency pulsed electrical stress regime, with a 20 A peak (Pulse 2), suffered an irreversible increase in vibration.

- Vibration levels under the 'Pulse 2' regime were considerably higher than any other test regime. This is interesting because the total energy delivered under this regime was only 25 % of that delivered under the DC regime, and 32 % of that delivered under the AC regime.

- The electrical stress regime which suffered the second greatest bearing vibration was the DC case. It can be seen that under DC electrical stress the bearing vibration increased steadily throughout the test duration.

- As expected, the bearing vibration is lowest for the case without any electrical stress.

This work indicates that the high frequency pulsed bearing currents caused by PWM operation of power electronic converters is particularly harmful to bearings. A variety of approaches have been suggested to mitigate bearing currents including [66], [67]:

- Insulated non-drive end bearing to prevent circulating currents.

- Shaft grounding - to provide an alternative path for the current rather than through the bearings.

- Insulated coupling between the machine and the encoder.

- Electrostatic shielding.

- Conductive lubricants - the capacitive nature of the bearings is largely derived from the lubricant. Therefore, by the addition of conductive particles in the lubricant a low impedance path can be provided thus preventing damaging discharges, The disadvantages are that this only seems to be effective for a short time, and that it increases abrasion.

- Ceramic bearings.

- Constrained power electronic converter PWM strategy in order to reduce the common mode voltage [68].

There is disagreement in the literature as to the importance of bearing currents. There is growing interest in the impact that power electronic converters operating PWM have upon bearing health. It has been stated that 30% of motor failures are attributable to bearing currents [69]. However, Drury argues that bearing failure to due electrical stress is relatively rare with bearing failures dominated by mechanical reasons [65]. In Chapter 8 research concerning the effect of bearing currents in wind turbine generators is presented.

**Rolling Element Skidding**

High speed rolling element bearings require loading in order to prevent sliding between the rolling elements and the raceway (i.e. skidding). Skidding occurs when the tractive force between the raceway and the rolling element is insufficient to overcome the cage drag and churning losses [70]. Skidding causes large surface shear stresses resulting in premature failure; it is characterised by surface initiated spalling (rather than the subsurface initiated spalling predicted by classical rolling contact fatigue theory).

**Thermal instability**

Because most materials expand as their temperature increases (see Equation 4.2) changes in temperature can result in a loss of internal clearances. At startup the machine is likely to be cold (in the case of a wind turbine generator, often only just above 0°C). Heat is generated in the bearings but the surrounding housing, with its large 'thermal inertia', is slower to warm up. Therefore, large temperature differences can develop resulting in the loss of operating clearance. This problem has been found in wind turbine gearboxes [71]. To mitigate this problem it may be necessary to locate the bearing in an area with sufficiently flexible housing and/or specify bearings with a large radial clearance. Alternatively, heaters could be fitted to reduce the temperature differential experienced by the bearings.

**Lubrication starvation**

Appropriate lubrication of bearings is critical for their reliable long-term performance. Bearing lubricants serve four main purposes [72]:

- To provide a film to separate the tribological surfaces.

- To protect the surface of the raceways and rolling elements from corrosion.

- To seal the bearing from foreign debris.

- To lower the thermal resistance, thereby minimising the bearing temperature.

Lubrication starvation leads to increased pitting fatigue and scuffing wear[2].

**Contamination**

Contaminant particles can cause abrasive wear thus initiating surface spalling and providing stress concentrations which increase the probability of fatigue failure.

**System Resonance**

Unexpected resonance can lead to severe loading of the bearings resulting in the rapid onset of fatigue failure. The stochastic nature of the wind means that the loading on the shaft is highly variable.

**Misalignment**

Misalignment can cause increased vibration and lead to earlier than expected fatigue failure. Misalignment can be a consequence of improper installation. However, it can also be a consequence of problems with the design.

If a shaft is too flexible this can allow significant displacement under bending loading resulting in alignment problems with bearings. Conversely, if a shaft or coupling is too stiff the system becomes intolerant to misalignment.

In wind turbine drivetrains subassemblies such as the generator and gearbox are usually mounted on rubber elements to reduce the drivetrain noise. However, these rubber elements may degrade with time, suffering creep or fatigue failure, resulting in misalignment between the gearbox and the generator.

Most multi-$MW$ wind turbines have compliant gearbox mounts. Under the application of highly variable off-axis loads on the low speed shaft (caused by the weight of the rotor

---

[2]Scuffing wear is defined by the American Society for Metals as localised damage by solid phase adhesion between surfaces undergoing sliding contact [73]

blades, wind shear, the tower shadow effect and turbulence) the gearbox moves on its compliant mounts. This results in misalignment between the gearbox and the generator which is accommodated by means of a flexible coupling. Nonetheless there is still a reaction force applied to the bearings due to the strain of the flexible coupling. This is investigated through a series of numerical simulations in Chapter 7.

### 4.2.3 Factors particular to wind turbines

Wind turbine generators endure a very arduous mission profile. The nature of the wind means that wind turbines are among the most fatigue loaded systems to be found, with wind turbine blades estimated to suffer $10^8$ cycles over the course of a 20 year life [74].

Undoubtedly the inertia of the turbine rotor has a filtering effect on the wind 'signal', removing some of the high frequency elements in the wind. However, preliminary investigations suggest that this filtering effect is not sufficient to remove all high frequency components associated with turbulence [75]. This rapidly fluctuating load is in contrast with the duty cycles of medium sized rotating electric machines in other industries. The number of startup transients is likely to be higher than in most other applications as a consequence of the diurnal peak in the van der Hoven wind energy spectrum (see Figure 4.8). In addition, the wind has been found to induce significant bending moments on the low speed shaft [76]. In direct-drive wind turbines these bending moments are experienced directly by the generator.

**The environment**

It should be remembered that the operating environment for a wind turbine generator is onerous. Temperatures will often fall as low as 1 °C, or even lower if the nacelle is not fitted with anti-condensation heaters. In addition, turbines are sometimes built in deserts where abrasive sand is whipped up by the wind and may find its way into the nacelle. Because of the height of the towers there is also a threat from lightning strikes. Lightning strikes can cause very severe transient loading of the generator. Again, this is unlike many industrial applications where machines operate in carefully controlled environments.
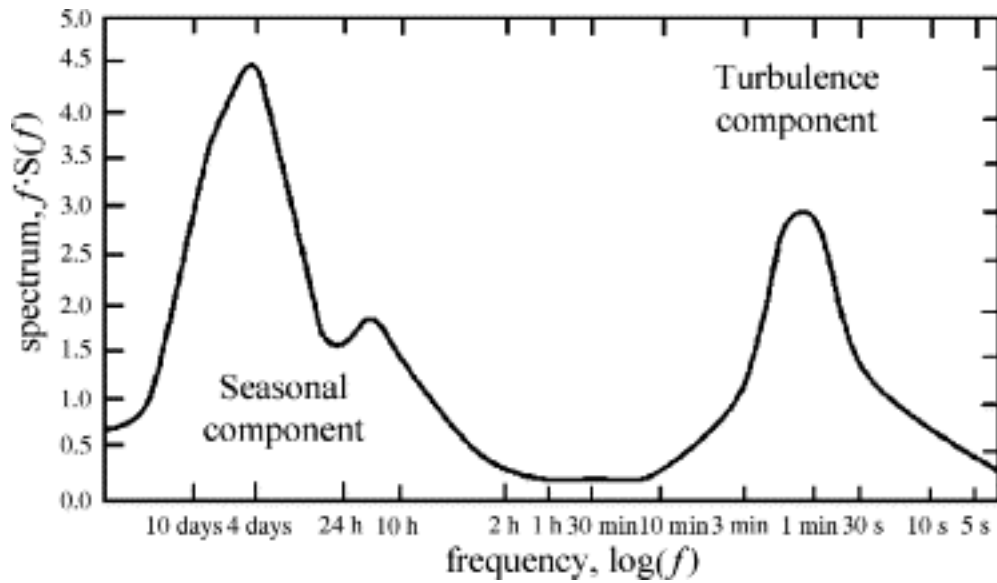
Figure 4.8: Wind induced acceleration fragility curves reproduced from [8]

Of particular relevance to the UK wind energy industry is the offshore environment, where weather is often more extreme and the presence of salt sea spray must be considered. Furthermore, difficulty of access for operation and maintenance means that offshore wind turbines must be able to survive in this extreme environment despite long service intervals (perhaps 12 months or more).

**Nacelle accelerations**

A 2 *MW* wind turbine would typically have a tower height of approximately 100 m. With such tall structures a degree of flexibility is unavoidable. Consequently, the nacelle may experience significant accelerations. In one study a lumped mass MDOF model of a wind turbine was used to estimate the nacelle accelerations experienced under wind loading. In the study it was predicted that under normal operating conditions the nacelle would experience accelerations great enough to damage wind turbine subassemblies. Interestingly, the generator is identified as the subassembly most susceptible to damage from base accelerations [19]. Experience from the field of earthquake engineering suggests that generator functionality can be affected by base accelerations in the range of 5-10 $m/s^2$ [77].

According to Deus-Osorio and Basu [19] the nacelle is very likely to experience accel-

erations in this range under normal operating conditions, see Figure 4.9. This study may provide useful input parameters to future computational models of the loading of wind turbine generators.
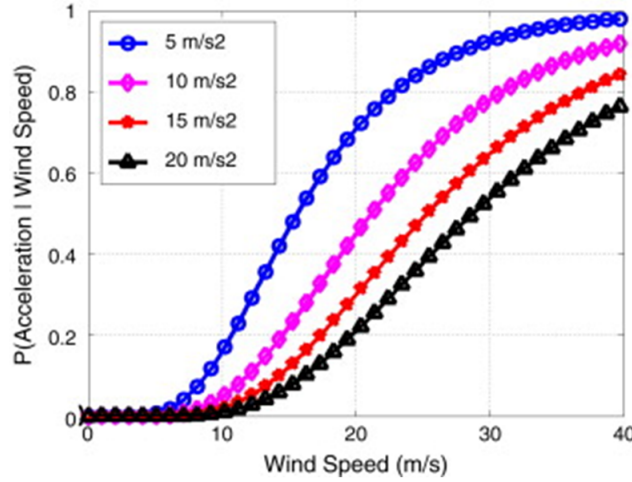


Figure 4.9: Wind induced acceleration fragility curves reproduced from [19]

## 4.3    Conclusions

Wind turbine failure rates are higher than is acceptable for large-scale deployment offshore. Moreover, the generator failure rates compare unfavourably with other industries and it is hypothesised that this is due to the particularly arduous nature of the loading and the environment in which wind turbines operate.

Direct-drive wind turbine architectures are favoured by some manufacturers and it is argued that by elimination of the gearbox the turbine reliability is improved. It has been shown that the situation is not quite so clear-cut, with some evidence presented that direct-drive wind turbines suffer higher generator failures. The reasons for this are not known, however, it is likely to be a combination of factors including the fact that the generators used in these architectures are more complex, the windings are longer, and the manufacture is less standardised. It may also be important that removal of the gearbox is exposing the generator to harsher transient loading due to fluctuation in the wind.

Generator failure modes, locations, and root causes have been explored. The bearings, stator winding arrangement, and sliprings and brushgear have been identified as the

sources of most generator failures.

The endwinding region and the ground insulation have been identified as crucial areas of the winding arrangement. It has been noted that the voids act, not only as geometric stress raisers, but also as potential sources of PD. The ground insulation has been found to suffer delamination under thermal loading, which can ultimately lead to serious turn-to-ground faults.

Bearing failure is also a complex matter with thermal instability, inappropriate housing, misalignment, bearing currents, and lubricant starvation all known to be root causes of bearing failure. There is a substantial literature devoted to bearings. Until recently bearing models were almost exclusively analytical, relying on Hertzian contact mechanical models. Increasingly, numerical analyses are being undertaken with the advances in available computing power. However, such models are complex due to the contact problem and importance of the lubricant fluid mechanics. One important outcome of Hertzian mechanics is that the point of maximum stress under contacting loads is actually subsurface. Thus, cracks initiate subsurface and propagate towards the surface eventually resulting in spalling.

The environment in which wind turbines operate is aggressive. The impact of the environment upon the wind turbine generator does not seem to be widely discussed in the literature. With increased deployment of wind turbines offshore, the impact of salt sea spray may become significant. Although the generator is protected inside the nacelle, the ingress of the salt sea spray may still be possible. If this were to occur the corrosive mechanisms initiated would interact with fatigue, resulting in an undesirable positive feedback mechanism which would hasten the onset of failure.

It has been suggested that an understanding of how the fluctuations in the wind translate into fluctuating load on the generator would be useful [78], and to the author's knowledge a detailed analysis is not currently provided in the literature. Such an understanding may form the basis of the development of new testing regimes for wind turbine generator manufacturers, as testing regimes currently embodied in standards are, arguably, not

appropriate for wind turbine generators given the stochastic nature of the loading.

An increased understanding of the transfer of the load through the drivetrain to the generator could perhaps also be useful for condition monitoring purposes, through, for example, the implementation of online rainflow counting of significant transients.

# Chapter 5

# Influence of the Weather upon Wind Turbine Reliability

## 5.1 Background

The relationship between reliability and availability is more acute in the rapidly growing offshore wind energy industry than conventional generation because the location and difficulties of access mean that failures can result in long downtimes, raising the COE from these sources. This chapter addresses the question: to what extent are WT reliability and availability affected by location and weather? This question is particularly important as the industry prepares to scale up offshore operations.

### 5.1.1 Previous Analysis

A study of WT reliability in Denmark [47] considered the effect of the Wind Energy Index, associated with wind speed, on WT failure rate. The study considered the operation, over 10 years, of a large mixed population of WTs distributed throughout Denmark, using data from the Windstats Newsletter (WSDK), and average wind speed data for the whole of Denmark. The statistical analyses presented in [47] were motivated by the observation that WT failure rates from Windstats in both Denmark (WSDK) and Germany (WSD) increased during identical months of bad winter weather [49] when weather conditions

over north western Europe were similar. The study clearly showed that high wind speeds reduced WT reliability; the cross-correlation between the wind speed and the failures was about 43% with a confidence level of 95%. The strength of the study was that it included a large number of turbines considered over an extensive period and, consequently, included a large number of failures. The weakness of the study was that it included many different designs of turbines and considered a monthly average wind speed over the whole of Denmark, thereby concealing potentially significant data.

### 5.1.2   This Analysis

New analysis presented in this chapter attempts to address the limitations of [47]. The failure rate and downtime data selected for this new study of the effect of weather on WTs have been taken from WMEP [33] which is managed by Fraunhofer IWES under the German publicly funded programme '250 $MW$ Wind' during a 17 year period. The WMEP programme collected 193,000 monthly operation reports and 64,000 maintenance and repair reports from 1500 WTs that have been collated and analysed, covering approximately 15,000 turbine years. It is considered to be the most thorough collection of publicly available onshore WT reliability data to date.

The same approach used by Tavner *et al.* in [47] is used here but the dataset includes only one particular WT type located in three different wind farms with potentially differing climatic and operating conditions. This approach attempts to build upon the work presented in [47].

## 5.2   Wind Turbines, Locations and Data

### 5.2.1   The Locations

In [47] the dataset included turbines located throughout Denmark. The geographic dispersion of the WTs meant that, at times, they will have experienced significantly different ambient conditions as weather fronts moved across Denmark. However, theses differences were neglected by averaging across the whole country. Despite this, a strong

cross-correlation between the weather data and the failure data was identified, but it was considered that a more geographically focussed study would be of value. Consequently, in this new analysis, three locations were identified, which complied with the twin criteria of having significant populations of the same WT type, and different geographic characteristics. Wind farms at the following locations were identified (see Figure 1):

- Fehmarn, located on a small island in the Baltic Sea, off the coast of Schleswig Holstein, Germany (N 54.46595, E 11.25536);

- Krummhörn, located on the North Sea Coast in Lower Saxony, Germany. (N 53.43858, E 7.048416);

- Ormont, located inland in the highlands in Rhineland Palatinate, Germany. (N 50.32546, E 6.44365).

## 5.2.2   Wind Turbine Failure Data

Each of the chosen locations operate two similar WT models, the Enercon E32/33, details given in Table 5.1, which were the last geared drive WTs manufactured by the company before it moved to manufacturing direct drive WTs. Although Enercon E32/33 WTs are of dated design, their technology is still relevant, particularly as they incorporate fully rated power electronic converters, a technology common in larger WTs. Moreover, high-quality meteorological data were available for the wind farms concerned (see Section 3.3). A comparative summary of the the WMEP and WSDK data are presented in Table 5.2 along with WMEP data used in the analysis here presented. The WMEP and WSDK surveys are very large but in order to isolate the variables of interest, it was necessary to consider only a subset of the WMEP data. Nevertheless, the data analysed here comprised 202 turbine years and 586 logged failures.

## 5.2.3   Weather Data

Weather data for these locations were available from two sources:

- Deutscher Wetterdienst (DWD) meteorological station data giving wind speed, temperature and humidity at 10 min intervals. The locations of the stations were within

|                      | E32/300                              | E33/300                              |
|----------------------|--------------------------------------|--------------------------------------|
| Rated power ($kW$)   | 300                                  | 330                                  |
| Rotor diameter ($m$) | 30                                   | 33                                   |
| Generator            | Synchronous (wound rotor)            | Synchronous (wound rotor)            |
| Drive                | Geared                               | Geared                               |
| Power control        | Variable speed, hydraulic blade pitch | Variable speed, hydraulic blade pitch |
| Power converter      | Fully rated                          | Fully rated                          |
| Production dates     | 1988-1993                            | 1988-1993                            |

Table 5.1: Enercon E32/E33 WT details [27]
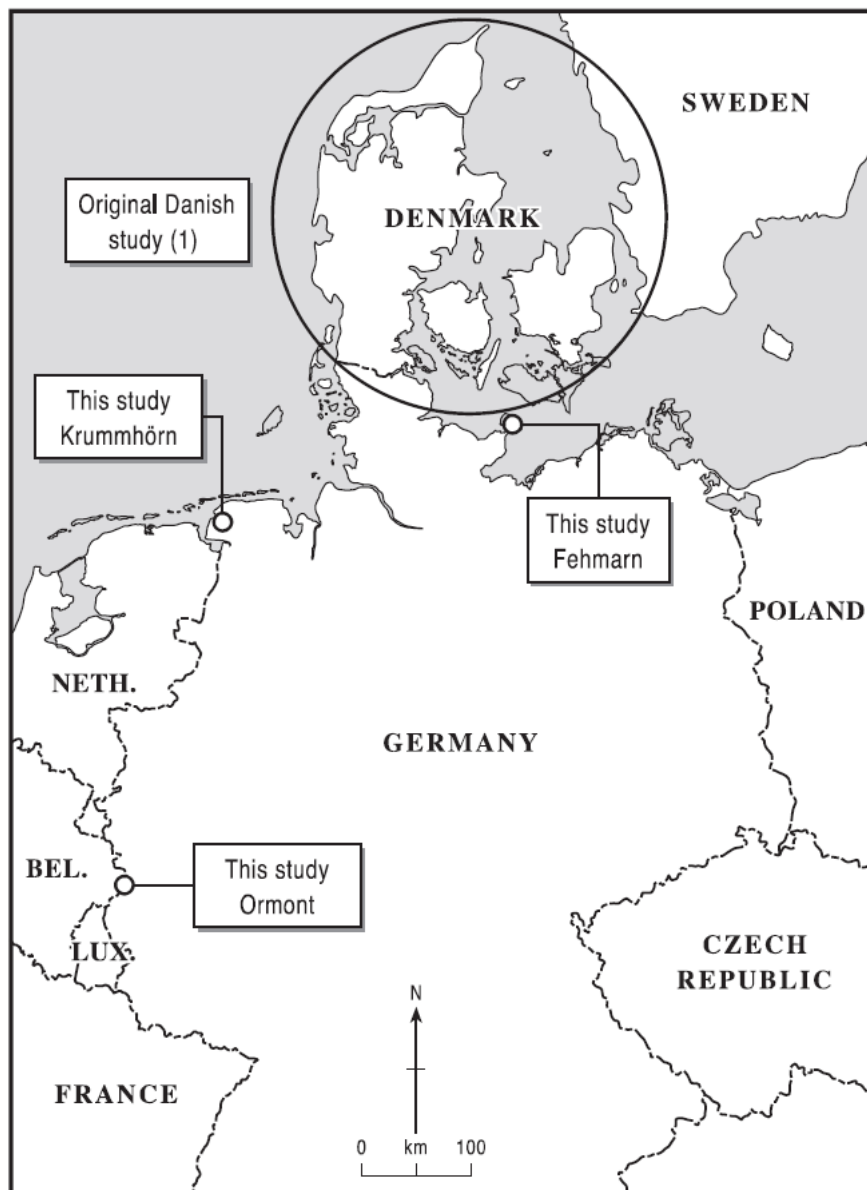


Figure 5.1: The three locations for this study

| | No. of WTs | No. of failures | Failures in cont. time series | Date wind farms est. | Years of available data | Total turbine-years studied |
|---|---|---|---|---|---|---|
| WSDK survey | 851-2345 | 13108 | - | 1994- | 10 | 15980 |
| WMEP survey | 1500 | 64000 | - | 1990- | 17 | 15400 |
| E32/33 WTs in WMEP survey | 136 | 5960 | - | 1990-1993 | 17 | 1357 |
| Fehmaarn (Ostzee) E32/33s | 9 | 252 | 199 | 1991 | 7.7 | 70 |
| Krummhörn (Nordzee) E32/33s | 16 | 987 | 339 | 1990-1992 | 6.5 | 104 |
| Ormont (German Highlands) E32/33s | 7 | 170 | 48 | 1991/1993 | 4.0 | 28 |

Table 5.2: Data details for the three wind farm locations in context with the WMEP and WSDK survey

    30 *km* of each of the three locations;

- Institut für solare Energieversorgungstechnik (ISET, now Fraunhofer Institute of Wind Energy Systems (IWES)) meteorological mast data giving maximum, minimum and mean wind speeds and wind speed standard deviation, temperature and humidity at 10 min intervals located at the Fehmarn and Ormont locations, but not at the Krummhörn location.

Weather data for Fehmarn and Ormont were taken from the on-site Fraunhofer IWES meteorological mast, and the weather data for Krummhörn were taken from a DWD mast at Emden-Flugplatz, 17 km from the location.

## 5.2.4 Quality of the Data

It has been acknowledged that Enercon E32/33 is a dated technology, but this turbine type has been chosen because of the significant number of Enercon E32/33s in the WMEP dataset, their presence at three disparate locations and because the E32/33s incorporated fully rated power electronic converters a technology relevant to more modern WTs. Thus, the findings of the present investigation should have wider applicability and may inform efforts to improve the reliability of other WT concepts.

## 5.3   Theoretical Basis

### 5.3.1   Cross-correlation

Cross-correlation is a time-domain technique used to measure the extent to which two signals are linearly related. The cross-correlation function of two stationary time-domain signals, $f(t)$ and $g(t)$, is given by

$$R_{fg}(\tau) = \int_{-\infty}^{\infty} f(t)g(t + \tau)\,\mathrm{d}t \tag{5.1}$$

This may be restated as

$$R_{fg}(\tau) = \lim_{T \to \infty} \frac{1}{2T} \int_{-T}^{T} f(t)g(t + \tau)\,\mathrm{d}t \tag{5.2}$$

where $T$ is the period of observation, that is, the signal length, and $\tau$ is the time lag between the signals. For sampled signals, this is written as

$$R_{fg}[m] = \lim_{N \to \infty} \frac{1}{2N+1} \sum_{-N}^{N} f[n]g[n+m] \tag{5.3}$$

where $N$ is the number of data points and $m$ is the lag. Note that in order to interpret this lag, as a time shift, the time series must be uniformly sampled.

The cross-correlation function can now be estimated where the signals $f(t)$ and $g(t)$ are of finite length. For sampled signals, the biased cross-correlation is computed by

$$R_{fg}[m] = \frac{1}{N} \sum_{n=1}^{N-m+1} f[n]g[n+m] \tag{5.4}$$

where the unbiased form is

$$R_{fg}[m] = \frac{1}{N - |m|} \sum_{n=1}^{N-m+1} f[n]g[n+m] \tag{5.5}$$

where $m = 1, \ldots, M + 1$.

Unbiased cross-correlation counters the reduction in cross-correlation coefficient as the

lag increases because of the reduced overlap of a pair of finite signal series being slid past one another. However, unbiased cross-correlation suffers from unbounded variance and may become unstable.

The cross-correlation coefficient is the normalized version of the cross-correlation obtained by setting the lag to zero and dividing by the signal power

$$C[m] = \frac{R_{fg}[m]}{[R_{ff}[0].R_{gg}[0]]^{1/2}} \tag{5.6}$$

so that the cross-correlation coefficient then lies between -1 and +1, where:

- $C = 1$ implies that $f[n]$ and $g[n]$ are perfectly positively correlated;
- $C = -1$ implies that $f[n]$ and $g[n]$ are perfectly negatively correlated;
- $C = 0$ implies that there is no cross-correlation between $f[n]$ and $g[n]$.

## 5.4   Results

Cross-correlations were computed to identify potential links between particular meteorological parameters and WT failures. A summary of the cross-correlation coefficients at zero lag is given in Table 5.3 (Krummhörn has fewer cross-correlation data because there was no on-site ISET meteorological mast). The daily values were aggregated into monthly periods and the cross-correlations were repeated. The data for the maximum wind speed, temperature variation and relative humidity were all taken from the DWD source and the mean wind speed and standard deviation of wind speed data were taken from ISET. The cross correlation plots of maximum wind speed with failures (data aggregated monthly) at the three sites are shown in Figure 5.2.

| Cross-correlation | Cross-correlation coefficent at zero lag | | | | | |
| --- | --- | --- | --- | --- | --- | --- |
| | Fehmarn | | Krummhörn | | Ormont | |
| | Daily Agg. | Monthly Agg. | Daily Agg. | Monthly Agg. | Daily Agg. | Monthly Agg. |
| Max wind speed X Failures | 0.23 | 0.76 | 0.30 | 0.76 | 0.10 | 0.56 |
| Mean wind speed X Failures | 0.22 | 0.74 | - | - | 0.13 | 0.55 |
| Standard deviation of wind speed X Failures | 0.22 | 0.73 | - | - | 0.13 | 0.57 |
| Temperature variation X Failures | 0.20 | 0.68 | 0.26 | 0.76 | 0.13 | 0.56 |
| Humidity X Failures | 0.22 | 0.73 | 0.30 | 0.75 | 0.13 | 0.55 |
| Max wind speed X Standard deviation of wind speed | - | 0.99 | - | - | - | 0.99 |

Table 5.3: Cross-correlation coefficients at zero lag for the three chosen wind farms
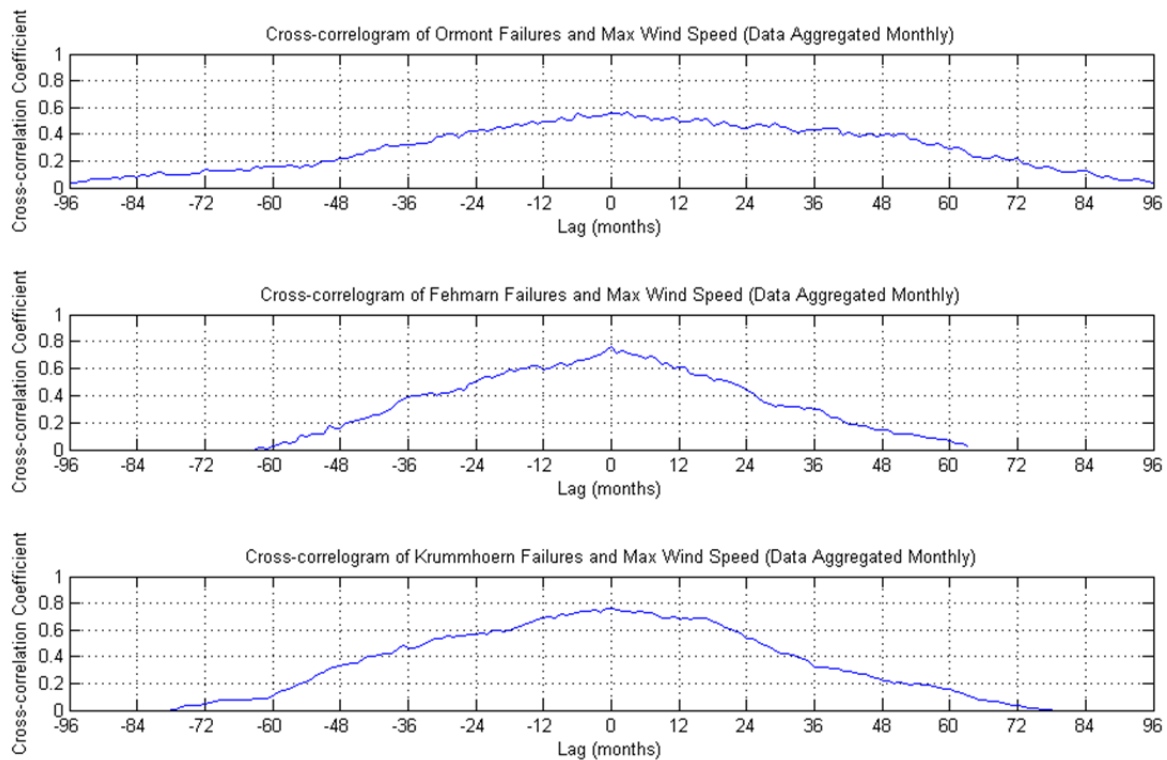


Figure 5.2: Correlograms for the three farms showing a correlation between WT failure and wind speed

## 5.5 Discussion

Whether failures were correlated with maximum wind speed, mean wind speed, standard deviation of wind speed, temperature or humidity the correlograms were found to be very similar. Initially, it was thought that this may be due to the presence of too many nulls in the failure data series. However, cross correlation of the different wind parameters with each other showed that in fact it is because of underlying relationships between the different meteorological parameters.

By comparing the correlograms obtained with the original daily data series, with the more statistically robust correlograms generated with monthy aggregated data, it was seen that the nulls in the failure data acted to mask the strength of the correlation between WT failure and weather.

## 5.6 Conclusions

The main findings were that:

- The failure rate trends for E32/33 type WTs in this study are similar to the failure rate trends obtained from previous WSD, WSDK and WMEP studies, despite the much smaller population of turbines considered in this study.

- Krummhörn, on the North Sea coast of Germany, had the highest average failure rates of all three sites but Fehmarn, on the Baltic Sea coast, had the highest maximum wind speeds.

- The cross-correlation of the data when in daily interval time series showed a weak positive correlation (10-23%) for all three sites. The weakness of the correlation is probably due to sparsity of the data given the small population size.

- There was significant cross-correlation (55-75%) between the failure data and the weather for all three sites when the data were aggregated into monthly quanta. When the data were monthly aggregated a higher cross-correlation coefficient has

been found in this study than in the previous study (40%). It is thought that this may be because the population was not so dispersed (geographically, or technologically) as in the previous study; the effect of this dispersion being to introduce noise.

## 5.7    Recommendations

One of the major limitations of this work was the small sample size. There were, in consequence, relatively few failures in the dataset and therefore many nulls in the 'failure signal'. If the constraints established at the start of this investigation, namely to consider only one turbine type at a number of specific locations, can be retained whilst performing the analysis on a larger population then greater confidence in the conclusions would be possible.

Having demonstrated a statistical correlation between wind speed and WT failure rates the following chapters take a different approach; specific failure modes are investigated using computational models to identify causality rather than merely correlation. But first the theoretical framework which undergirds these numerical analyses is described in Chapter 6.

# Chapter 6

# Theoretical Fundamentals of Bearings

## 6.1  Introduction

Rolling element bearings have been used for millenia; the concept is simple with rolling replacing frictional sliding, the consequence of which is to significantly reduce the energetic effort required. Bearing technology developed rapidly during the industrial revolution, finding an increasing number of applications but also resulting in many tragedies due to the effects of fatigue which were not understood. The last century has seen continuous development in the understanding of tribology.

In this chapter an overview is presented of the fundamental tribology and bearing theory underlying this thesis. It begins with an overview of the relevant metal fatigue theory before introducing the basis of contact mechanics. These two engineering sciences are the foundation of rolling contact fatigue life calculation, which is discussed before finally outlining elastohydrodynamic lubrication (EHL) and introducing the important Hamrock-Dowson equation which is used to compute the bearing minimum film thickness.

## 6.2   Fatigue of Metals

Many mechanical components fail under stresses below their ultimate strength due to fatigue, so called because early theories posited that the metal became crystalline under the cyclic loading and, therefore, 'tired'. In fact fatigue failure is a process of crack initiation, at a microscopic localised defect, followed by growth (the subject of fracture mechanics). Although it is often convenient to consider materials as continua with homogeneous macro properties, in fact at microscopic level two apparently identical samples are in fact very different crystalline structures with randomly oriented slip planes and randomly distributed dislocations, inclusions and microcracks. This microscopic variation, when viewed at a macroscopic level, means that fatigue is a statistical phenomenon. This will be important in the calculation of bearing fatigue lives in Section 6.4.

For high-cycle fatigue, i.e. where the stress cycles remain within the region of elasticity, material fatigue characteristics may be represented by means of an $S$-$N$ curve, see Figure 6.1. If a single graph is plotted it is typically the 50% survival probability contour and it indicates the number of cycles, $N$, that may be survived at stress amplitude $S$. In bearing fatigue life calculation it is common to refer to the $L_{10}$ fatigue life which is the number of load cycles that 90% of the population of bearings would be expected to survive. For low-cycle fatigue, typically where the number of cycles to failure is less than $10^5$, plasticity dominates and the $S$-$N$ curve is no longer appropriate; instead it is necessary to treat the problem using the strain-life ($\epsilon$-$N$) approach. This will not, however, be discussed any further here because the number of stress cycles experienced by high speed rolling element bearings, used in wind turbine generators, is in the region of high-cycle fatigue.

## 6.3   Hertzian Contact Mechanics

In 1881 Hertz published his theory of elastic contact which has been of lasting significance and is still the basis of much work in the field of contact mechanics today. Hertz theory of contacting mechanics applies in general to two surfaces where:

- The radii of curvature of the contacting bodies are large compared with the radius
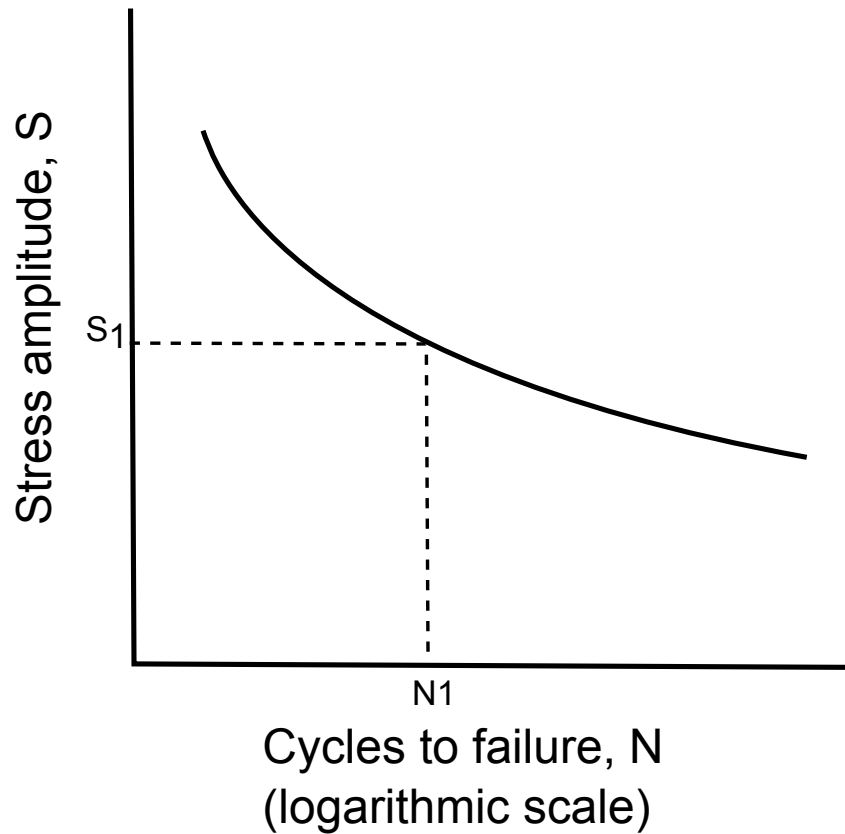
Figure 6.1: A typical S−N curve (for stress level, $S_1$ the number of cycles to failure is $N_1$)

    of the contact area

- The contact is frictionless

- The contacting surfaces are continuous and nonconforming.

Although the assumption of completely frictionless contact is never true, Hertzian contact theory gives a close approximation of the contact area and maximal shear stress depth in rolling element bearings so long as the bearing is appropriately lubricated and the other assumptions remain valid.

If the raceway and the ball are considered to be in non-conforming contact, and the surface roughnesses are neglected, Hertzian theory of elastic contact may be used to approximate bearing contact area, $A$. In Chapter 9 it is described how this is used to model EDM in wind turbine generator bearings.

First the relative radius of curvature, $R$, is calculated

$$R = \frac{R_1 R_2}{R_1 + R_2} \tag{6.1}$$

where $R_1$ is the radius of the ball, $R_2$ is the radius of the raceway. The raceway is modelled as a flat surface, so for the purposes of computation it is set to a very large number $(10^9 R_1)$ and a convergence plot is used to confirm that this satisfies the present requirements.

According to the Hertz theory of elastic point contact the radius of the contact circle, $a$, is given by

$$a = \left( \frac{3PR}{4E'} \right)^{1/3} \tag{6.2}$$

where $P$ is the applied load, and $E'$ is defined by

$$E' = \frac{1}{((1 - \nu_1^2)/E_1) + ((1 - \nu_2^2)/E_2)} \tag{6.3}$$

with $E$ and $\nu$ being, respectively, the Young's modulus and Poisson's ratio of the two contacting materials.

## 6.4   Rolling Contact Fatigue of Bearings

Analytical treatments of rolling contact fatigue (RCF) are of statistical nature. On a micro-scale the crystalline structure of the alloys used in bearings is not homogenous. There is a distribution of the material properties throughout the alloy. The cyclic loading over a region of the material therefore yields crack growth initiating from some local weak point. RCF lives are, consequently, highly variable with apparently identical specimens under controlled loading experiencing widely varying failure times.

Present day RCF lifetime equations may be considered to have their genesis in the work of Lundberg and Palmgren in the 1940s.

If the stressed region of material is discretised in $m$ similar volumes and $M_i$ is allowed to represent the probability of failure, with $S_i$ the probability of survival, for the $ith$ element

then

$$S = 1 - M = \prod_{i=1}^{m}(1 - M_i) \tag{6.4}$$

The probability of failure in the stressed volume may be represented by [79]

$$M = 1 - e^{-\int_V f(x)dv} \tag{6.5}$$

Therefore

$$S = 1 - \left(1 - e^{-\int_V f(x)dv}\right) \tag{6.6}$$

Taking the natural logarithm

$$\ln(S) = -\int_V f(x)dv \tag{6.7}$$

which can be rearranged to give

$$\ln\left(\frac{1}{S}\right) = \int_V f(x)dv \tag{6.8}$$

The stressed volume, $V$, may be defined as

$$V = D_y Z_0 l_v \tag{6.9}$$

where $D_y$ is the contact ellipse diameter (along the y axis), $Z_0$ is the depth to the maximum shear stress and $l_v$ is the axial length of the stressed volume.

A power function of shear stress, $\tau_0$, the number of stress cycles, $J$, and the depth of the maximum shear stress, $Z_0$, was chosen by Lundberg and Palmgren to represent the stress function

$$f(x) = \tau_0^{c_1} J^{c_2}/Z_0^{c_3} \tag{6.10}$$

This gives the well known Lundberg-Palmgren equation

$$\ln\left(\frac{1}{S}\right) = \frac{\tau_0^{c_1} J^{c_2} D_y l_v}{Z_0^{c_3-1}} \tag{6.11}$$

Thus, noting that for given bearing and loading $\tau_0$, $D_y$, $l_v$ and $Z_0$ are constant, it may be observed that

$$\ln\left(\frac{1}{S}\right) \propto J^{c_2} \tag{6.12}$$

Then if

$$J = \frac{L}{A} \tag{6.13}$$

where $L$ is life and $A$ is a constant, equation 6.12 may be written

$$\ln\ln\left(\frac{1}{S}\right) = c_2 \ln\left(\frac{L}{A}\right) \tag{6.14}$$

Thus a probabilistic relationship between survival probability and life, which may be recognised as the Weibull distribution, has been arrived at. It is this Weibull relationship, founded upon the work of Lundberg and Palmgren in the 1940s, which remains the basis of $L_{10}$ bearing life calculations (i.e. where $S = 0.9$) using the bearing dynamic load capacity, $C$, and the equivalent bearing load, $F_e$, with

$$L = \frac{C}{F_e}^m \tag{6.15}$$

where the bearing exponent, $m$, is 3 for cylindrical rolling element bearings and (10/3) for spherical rolling element bearings.

### 6.4.1   ISO 281:2007

The theory outlined above is the basis of the ISO 281:2007 bearing fatigue life calculations. The fatigue lives referred to in the analysis of gearbox-generator misalignment, presented in the next chapter, were computed using ISO 281:2007 so an brief overview of

the standard is given here.

### Radial ball bearing ratings

The basic dynamic radial load rating, $C_r$, (in Newtons) for a radial ball bearing is

$$C_r = b_m f_c (i cos(\alpha)^{0.7} Z^{2/3} D_w^{1.8} \tag{6.16}$$

if $D_w \leq 25.44mm$ and

$$C_r = 3.647 b_m f_c (i cos(\alpha)^{0.7} Z^{2/3} D_w^{1.4} \tag{6.17}$$

if $D_w > 25.44mm$, where $b_m$ is the rating factor (dimensionless parameter, varies with bearing type and design), $D_w$ is the nominal ball diameter ($mm$), $f_c$ is a factor which depends on the bearing geometry (dimensionless), $i$ is the number of rows of rolling elements, $Z$ is the number of rolling elements per row and $\alpha$ is the nominal contact angle (degrees).

The dynamic equivalent radial load, $P_r$, is defined by the empirical relationship

$$P_r = XF_r + YF_a \tag{6.18}$$

where $F_r$ and $F_a$ are the actual radial and axial bearing loads ($N$) and $X$ and $Y$ are dimensionless factors the values of which are dependent upon the bearing type and geometry.

### Radial roller bearing ratings

For radial roller bearings the approach is the same, but the equations are modified for line contact. The basic dynamic radial load rating becomes

$$C_r = b_m f_c (i L_{we} cos(\alpha))^{7/9} Z^{3/4} D_w^{29/27} \tag{6.19}$$

where the new parameter, $L_{we}$, is the effective roller length ($mm$) which is the theoretical maximum length of the contact between a roller and whichever raceway has the

shortest contact. The dynamic equivalent radial load is calculated according to Equation 6.18 unless $\alpha = 0$ in which case it becomes

$$P_r = F_r \tag{6.20}$$

**Calculating the fatigue life**

The $L_{10}$ life, defined as the number of revolutions (in millions) that 90 % of bearings would survive before the first manifestation of fatigue damage in one of the raceways or rolling elements, is defined as

$$L_{10} = a_{iso} \left( \frac{C_r}{P_r} \right)^e \tag{6.21}$$

where $e$ is a dimensionless exponent which is a function of bearing type; $e = 3$ for ball bearings and $e = 10/3$ for roller bearings. The factor $a_{iso}$ is incorporated as part of the 2007 amendment to ISO 281 to account for the existence of a fatigue load limit thereby yielding more accurate fatigue life calculations at low loads. $a_{iso}$ captures the S-N characteristic of the raceway and rolling element metals so it can be said that it is a function of the fatigue stress limit, $\sigma_u$, and the actual stress, $\sigma$, experienced by the raceway, thus

$$a_{iso} = f \left( \frac{\sigma_u}{\sigma} \right) \tag{6.22}$$

For practical purposes it is easier to equate this to the loads on the bearing by introducing the fatigue load limit, $C_u$, so that

$$a_{iso} = f \left( \frac{C_u}{P} \right) \tag{6.23}$$

where $C_u$ is defined as the load at which the fatigue stress limit is just reached at the most heavily loaded raceway contact. The value of $C_u$ is a function of the internal geometry of the bearing, the manufacturing quality and the fatigue limit of the raceway

steel. ISO 281:2007 should be consulted for a full account of the bearing life calculations including more details on the calculation of $a_{iso}$.

## 6.5 Rolling Element Bearing Kinematics

An understanding of the principal geometry of the bearing, see Figure 6.2, yields the possibility of kinematic analysis of the bearings. The basic equations are outlined below.
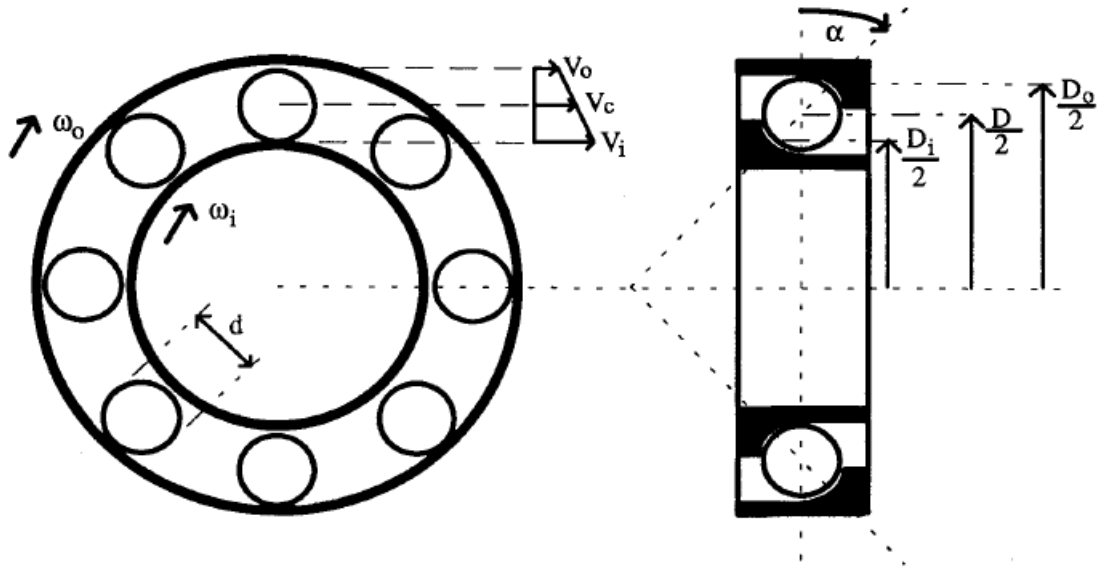


Figure 6.2: Schematic diagram of a ball bearing, reproduced from [20]

For rolling element bearings, typically used in wind turbines, from the geometry if a constant operating contact angle, $\alpha$, is assumed then the pitch circle diameter is approximately

$$D = \frac{D_i + D_o}{2} \tag{6.24}$$

where $D_i$ and $D_o$ are the outer and inner raceway diameters respectively. If the rolling element diameter is given by $d$ then it can be stated that

$$D_i = D - d\cos(\alpha)$$
$$D_o = D + d\cos(\alpha) \tag{6.25}$$

In wind turbine drivetrains the outer raceway is typically fixed ($V_o = 0$) and the inner

raceway velocity is given by

$$V_i = \omega_i \frac{D_i}{2} \tag{6.26}$$

Assuming no slip, the cage velocity is then

$$V_c = \frac{\omega_i(D - dcos(\alpha))}{4} \tag{6.27}$$

or, more usefully, as angular speed (in $Hz$)

$$f_{cage} = \frac{f_i(1 - \frac{d}{D}cos(\alpha))}{2} \tag{6.28}$$

The important ball-pass frequencies may be now be derived. These frequencies find their main application in condition monitoring, where the synchronous impulsive excitation caused by pitting of the tribological elements may be detected to give early warning of the onset of bearing failure. In this thesis they find their use in the simulation of electrostatic discharge machining (EDM) of rolling elements bearings (see Chapter 8).

Beginning with the relative frequency of the rolling elements with respect to the inner and outer raceways,

$$f_{ri} = f_{cage} - f_i \tag{6.29}$$

and

$$f_{ro} = f_o - f_{cage} \tag{6.30}$$

Substituting Equation 6.28, and recalling that $f_c = 0$, for $Z$ rolling elements the inner and outer raceway ball pass frequencies become

$$f_{bpfi} = -Zf_i\frac{(1 + \frac{d}{D}cos(\alpha))}{2} \tag{6.31}$$

and

$$f_{bpfo} = -Zf_i \frac{(1 - \frac{d}{D}cos(\alpha))}{2} \tag{6.32}$$

## 6.6  The Hamrock-Dowson Equation

In order to model the electrical characteristics of the generator ball bearings the film separation in the contact area must be calculated. It was in the mid twentieth century that significant advances were made in tribology which led eventually to the theory of elastohydrodynamic lubrication (EHL). Practical experience indicated that lubricated gears were not usually experiencing metal to metal contact, but the classical theory did not account for this. It became clear that the influence of elasticity of the contact surfaces and, because of the small non-conforming contact area, very high pressure upon the lubricant must be at the root of this newly observed phenomenon. Progress was made by considering these two parameters separately, but it was hampered because the problem was inherently one in which the solid elastic and fluid viscosity effects were coupled. Yet the computational effort to solve this coupled problem was very large, and it was not until 1959 when Dowson and Higginson used an inverse solution approach that a simultaneous solution of the elasticity and Reynolds equations was found . Their approach was to assume a pressure distribution and then, using the Reynolds equation, calculate the film shape required to give this pressure distribution. This was then compared to the film shape computed by elasticity and changes could be made to the assumed pressure distribution to iteratively arrive at a reasonable agreement between the two distributions.

For most practical purposes the important parameter in EHL theory is the minimum film thickness. To save the effort of a full coupled solution of the elastic and Reynold equations for every analysis minimum film thickness equations based upon the dimensionless groups of the influencing parameters, tuned to the coupled equations, were developed. The Hamrock-Dowson equation for the minimum film thickness for fully flooded, isothermal, elastohydrodynamic point contacts [80] is

$$H_{min} = 3.63 U^{0.68} G^{0.48} W^{-0.073} \left(1 - e^{-0.68k}\right) \tag{6.33}$$

where the following dimensionless groups are defined:

- Dimensionless film thickness

$$H = \frac{h}{R_x} \tag{6.34}$$

where $h$ is the film thickness and $R_x$ is the relative radius of curvature (see Equation 6.1) in the $x$ direction.

- Dimensionless speed parameter

$$U = \frac{\eta_0 u}{E' R_x} \tag{6.35}$$

where $\eta_0$ is the atmospheric viscosity, $u$ is the surface velocity in the $x$ direction

- Dimensionless material parameter

$$G = \frac{E'}{p_{iv,as}} \tag{6.36}$$

where $p_{iv,as}$ is the asymptotic isoviscous pressure.

- Dimensionless load parameter

$$W = \frac{P}{E' R_x^2} \tag{6.37}$$

- Ellipticity parameter

$$k = \frac{a}{b} \tag{6.38}$$

where $a$ is the semimajor axis of the contact ellipse and $b$ its semiminor axis ($k = 1$ for point contact).

The Hamrock-Dowson minimum film thickness formula (Equation 6.33) has been widely accepted as a reasonable approximation of the minimum film thickness for non-conformal point contacts.

## 6.7 Summary

An overview of tribology and bearing theory has been presented. This lays the foundations for the following chapters. Chapter 7 presents the analysis of gearbox-generator misalignment which investigates whether high WT generator failure rates may be, in part, caused by misalignment between the gearbox and the generator under operation. Chapter 8 seeks to understand the interaction between the mechanical and electrical systems of the WT drivetrain. Specifically it explores whether the common-mode signal associated with the PWM switching of the power electronic converter may cause damaging currents to flow through the generator bearings.

# Chapter 7

# The Impact of Gearbox-Generator Misalignment

## 7.1 Introduction

In order to minimise the cost of energy (COE) from wind it is necessary to increase reliability and reduce unplanned downtime. The link between reliability and availability is particularly acute in the offshore wind energy sector, where even minor reliability issues can severely reduce availability due to the difficulties associated with access [81]. Unfortunately many drivetrains are suffering premature bearing failures. These bearing failures are very costly, not least because of the associated unplanned downtime.

Wind turbines, unlike traditional generation plant, experience highly stochastic loading due to the fluctuating nature of the wind, which can be difficult to characterise. There is evidence of a positive correlation between wind speed, the standard deviation of wind speed (which is used as a proxy for turbulence) and WT failures (see Chapter 5). In this chapter computational analyses are used to investigate misalignment between the gearbox and the generator and to understand whether gearbox-generator misalignment could be one of the root causes of premature WT generator failure.

Moreover, WTs are often exposed to extreme ambient conditions, and can be located in very remote regions on shore and offshore. This creates design challenges and also

logistical challenges for operation and maintenance (O&M); reliability is, therefore, closely linked to COE [82].

Numerous studies [31, 46, 83**?** , 84] have been undertaken to obtain the distribution of failures by assembly in WTs. It has been found that the gearbox and generator failure rates are unacceptably high. Furthermore, the downtime for these failures is amongst the highest of all WT assemblies, because often the entire gearbox or generator needs to be replaced which requires the deployment of a large crane. These cranes are costly, and may take some days or weeks to deploy. Offshore it is not unusual for rough weather to prevent access for O&M for weeks at a time. In 2010 Chen and Alewine [17] published the findings of a survey of over 800 failed WT generators, which showed that the dominant source of failures in multi-megawatt WT generators is the bearings (see Figure 4.4). To date, understandably, much attention has been given to blade reliability, but it is now clear that drivetrain bearing failures can have a significant impact upon the COE [85].

## 7.2   Misalignment

Although many different drivetrain concepts are used in multi-megawatt WTs, the most common is that shown in Figure 7.1. It consists of a low speed shaft supported on one or two bearings and a three stage gearbox, which drives a high speed generator via a flexible coupling.

Typically the low speed shaft operates at 15-23 $rpm$ while the high speed output of the gearbox is at 1200-1800 $rpm$. To achieve this gear ratio (approximately 1:80) a three stage gearbox with one planetary and two helical stages is commonly employed (see Figure 7.2).

The gearbox is mounted to the bedplate by the torque arm mounts; the purpose of this mounting is to prevent torque roll rather than to support the weight of the gearbox, which is instead cantilevered from the main bearings. Conventional WT drivetrains are supported on rolling element bearings, with those in the gearbox being oil lubricated and those in the generator greased.

Misalignment is a very common problem for rotating machinery; estimates suggest that misalignment may be the root cause of 20-30% of downtime of rotating plant across a wide
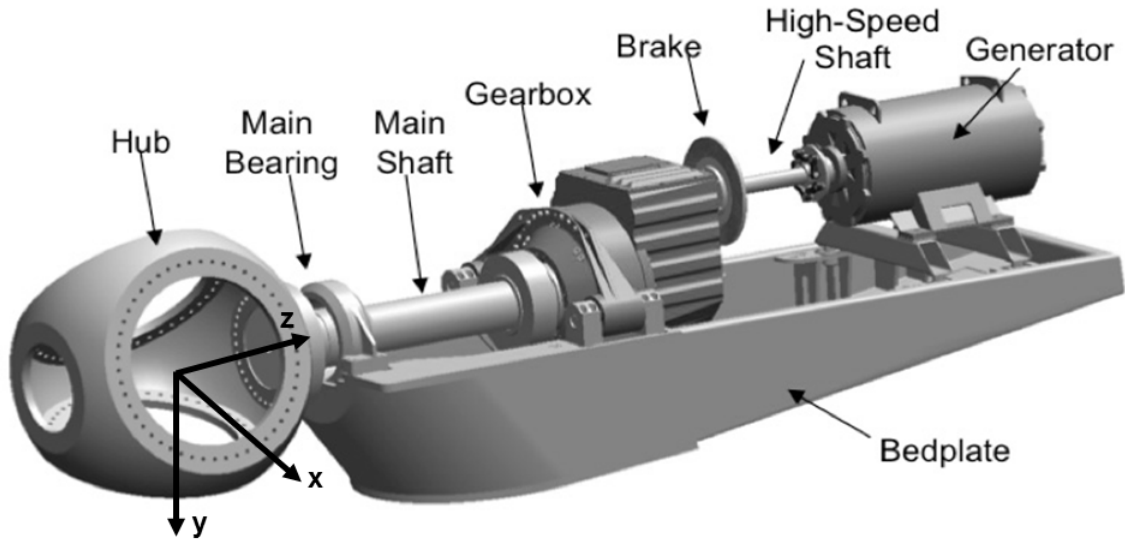
Figure 7.1: Typical multi-$MW$ WT drivetain (reproduced from [21], the coordinate system has been added)
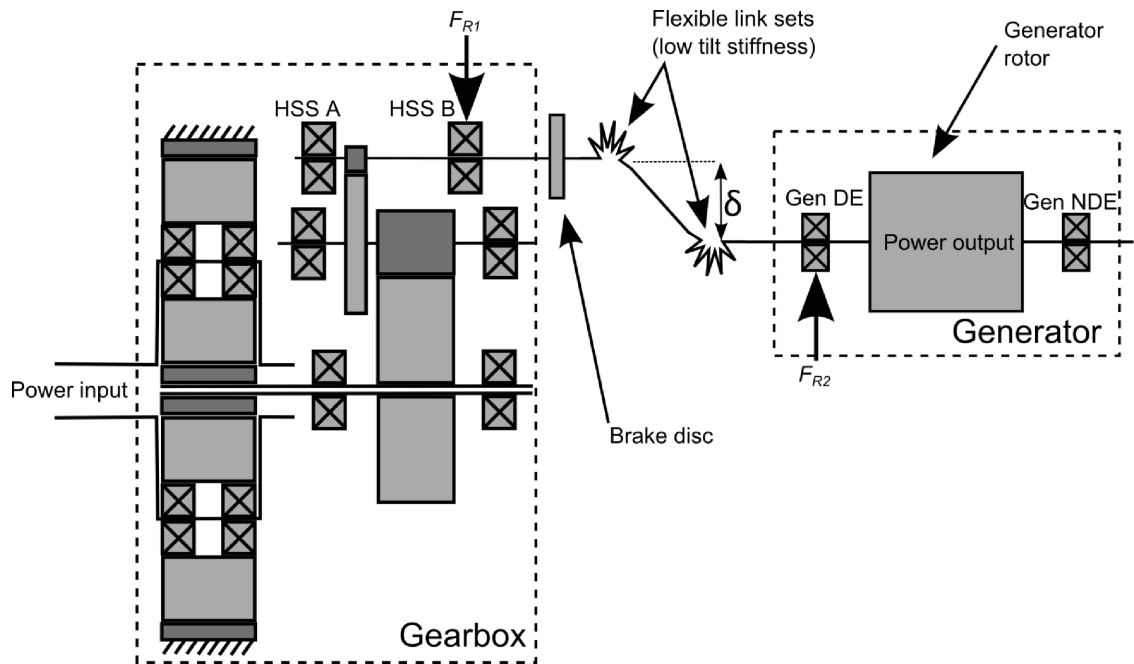


Figure 7.2: Three stage WT gearbox flexibly coupled to the generator ($F_{R1}$ and $F_{R2}$ indicate reaction forces caused by misalignment; $\delta$ denotes the misalignment)

range of industrial applications [86]. In 2011 McNiff *et al.* presented experimental data from a 750 $kW$ test rig which showed significant misalignment between the gearbox and generator [87]. In the same year Whittle *et al.* presented the results of a computational parametric analysis which was undertaken to evaluate the sensitivity of the generator and gearbox HSS bearing fatigue lives to parallel misalignment [88]. This was motivated by the high failure rate of the gearbox HSS and generator bearings coupled with the insight that the rubber bushings of the gearbox torque arm mounts have a relatively low stiffness ($ky \approx 40kN/mm$, using the coordinate system shown in Figure 7.1). Current practice is to use relatively compliant rubber elements in the torque arm mounting arrangement to control noise and vibration. The low stiffness of these elements means that they undergo large strains at rated torque. Because in a typical three stage WT gearbox the output shaft is off-centre this torque induced rotation of the gearbox causes misalignment between the gearbox and the generator. This is illustrated in Figure 7.3, in which it can be seen that the rotation of the gearbox causes a linear displacement, denoted $\delta$, in the output shaft. This misalignment, $\delta$, is also shown in diagrammatic form in the $yz$ plane in Figure 7.2.

Misalignment between the generator and the gearbox is accommodated by means of a flexible coupling. The restoring force of the coupling must be reacted at the generator and gearbox HSS bearings, as illustrated in Figure 7.1. The bearing types usually used for the gearbox HSS and generator are given in Table 7.1 [89].

In practice, a full understanding of the behaviour of a WT drivetrain can only be gained by undertaking a sophisticated analysis including the 3D dynamic response. For example, Heege *et al.* [38] demonstrate that for large turbines, various sources of excitation can give rise to periodic dynamic 3D orbits of the misalignment between the gearbox and the generator. In 2011 Helsen *et al.* used advanced multi-body modelling techniques in order to describe the complex modal behaviour of large WT gearboxes [39]. However, there are significant complexities involved in undertaking a full dynamic simulation and there is recognition in the industry of the need for experimental validation of these multi-body

| Bearing | Type |
| --- | --- |
| HSS A | Cylindrical or tapered cylindrical rolling element bearing |
| HSS B | A single row or back-to-back tapered cylindrical rolling element bearing(s) |
| Gen DE | Deep groove ball bearing |
| Gen NDE | Deep groove ball bearing |

Table 7.1: Gearbox HSS and generator bearing types

simulations, which are capable of capturing the dynamic behaviour of the turbine [40]. The output of these dynamic simulations must also be linked to a fatigue calculation and here some compromises must be made in order to minimise the computational effort of the operation. Moreover, the system dynamics will be strongly dependent on the specification of individual drivetrain components and their couplings. For these reasons, it is currently common practice to make a quasi-static assumption in the design process and, for example, in understanding drivetrain loading utilising operational data such as those obtained from SCADA [90, 91].

In the following section numerical simulations of a 750 *kW* drivetrain are presented. The results of these simulations showed that misalignment between the gearbox and the generator could have a significant influence upon the fatigue life of the generator bearings. Hence a second, more detailed, set of simulations was carried out using a model of a 2 *MW* WT drivetrain (see Section 7.4). The analyses presented here are quasi-static simulations of a complete WT drivetrain. The methodology used provides a generalised insight from the analysis of two specific cases. However, the influence of misalignment on bearing fatigue life, and the optimisation of the mitigation, will vary greatly from turbine to turbine, and will also be affected by enhancing the analysis by including dynamic effects. Thus for practical application, a full analysis is recommended for each turbine considered.

## 7.3 A 750 *kW* Computational Study

### 7.3.1 Bearing fundamentals

Wind turbine drivetrains are supported on rolling element bearings which are designed to last for twenty years based upon $L_{10}$ bearing fatigue life calculations – the premise of
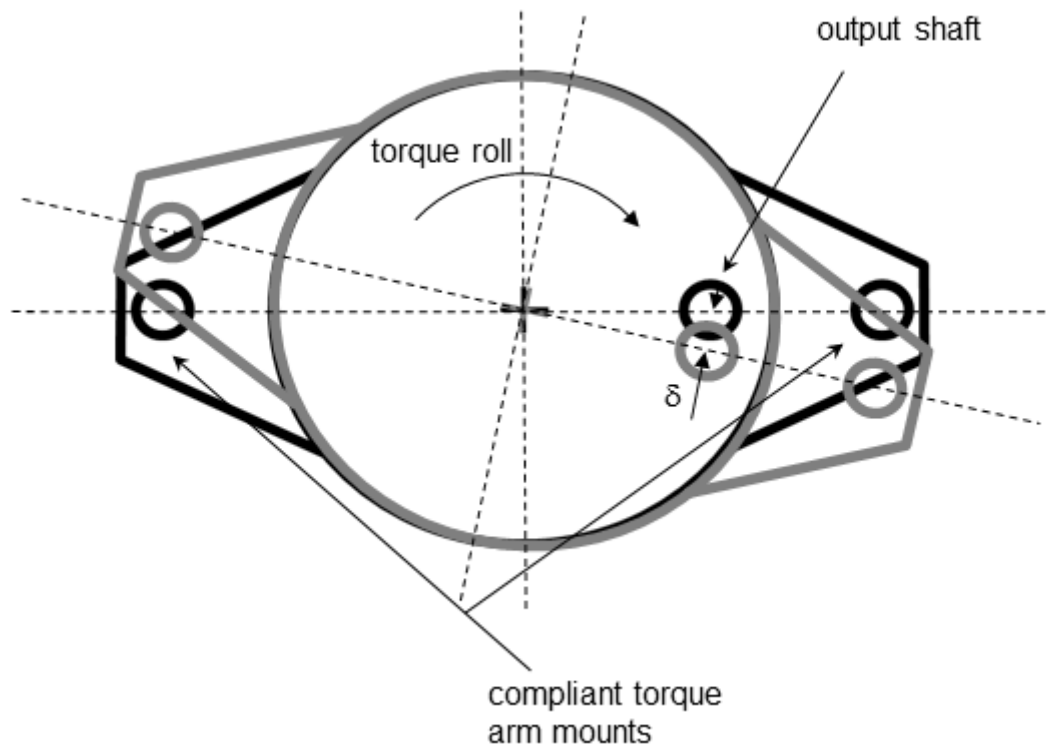
Figure 7.3: Displacement of gearbox under load induces gearbox-generator misalignment

which is that bearings ultimately fail under rolling contact fatigue.

**Rolling contact fatigue**

Classical fatigue damage in rolling element bearings is characterised by subsurface crack growth, as explained by Hertzian contact mechanics [58]. These subsurface cracks propagate towards the surface and eventually cause small particles to break free, forming pitting damage. These particles hasten the onset of failure by causing abrasion of the raceways and rolling elements.

A range of bearing life prediction methods exist, but they are mostly based upon the assumption that ultimately the bearing fails by classical rolling contact fatigue, due to the cyclic nature of the loading under rolling contact [92]. In the numerical simulations that are presented in this chapter the bearing fatigue lives have been calculated according to ISO 281:2007 [93] which is based upon the Lundberg-Palmgren equation [94, 95]. For details of the ISO 281:2007 $L_{10}$ calculations and their theoretical basis refer to Chapter 6.

## 7.3.2   Numerical simulations

A typical 750 *kW* variable speed wind turbine was modelled using RomaxWIND, a pro-
prietary drivetrain design and analysis software package [96]. The RomaxWIND software
has been validated using the NREL GRC test rig [97] and is a GL certified design and
analysis tool. The drivetrain comprised a three stage gearbox (one planetary stage, and
two helical stages) flexibly coupled to a DFIG. The gearbox HSS bearing arrangement
comprised one upwind cylindrical rolling element bearing, with downwind back-to-back
taper rolling element bearings to react the axial loading from the helical gear. The gen-
erator rotor was supported by two ball bearings.

The flexible coupling was modelled as a composite structure gaining its flexibility from
the two linksets at each end which have low tilt stiffness. This type of flexible coupling is
commonly employed in wind turbine drivetrains. The analysis could be scaled, without
difficulty, to larger multi-megawatt turbines. A representation of the model is shown in
Figure 7.4.
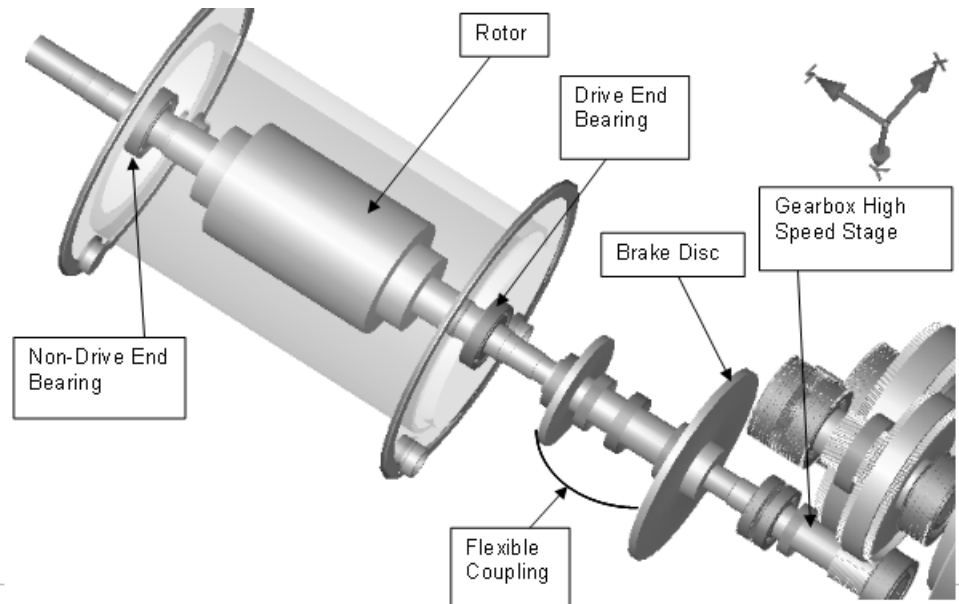


Figure 7.4: Model of Wind Turbine Drivetrain and Generator in RomaxWIND Drivetrain
Analysis Software

Using GH Bladed [98]a system model of the WT was used to generate a twenty year
time series of load data. This model included an aeroelastic description of the blades

and simplified drivetrain dynamics (torsional stiffness only) to derive a set of load data that is considered representative of WT load spectra. These data were 'binned' according to torque and speed, thus generating a 3-D histogram defining the number of cycles for each operational point. The set of load cases was then solved quasi-statically using Ro-maxWIND in which the shafts are modelled as Timoshenko beams and the gear contact stresses solved by employing non-linear analytical contact mechanics. The bearing dy-namic equivalent radial loads were then be calculated and the bearing $L_{10}$ fatigue damage computed according to ISO 281:2007 using the RomaxWIND software. It was important to model the whole drivetrain in order to solve the coupled non-linear solutions for the system. The bearing fatigue damage for each load case was summed according to Miner's principle (see Figure 7.5).

In practice, a full understanding of the behaviour of a WT drivetrain can only be gained by undertaking a sophisticated analysis including the 3D dynamic response. For example, Heege *et al.* [38] demonstrate that for large turbines, various sources of excita-tion can give rise to periodic dynamic 3D orbits of the misalignment between the gearbox and the generator. In 2011, Helsen *et al.* used advanced multi-body modelling techniques to describe the complex modal behaviour of large WT gearboxes [99] However, there are significant complexities involved in undertaking a full dynamic simulation, and there is recognition, in the industry, of the need for experimental validation of these multi-body simulations capable of capturing the dynamic behaviour of the turbine [40]. The output of these dynamic simulations must also be linked to a fatigue calculation, and here, some compromises must be made to minimize the computational effort of the operation. More-over, the system dynamics will be strongly dependent on the specification of individual drivetrain components and their couplings. For these reasons, it is currently common practice to make a quasi-static assumption in the design process and, for example, in un-derstanding drivetrain loading by utilizing operational data such as those obtained from SCADA [90, 91]. In this chapter, a potential failure mechanism that does not appear to have been addressed in the literature is investigated, that of WT bearing failure due to

misalignment between the gearbox and the generator. Quasi-static analyses of a complete
WT drivetrain have been undertaken to calculate the gearboxgenerator misalignment and
then to compute its influence upon bearing loading and fatigue life.
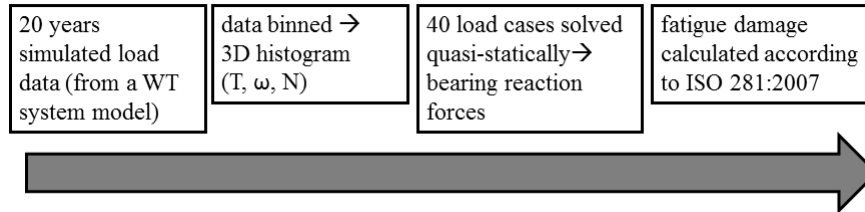


Figure 7.5: Computational strategy

.

A two-dimensional sensitivity study was carried out to investigate the sensitivity of the
bearing fatigue damage to (a) the coupling linkset tilt stiffness and (b) the misalignment
between the gearbox high speed shaft and the generator. The results are presented in
Figures 7.6 – 7.9.

The main findings of this preliminary sensitivity study were:

- In this analysis the aligned system is well within the fatigue envelope for the gen-
  erator drive end (DE) bearing; 20 years load history accrued approximately 40%
  fatigue damage.

- For misalignment between 0 $\mu m$ and -3000 $\mu m$, increasing the coupling stiffness
  resulted in reduced contact stresses at the generator DE bearing.

- For negative misalignments greater than 3000 $\mu m$ the fatigue life of the generator
  DE bearing was reduced by increasing the tilt stiffness of the coupling linksets.

- Positive misalignment countered the bearing loading due to the generator rotor self
  weight at the DE bearing, at the cost of increased loading of other bearings.

- As the coupling tilt stiffness is increased the maximum contact stress increases
  resulting in a significant reduction in the fatigue life for positive misalignments over
  3000 $\mu m$.
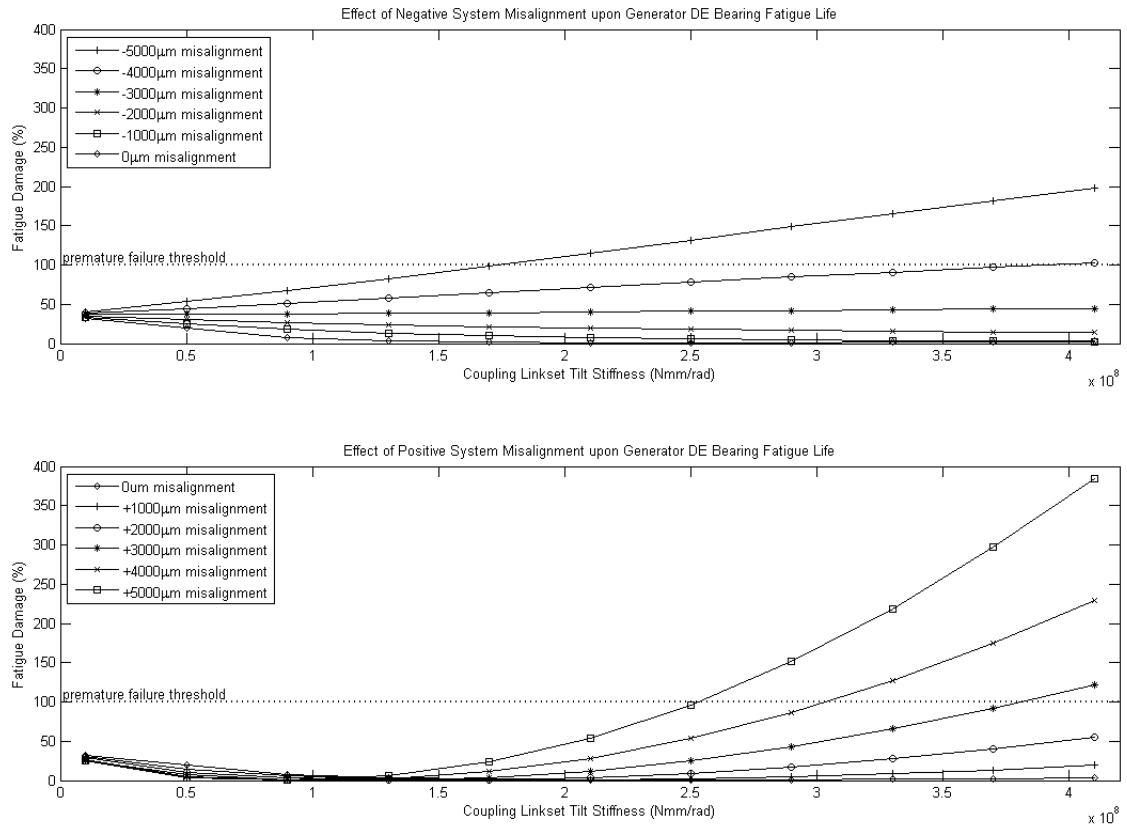
Figure 7.6: Fatigue Damage of the Generator Drive End Bearing

This preliminary study showed that a feasible methodology to solving the problem of WT gearbox-generator misalignment had been identified. However there remained three important questions:

- What is the likely magnitude of misalignment between gearboxes and generators in multi-$MW$ wind turbines?

- What are the stiffness characteristics of the couplings? It was found that most coupling manufacturers publish only an allowable misalignment range, rather than specifying stiffness characteristics.

- How did the problem scale to multi-$MW$ turbines?

Further numerical simulations were carried out in order to answer these questions. These analyses were carried out using a model of 2 $MW$ WT drivetrain. The mounting
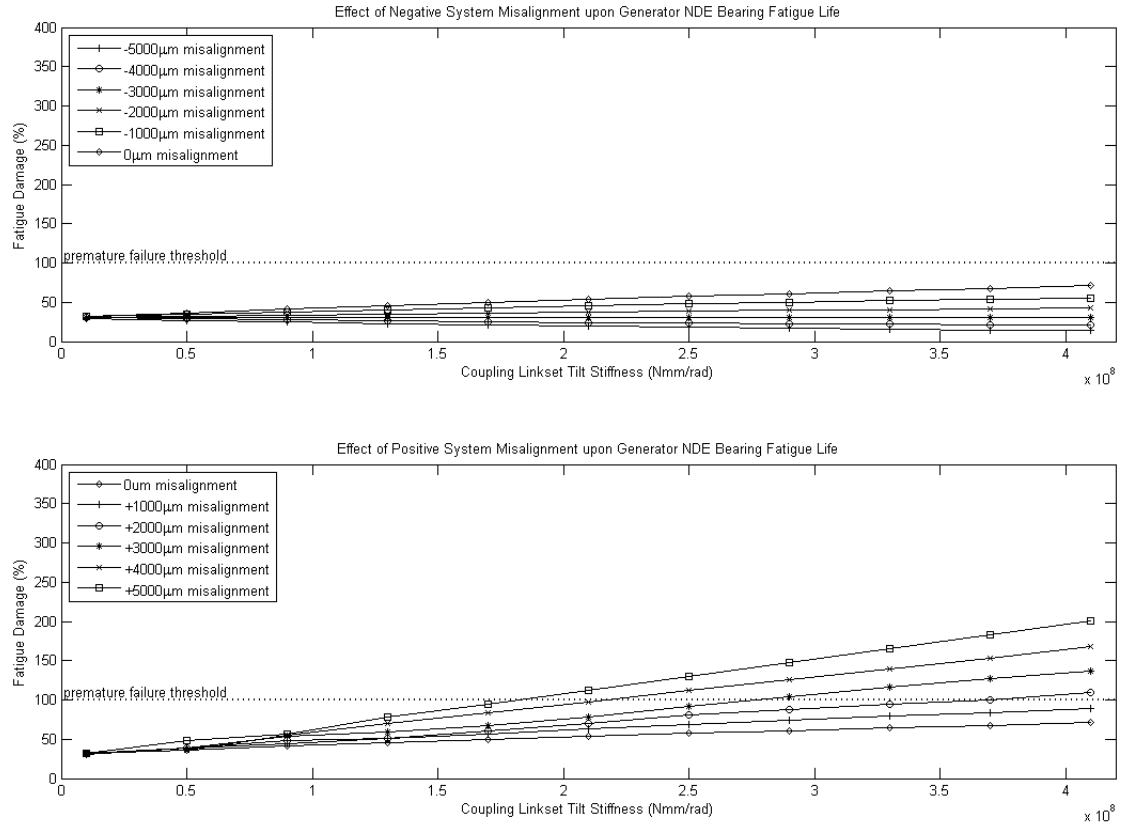
Figure 7.7: Fatigue Damage of the Generator Non Drive End Bearing

arrangements of the drivetrain (including detailed geometry for the bedplate and gearbox housing) and the flexible coupling tilt stiffness were known [1].

# 7.4  A 2 *MW* Computational Study

## 7.4.1  Numerical Modelling Approach

A series of computational simulations was performed in order to:

- Compute the gearbox-generator misalignment due to displacement of the gearbox under load;

- Predict the impact of this misalignment upon the fatigue lives of the gearbox HSS bearings and generator bearings.

[1]The 2 *MW* WT drivetrain modelled in this chapter is from a real commercially available turbine. The commercial sensitivity of the data prohibits the publication of certain details pertaining to the model
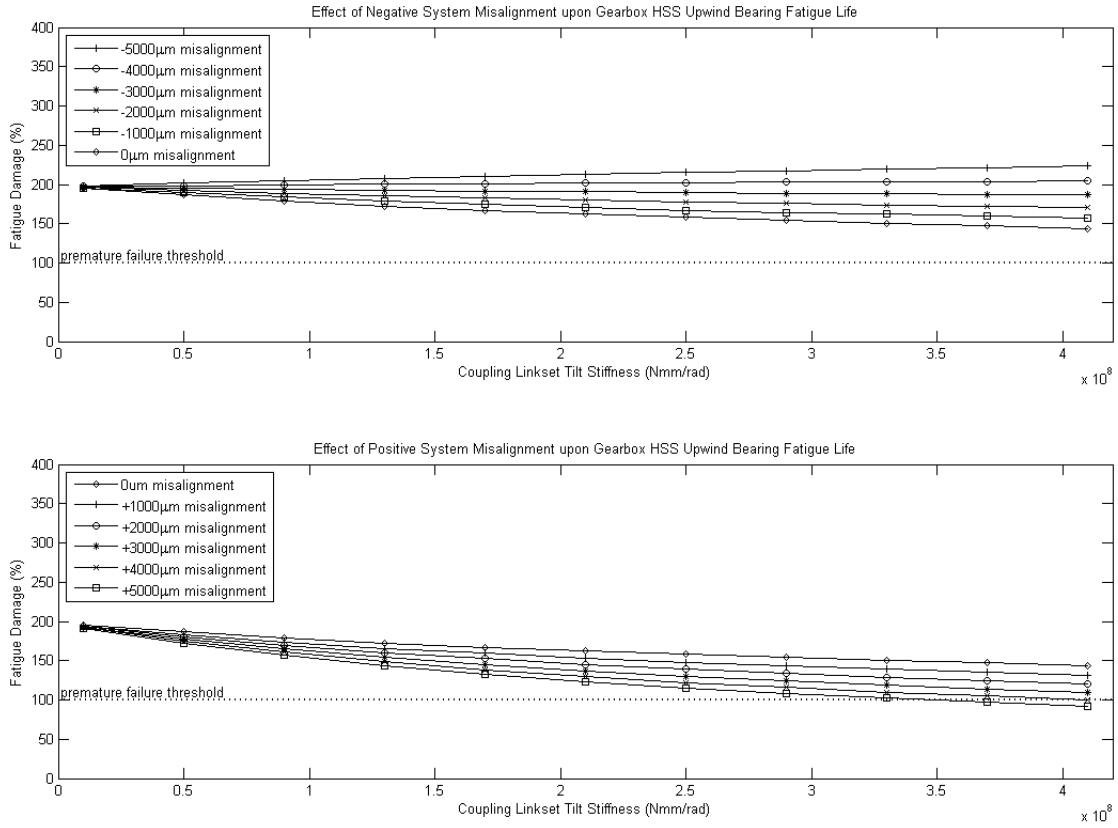
Figure 7.8: Fatigue Damage of the Gearbox High Speed Stage Upwind Bearing

The same computational strategy that had been used in the analysis of the 750 $kW$ drivetrain was again employed to perform numerical simulations of the 2 $MW$ drivetrain. Another system model of the WT was used to generate a twenty year time series of load data. However this time the data were binned according to torque, speed and the non-torsional loads (forces $F_x$,$F_y$,$F_z$ and moments $M_x$,$M_y$) to generate forty load cases (see Figure 7.10), each of which could be solved quasi-statically, in RomaxWIND, to compute the stresses and strains in the drivetrain. Note that in the previous sensitivity analysis, using the 750 $kW$ drivetrain, the non-torsional loads were neglected. Here, however, they are included in order more accurately to represent the movement of the gearbox on its compliant mounts. The coordinate system used throughout is that shown in Figure 7.1.

In order to determine the most efficient computational model that would sufficiently accurately capture the stiffness characteristics of this complex problem, four different
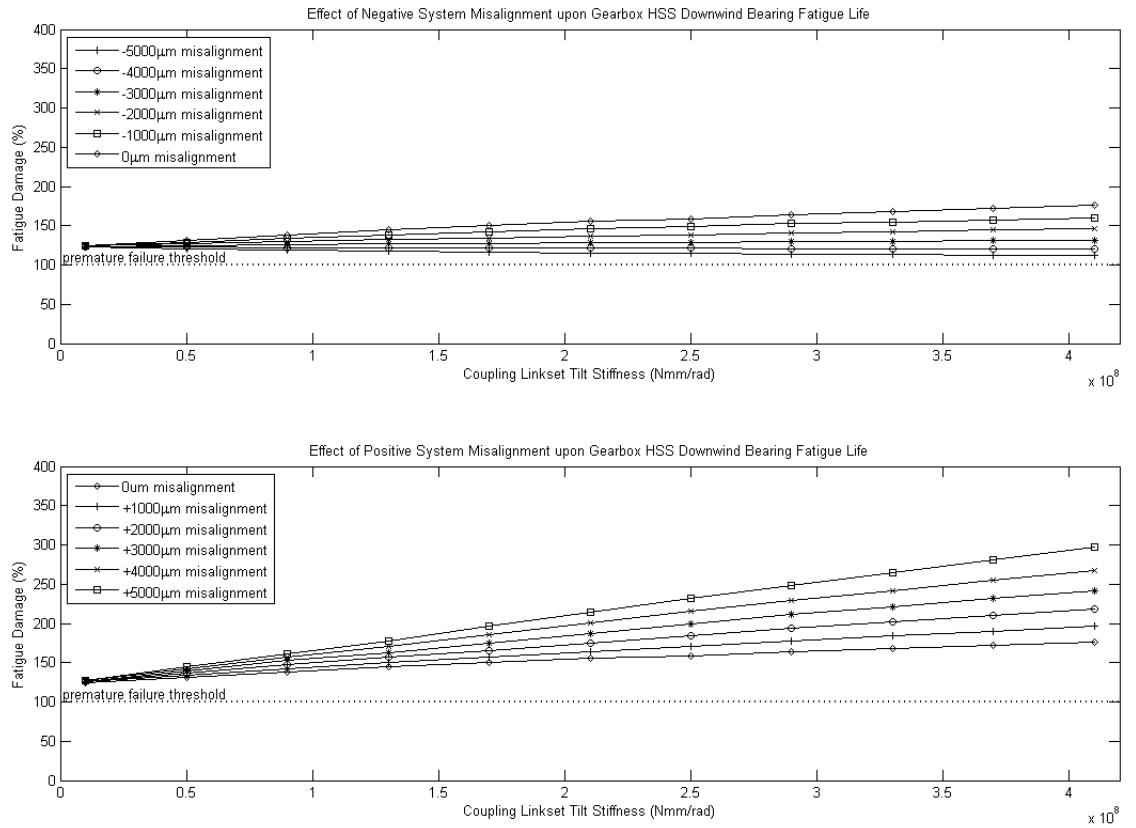
Figure 7.9: Fatigue Damage of the Gearbox High Speed Stage Downwind Bearing
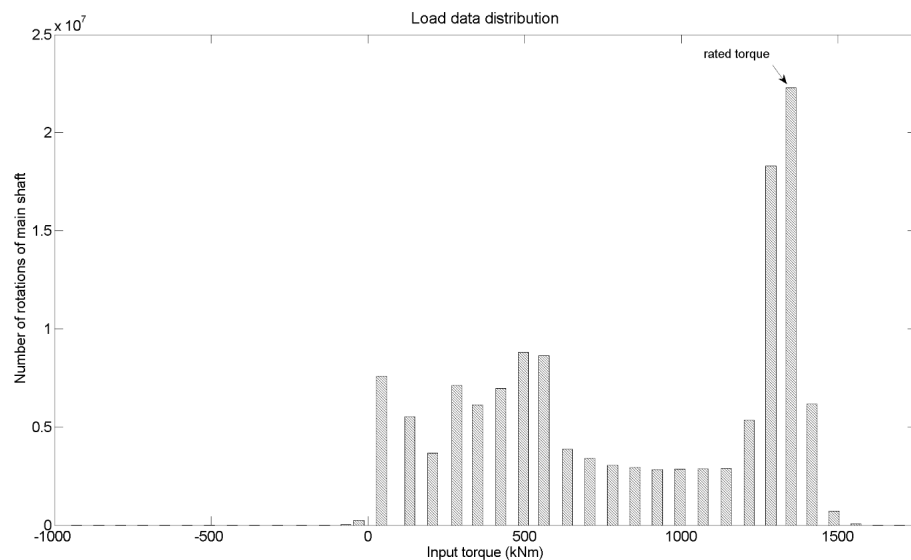


Figure 7.10: Twenty years of simulated load data binned according to torque, speed and non-torsional loads (note the small number of cycles at negative torque; these negative torque cycles are due to transient events such as braking, or gusts in the wind)

| Case | Mount | Housing | Bedplate |
|------|-------|---------|----------|
| 1 | Rigid | Rigid | Rigid |
| 2 | Compliant | Rigid | Rigid |
| 3 | Compliant | Compliant | Rigid |
| 4 | Compliant | Compliant | Compliant |

Table 7.2: Drivetrain Models

representations of the same 2 $MW$ drivetrain were considered. In the first, the benchmark, the drivetrain was rigidly mounted; the second included the gearbox torque arm mount compliance, but neglected the compliance of the housing and bedplate; the third model included both the mount compliance and the housing compliance; the fourth model was the most detailed with the compliance of the mount, housing and bedplate included in the model. The housing and bedplate compliances were included using FE models provided by Romax. These four cases are summarised in Table 7.2.

In the generator model the rotor was supported on two deep groove ball bearings, which were directly grounded (i.e. the generator housing and bedplate compliance were neglected). This was justified since the misalignment between the generator and gearbox is likely to be dominated by the gearbox displacements under operational loads.

The final, but important, parameter in the model described in this section is the tilt stiffness prescribed for the flexible couplings. There is a range of flexible couplings on the market; the type used in WT drivetrains typically gain their flexibility by means of two arrangements of links (one at each end). The tilt stiffness of the flexible coupling link set adopted for the numerical model of the drivetrain was 5 $kNm/rad$, i.e. that of the Centalink 71 coupling [100].

## 7.4.2   Results

The results of the numerical simulations using the 2 $MW$ WT drivetrain model are now presented beginning with the displacement data. After which the bearing fatigue life calculations are presented and mitigation options are discussed.

**Displacement**

The magnitude of the misalignment between the gearbox HSS and the generator shaft in the $xy$ plane (axial displacement is neglected) for the four different modelling cases, presented in Table 7.2, is shown in Figure 7.11. In case 1 (rigidly mounted) a misalignment of approximately 1000 $\mu m$ is observed under rated torque; this misalignment is due to the compliance of the bearings and the shaft under significant radial loading at the HSS gear set. By comparison of the magnitude of misalignment for the other cases it may be seen that the housing and bedplate compliances have a small influence upon the gearbox-generator misalignment ($< 300\mu m$). In the analysis that follows the full model is used (case 4) but such a detailed model is not essential. The gearbox housing and bedplate compliances may be neglected where these data are not available. These compliances may also be neglected where computational or time constraints are severe when computing gearbox-generator misalignment since, as may be seen from Figure 7.11, the misalignment is mainly a function of the torque arm mount stiffness.
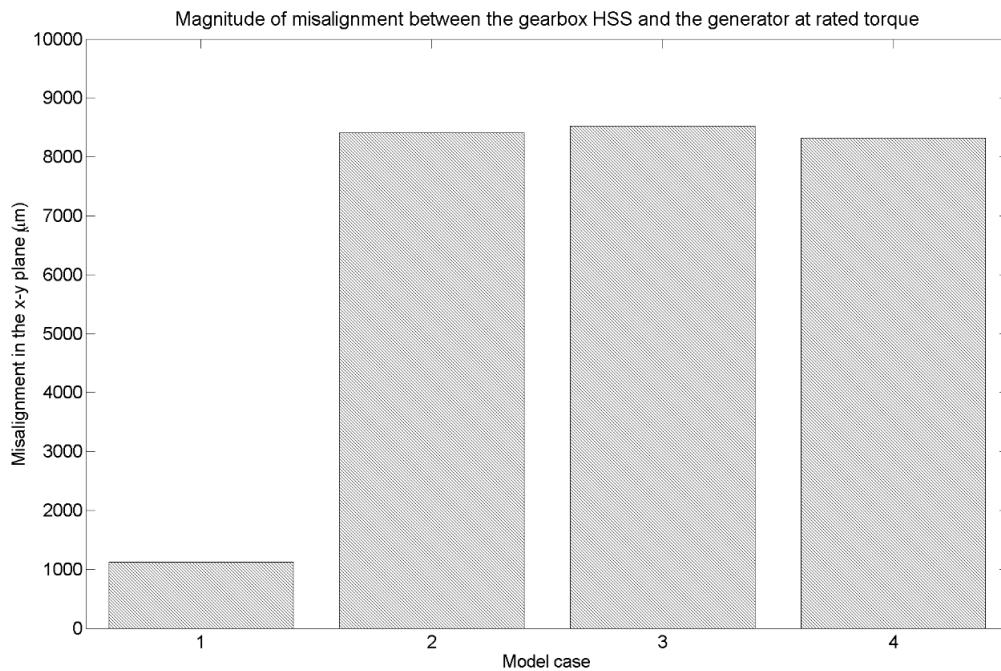


Figure 7.11: Impact of component compliances for the model cases as defined in Table 7.2

**The bearing loads**

Before presenting the bearing load results from the numerical simulations it is germane first to discuss low load requirements for rolling element bearings.

In a very lightly loaded bearing the force normal to the contact is insufficient for the elastohydrodynamic tractive force to overcome the cage drag and churning losses. Therefore, the actual cage frequency is a little below the theoretical cage frequency and the raceway will skid past the rolling elements [101, 102]. Whereas in Hertzian contact the maximum shear stress is below the surface, the presence of skidding can result in a larger shear stress at the surface. These surface stresses render the bearing fatigue life calculations outlined in Chapter 6 invalid. Rolling element bearing skidding is not a well understood phenomenon and, consequently, there is a range of different low load requirements used in industry. For deep groove ball bearings (such as those used in WT generators), one bearing manufacturer has developed the relationship

$$F_{rm} = k_r(\nu n/1000)^{2/3}(d_m/100)^2 \tag{7.1}$$

where $F_{rm}$ is the minimum radial load required ($kN$) to avoid skidding; $k_r$ is the minimum load factor (this dimensionless parameter is a function of the bearing geometry and is obtained from the bearing datasheets); $\nu$ is the oil kinematic viscosity ($mm^2/s$) at the operating temperature; $n$ is the number of shaft revolutions per second and $d_m$ is the bearing mean diameter ($mm$) [103]. Other manufacturers opt for simpler and more conservative minimum load requirements of either 1% [104], or 2% [105] of the dynamic load rating of the bearing.

Having seen that significant misalignments – 8500 $\mu m$ at rated torque – between the gearbox and generator are caused by rotation of the gearbox under torsional loading this section considers the effect of the misalignment upon the loads transmitted through the bearings and thence on their fatigue lives. Figure 7.12 shows the radial and axial loads on the gearbox HSS bearings with no generator nominal offset (0 $\mu m$) and a large nominal offset of the generator (10,000 $\mu m$). Applying a nominal generator offset of 8500 $\mu m$ aligns

the drivetrain for rated torque; the bearing reaction forces for this case lie in between the two graphs (0 $\mu m$ and 10,000 $\mu m$) shown in Figure 7.12, but for clarity these data were not graphed.

For the gearbox HSS bearings the loading is a linear function of the absolute torque. These bearing forces are reacting the contact forces in the HSS helical gear set. At rated torque inclusion of misalignment in the computation changes the radial load on HSS A and HSS B by 20% and 15% respectively (refer to Figure 7.2 for the definition of HSS A and HSS B); i.e. at rated torque the HSS bearing loading is primarily due to the gear contact.
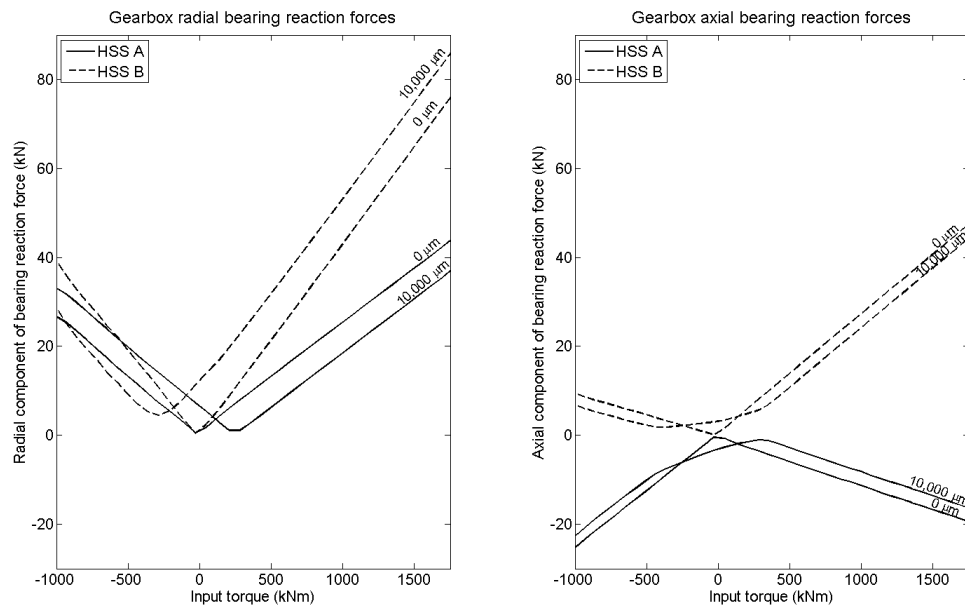


Figure 7.12: Gearbox HSS bearing reaction force as a function of torque

For a 2 *MW* DFIG the generator bearings typically have a load of 9.8 $kN$ to 12.3 $kN$. The radial loading on the generator bearings is only about 33% of that on the upwind HSS bearing (HSS A), or 19% of the force on the HSS downwind bearing (HSS B). Thus, whilst the restoring forces of the coupling under misalignment have a small influence upon the gearbox HSS bearing loads, the same cannot be said for the loading of the generator bearings, as shown in Figure 7.13. It may be seen that the generator drive-end (DE) bearing loading is, as expected, much more sensitive to misalignment than the non-drive

end (NDE) bearing. When the system was statically aligned and operating at rated torque the generator DE bearing load was 160% that of the NDE bearing, i.e. the system was very imbalanced.

The graphs in Figure 7.13 show the generator bearing reaction forces as a function of torque for a range of nominal generator offsets (0 – 10,000 $\mu m$) in the y direction. The low load requirements for the conservative design choice (bearing designation 6330, see Table 7.3) are also plotted on Figure 7.13 – under all but the most severe conditions the low load requirements are met. However, low load phenomena are not well understood, therefore a greater factor of safety, with regards to this requirement, may be preferred by some OEMs.
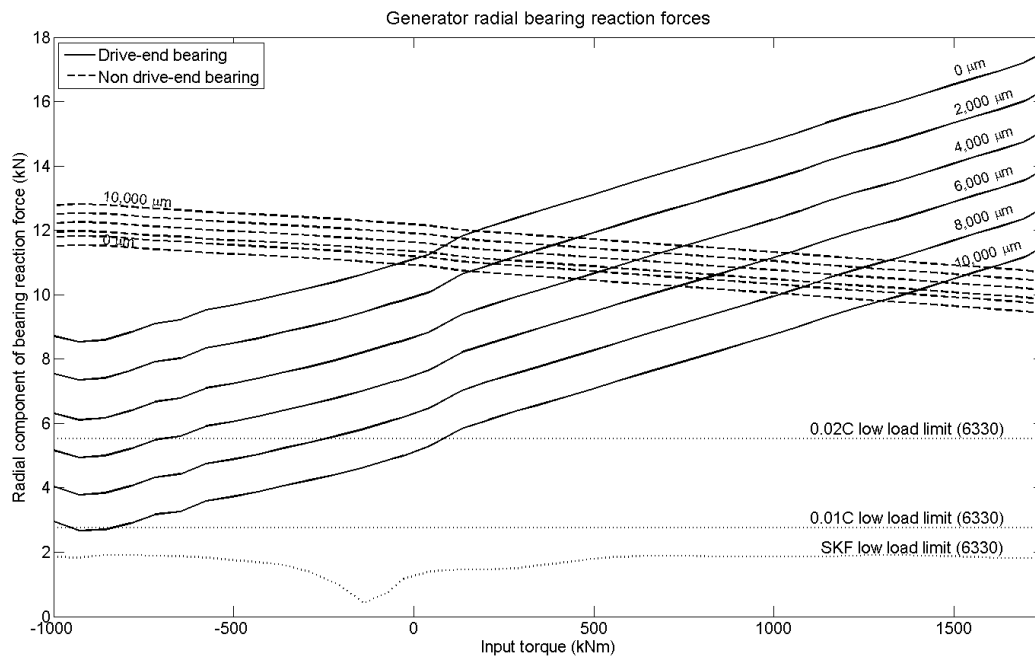


Figure 7.13: Generator radial bearing reaction forces

Having seen that gearbox-generator misalignment can significantly alter the generator bearing loads the following sections consider the impact upon the bearing fatigue life and appropriate mitigation measures.

| Bearing | $C(kN)$ | $C_0(kN)$ | $C_u(kN)$ | $0.01C(kN)$ | $0.02C(kN)$ |
|---------|---------|-----------|-----------|-------------|-------------|
| 61930 | 88.4 | 93 | 2.9 | 0.884 | 1.768 |
| 6230 | 174 | 166 | 4.9 | 1.74 | 3.48 |
| 6330 | 276 | 285 | 7.8 | 2.76 | 5.52 |

Table 7.3: Ball bearing data used in generator model ($C$ is the dynamic rating, $C_0$ is the static rating, $C_u$ is the fatigue load limit)

### 7.4.3 Mitigating Misalignment

Two strategies for mitigating the effects of gearbox-generator misalignment were considered:

1. Over-rating the generator bearings. Three different ratings were considered for the generator bearing, varying from a lean design (bearing designation 61930) to a conservative approach (bearing designation 6330)- see Table 7.3 for details;

2. Imposing a nominal offset on the generator to reduce operational misalignment (i.e. apply static misalignment to the generator).

**Over-rating the generator bearings**

A simple approach to mitigate misalignment is to increase the bearing $L_{10}$ fatigue life by increasing the bearing rating. This option is attractive for two reasons:

- The generator deep groove ball bearings are relatively inexpensive. If costly downtime can be avoided by using larger, more expensive, bearings the cost-benefit analysis is likely to be favourable;

- It is a simple solution requiring very little detailed system knowledge.

Three bearing selections were considered for the 2 *MW* generator in this test case. For the twenty-year simulation the accumulated fatigue damage was calculated for each bearing choice and these data are shown in Table 7.4.

It may be seen that the smallest bearing selected has very imbalanced fatigue damage for the DE and NDE bearings, due to the effect of misalignment. The second option, bearing 6230, still betrays the presence of misalignment with the DE bearing having twice

| Bearing | Fatigue Damage (%) | |
|---|---|---|
| | Gen DE | Gen NDE |
| 61930 | 250 | 50 |
| 6230 | 20 | 10 |
| 6330 | 3 | 2 |

Table 7.4: Generator bearing fatigue damage (where 100 % corresponds to the $L_{10}$ fatigue life) for three different bearing selections over simulated twenty year design life

the fatigue damage of the NDE bearing. The most conservative design choice, bearing 6330, has loading only slightly greater than the infinite fatigue life asymptote.

However, although over-rating the bearing will give a longer $L_{10}$ fatigue life, it may actually reduce the serviceable life of the bearing if the load is insufficient to prevent the bearing from skidding [57]. This is particularly problematic in WT generators because the bearings must be able to withstand significant thermal growth. Upon start-up the bearing temperature will increase more rapidly than the surrounding housing, which has a large thermal inertia, and this leads to a loss of operating clearance [71]. The bearings must have a large enough internal clearance to accommodate the thermal expansion but this makes the rolling elements more prone to skidding. The necessity of ensuring sufficient operating clearance under thermal instability therefore makes WT bearings more likely to suffer from skidding and so increasing the probability of skidding still further by over-rating bearings may be inadvisable.

**Nominally offset generator**

An alternative strategy is to apply a nominal offset to the generator such that the system moves into alignment under the application of a load. Such a system might be designed to become fully aligned under rated torque. However, here the prospect is considered that the optimum fatigue life may arise for a system that has a somewhat different nominal offset.

The effect of applying a nominal offset to the generator upon its bearing fatigue lives is shown in Figures 7.14 and 7.15 which compare the fatigue damage accumulation in the forty simulated load cases for the drivetrain statically aligned (offset = 0 $\mu m$) and when it is aligned for the rated torque (offset = 8500 $\mu m$). Aligning the drivetrain for the rated

torque not only reduces the fatigue damage on the DE bearing at high torque, but also reduces it at low torque levels. This is because the misalignment at low torque unloads the DE bearing so it comes at the cost of slightly increased damage to the NDE bearing.
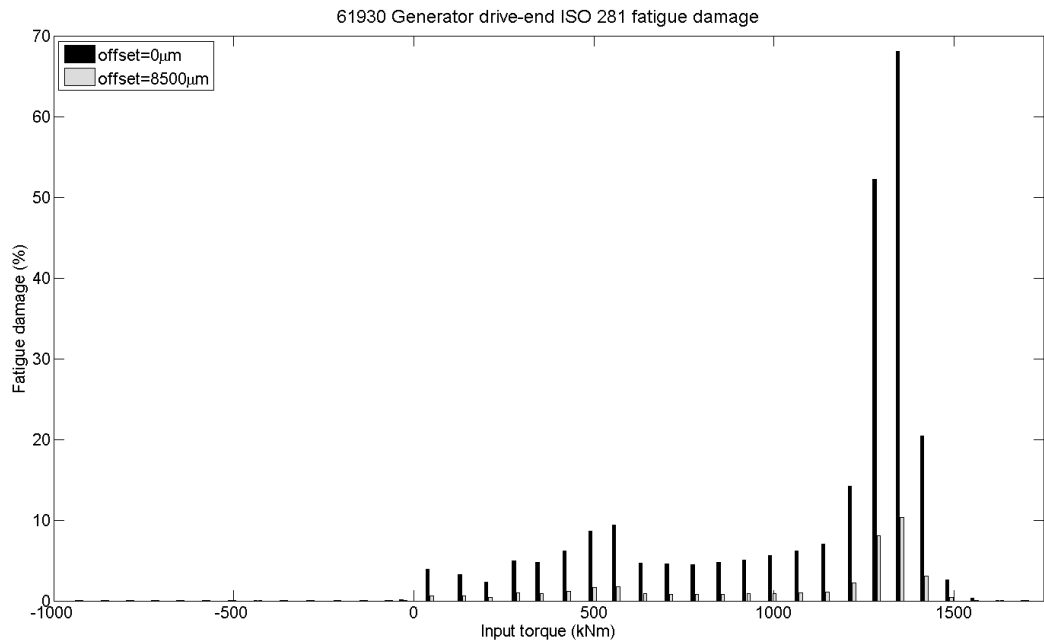


Figure 7.14: 61930 generator drive-end ISO 281 fatigue damage
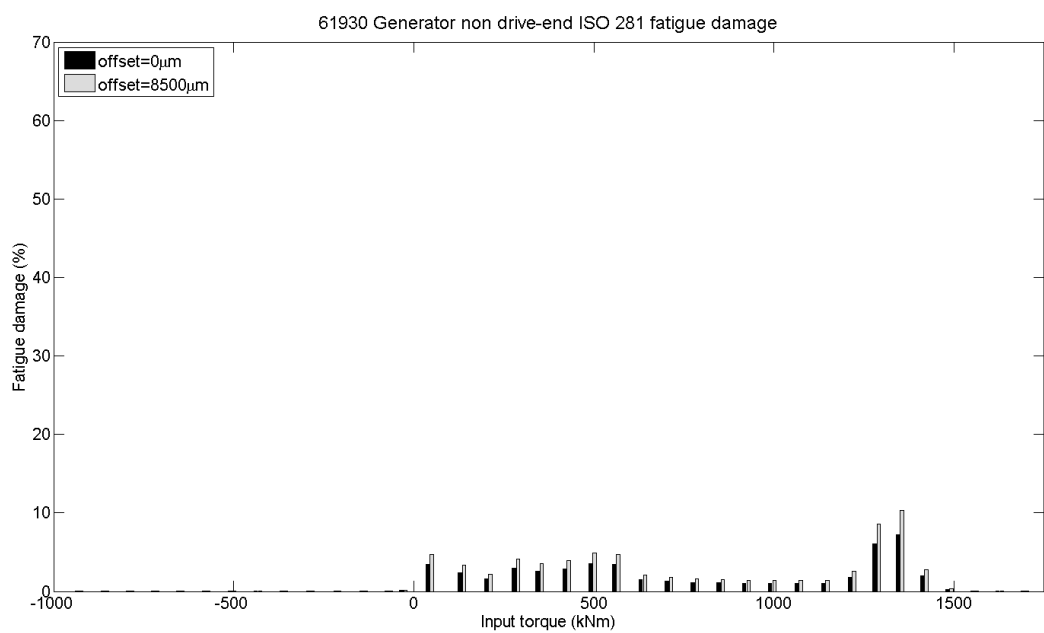


Figure 7.15: 61930 generator non drive-end ISO 281 fatigue damage

The influence of the nominal generator offset upon the bearing fatigue damage accrued over the twenty-year simulation, for the gearbox HSS and generator (for bearing 61930 and 6230), is shown in Figure 7.16. The gearbox HSS bearings are not significantly affected by misalignment because the coupling reaction forces are small compared to the gear loading; the generator bearings, particularly the DE bearing, are sensitive to misalignment. It is interesting to note that for the leanest generator specification (bearing 61930) nominally offsetting the generator is sufficient to make the difference between meeting the target $L_{10}$ bearing fatigue life or not. The more conservative design, using a 6230 type bearing, should not encounter fatigue problems even when statically aligned. However, it may still be better to offset the generator to reduce vibration and reduce the probability of coupling failure.

The optimal generator offset is a function of the specific drivetrain configuration. Hence, to optimise the generator offset, it would be necessary to undertake the analysis for each drivetrain. In particular, it is important that the torque arm mount and flexible coupling stiffnesses are correctly specified, since the model is sensitive to these parameters. Moreover, the optimal generator offset is also a function of the wind conditions for the particular WT location. Different wind conditions will give a different shape to the load data histogram (Figure 7.10). Therefore, for a given WT, high wind speed sites will require larger generator offsets than low wind speed sites. In fact, it is not a simple matter to define the optimal generator offset even for a given WT subjected to known loading. By reference to Figure 7.16, it may be seen that alignment for the rated torque gives imbalanced generator bearing fatigue lives. This is because the variable nature of the wind means that the WT is not operating at rated power for much of the time. Therefore, a better solution may be to align the turbine for 70% of rated torque which yields balanced fatigue damage for the generator bearings, albeit resulting in imbalanced loading at rated operation.
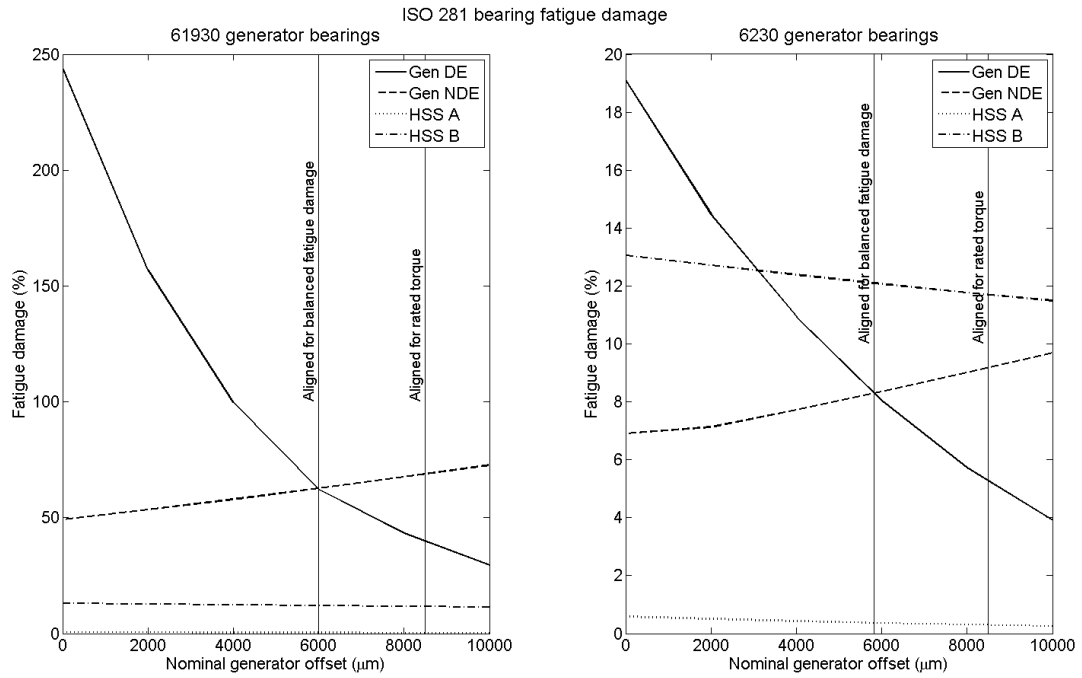
Figure 7.16: The sensitivity of the ISO 281 bearing fatigue damage to the generator offset

## 7.5   Conclusions

For a typical 2 $MW$ geared WT, significant misalignment between the gearbox and the generator results from the compliance of the gearbox torque arm mounts. Depending upon whether this misalignment loads, or unloads, the generator DE bearing it could decrease the bearing $L_{10}$ fatigue life, or increase the probability of failure due to skidding. The NDE bearing could also be affected by misalignment, but gearbox bearings are less likely to be affected by radial misalignment as they must be rated for significantly greater loading from the HSS helical gear set.

In modelling global gearbox displacement the gearbox torque arm mount stiffness is critical. The gearbox housing and bedplate compliances may be neglected for the present purpose if necessitated by computational constraints or unavailability of data. The need for integrated system analyses of WT drivetrains has been demonstrated, and this requires OEMs to collaborate in order to understand the interactions between WT subassemblies.

The present quasi-static analysis showed that the interactions between drivetrain assemblies are important, and that large gearbox-generator misalignments can occur, which

may cause increased fatigue damage to the generator bearings. Promising advances are being made in the application of multi-body simulation techniques capable of describing the dynamic behaviour of WT drivetrains (see, for example, [40, 99, 106]). In the future, the analysis could be enhanced by incorporating dynamic effects in order to quantify the influence of dynamic loading upon the gearbox HSS and generator bearings. Of particular interest may be the contribution that extreme load events, such as emergency stops, make to the gearbox HSS and generator bearing fatigue lives.

Another way in which the research could be enhanced, in the future, is by improving the characterisation of the flexible coupling. Many different coupling designs are used in the wind industry and it is likely that a range of tilt stiffnesses will be found. Moreover, most datasheets for couplings do not specify the stiffness and even where they do it is assumed to be linear. It may be that this linear characterisation of the coupling stiffness is insufficient and that at higher strains the assumption is not valid. Laboratory testing of a range of flexible couplings would allow greater fidelity in the numerical simulation of gearbox-generator misalignment.

The practice of over-rating bearings to increase their $L_{10}$ fatigue life is not recommended for WT generators. These bearings need large internal clearances to accommodate the thermal instability inherent in this application; this makes them prone to skidding which is one possible cause of premature failure. Therefore, it is proposed that gearbox-generator misalignment be mitigated by means of a nominal generator offset, rather than over-rating the generator bearings. This requires a careful analysis of the drivetrain, but the potential to increase availability, thereby reducing the risk to investors, may reduce the COE enough to justify the small additional capital cost involved.

# Chapter 8

# Bearing Currents

## 8.1 Introduction

It has been known for many years that currents flowing through the bearing are a source of failure in rotating electrical machines. High voltages arise due to the capacitive effect of the lubricant; eventually discharge may occur which leads to erosion damage known as EDM which can advance the onset of fatigue failure. Historically, bearing currents were caused by electrostatic charging and magnetic flux asymmetries [18]. The first of these mechanisms, electrostatic charging, is due to friction which leads to a build up of charge, and a DC voltage along the shaft, followed by discharge through the bearings. Conversely, magnetic flux asymmetries lead to an AC voltage along the shaft at frequencies of the same order as the electrical supply frequency (under 100 $Hz$). With the widespread adoption of power electronic converters in WT architectures another source of bearing currents became important [107], this is discussed in the next section.

## 8.2 The Common-Mode Signal

The widespread use of power electronics leads to increased risk of harmful bearing currents because of the common-mode signal associated with PWM switching [108, 109]. The line voltages are phase shifted such that as sinusoids they instantaneously sum to zero. However, when power electronics are used they do not instantaneously sum to zero so the

neutral point has a zero sequence voltage, which drives the parasitic circuit in which the bearings are conductive (see Figure 8.1).
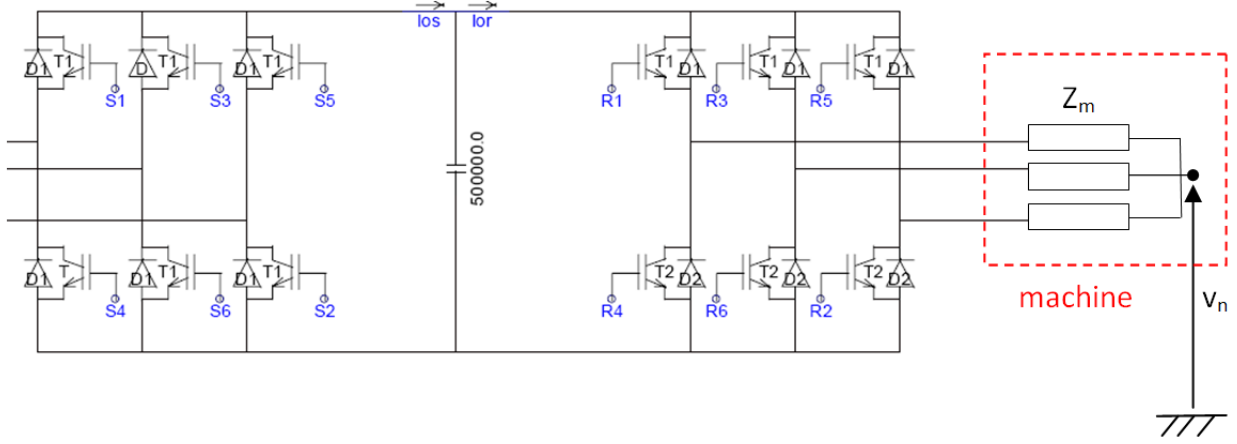


Figure 8.1: Three phase back-to-back converter

The voltages across the three phases of the electrical machine are given by

$$
\begin{aligned}
v_a - v_n &= R_m i_a + L_m \frac{di_a}{dt} \\
v_b - v_n &= R_m i_b + L_m \frac{di_b}{dt} \\
v_c - v_n &= R_m i_c + L_m \frac{di_c}{dt}
\end{aligned}
\tag{8.1}
$$

where $v_a$, $v_b$, $v_c$ are the converter output phase voltages; $i_a$, $i_b$, $i_c$ are the line currents; and $v_n$ is the common mode voltage.

Summing the set of equations in (8.1) gives

$$
v_a + v_b + v_c - 3v_n = (R_m + L_m \frac{d}{dt})(i_a + i_b + i_c)
\tag{8.2}
$$

and since $i_a + i_b + i_c = 0$, the common-mode voltage in the motor is given by

$$
v_n = \frac{v_a + v_b + v_c}{3}
\tag{8.3}
$$

It is this common-mode voltage which drives the leakage current from the inverter-fed windings, through the bearings, to ground. The common mode signal used in the

computational work presented in this chapter was generated using a model of a 2 *MW* DFIG developed by Prof. Li Ran, see Figure 8.2.
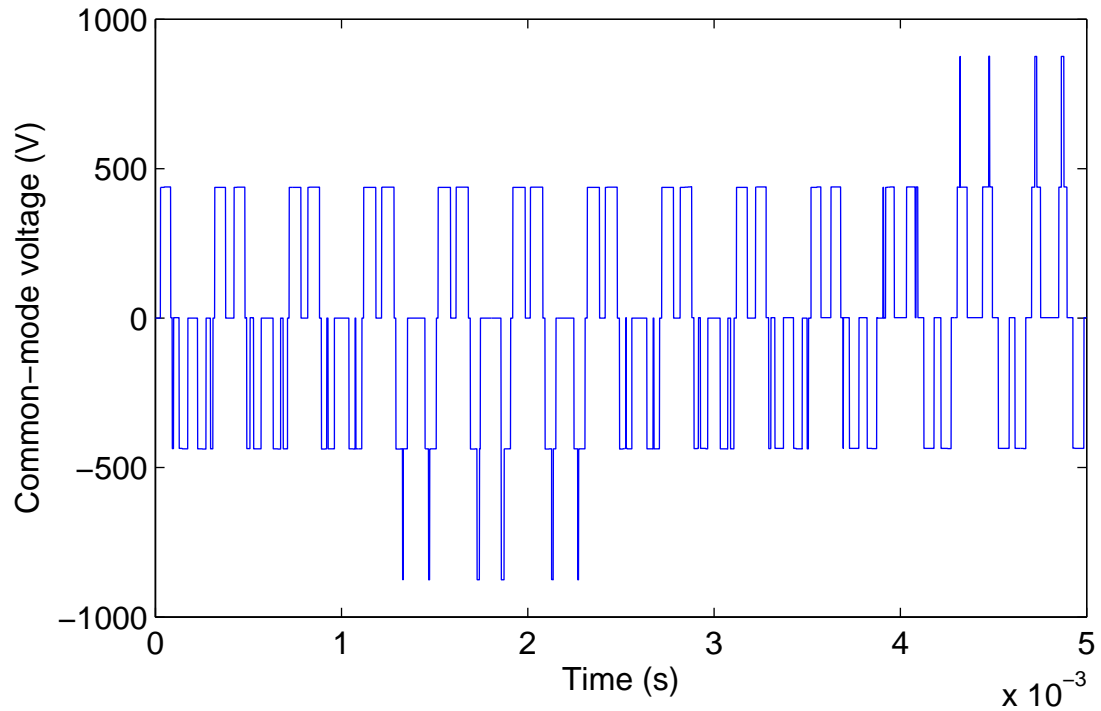


Figure 8.2: Common-mode signal from 2 *MW* DFIG wind turbine model provided by Prof. Li Ran

## 8.3    The Stray Circuit

As inverter-fed machines became more widespread in the 1990s, research effort was expended in order to develop models that described the leakage currents that were observed. Ogasawara and Akagi noted that the waveform of the leakage current resembled that of an LCR series resonant circuit and, therefore, proposed an LCR equivalence circuit to describe the observed high frequency leakage current [108] (see Figure 8.3a). Chen *et al.* developed a lumped parameter parasitic coupling circuit based upon transmission line theory [110]. The proposed circuit combined the properties of the series resonant LCR described above with a simple electrical model of the bearing and a capacitance for the airgap (see Figure 8.3b). These models were valuable descriptions of the phenomenon and elucidated the mechanism by which these bearings currents arise. However, the parame-

(a) LCR Series resonant circuit proposed by Ogasawara and Akagi [108]

(b) Circuit incorporating bearing model, proposed by Chen *et al.* [110]

(c) Capacitive divider proposed by Busse *et al.* and later used by Muetze [111]
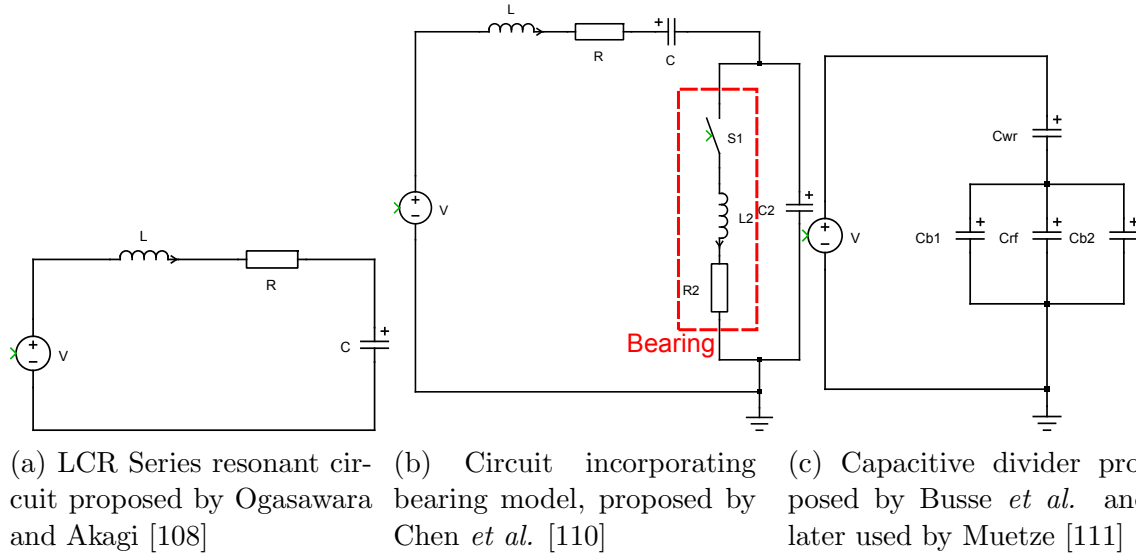
Figure 8.3: Review of parasitic circuit models

ters of the models could not be easily calculated; the circuits had to be tuned to empirical data and so could not be used to predict the likely magnitude of any potential bearing current for a given machine.

Busse *et al.* investigated the problem of bearing currents; this time providing a basis for calculation of the key capacitances in the stray circuit [22, 112]. By considering the stray circuit as a capacitive divider (See Figure 8.3c) Busse *et al.* introduced the concept of the "bearing voltage ratio" (BVR) where

$$BVR = \frac{v_b}{v_n} = \frac{C_{wr}}{C_{wr} + C_{rf} + 2C_b} \tag{8.4}$$

where $v_b$ is the voltage across the bearings, $v_n$ is the common mode voltage, $C_{wr}$ is the winding-rotor capacitance, $C_{rf}$ is the rotor-frame capacitance, $C_{wf}$ is the winding-frame capacitance, $C_b$ is the bearing capacitance.

A decade later Muetze *et al.* used this simplified approach and calculated stray capacitances in order to predict the BVR for six machines over a wide power range (11 to 500 $kW$)[111]. The efficacy of the model was demonstrated experimentally and the BVR was shown to be a useful indicator of susceptibility to EDM.

A sketch of a machine is shown in Figure 8.4 with the most important capacitances
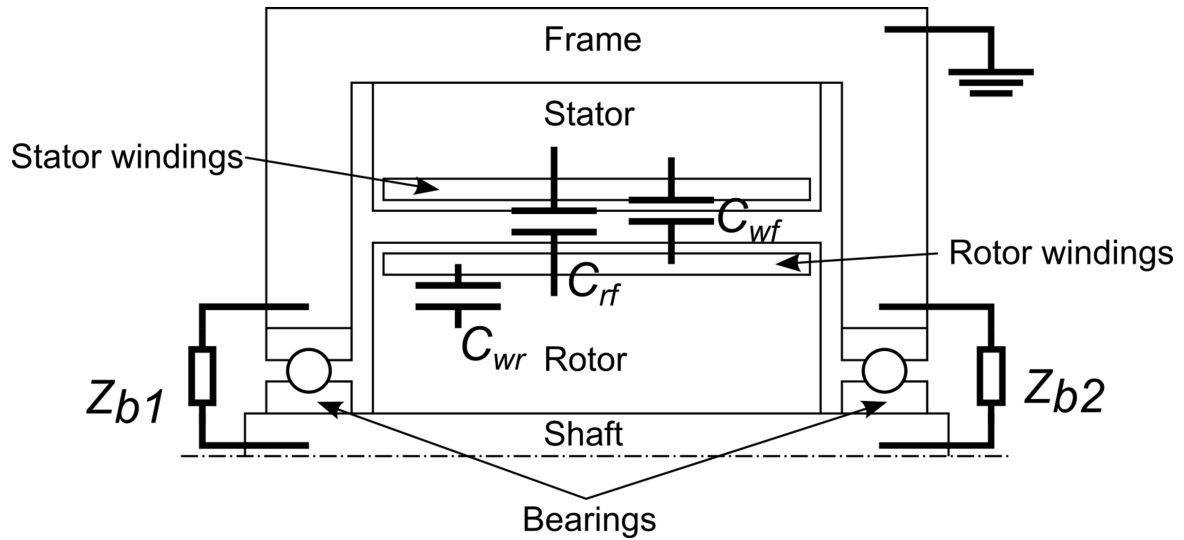
Figure 8.4: The stray capacitances in a rotor-fed electrical machine. Note that the stator frame is earthed and that the bearings are represented more generally as impedances, $Z_{b1}$ and $Z_{b2}$, rather than capacitances as in the BVR equation developed by Busse *et al.*).

for the stray circuit indicated. The model used in the analysis presented in this chapter builds upon those described above, particularly Muetze's, but a more advanced electrical description of the bearing is incorporated. In the literature the attention has been on stator–fed machines, but WT generators are often rotor-fed; this changes the capacitive coupling and, therefore, is important when considering the common-mode characteristics of the machine. In this research the vulnerability to EDM of rotor-fed machines is considered, by means of numerical simulations. Moreover, the model is of a larger machine (2 $MW$) than those previously considered in the literature.

The capacitive coupling between the inverter-fed windings and the rotor, $C_{wr}$, is critical. The normal route to earth for high frequency (HF) parasitic currents is to the rotor and then to the earthed stator frame via the bearings. However, there also exists coupling between the windings and the stator, $C_{wf}$. Although it is thought that this capacitance may usually be neglected when considering EDM it may become important if the rotor is earthed by a very low impedance path (e.g. through the gearbox in the case of a WT)[111]. In this case the winding-frame ground current may pass through the bearings and earth via the rotor. As long as an appropriate flexible coupling between the gearbox and the generator is used, and the frame earthing cable is not damaged, this is unlikely

to be of concern in WTs.

There is another mechanism by which bearing currents may flow. All of the previous descriptions of bearing currents may be said to be non-circulating, they pass from the windings and out of the machine to ground. There is, however, an alternative path to ground than that through the bearings. The inverter-fed windings are capacitively coupled to the earthed stator frame, as well as to the rotor, therefore ground currents may pass this way. Lipo *et al.* [113] showed that this causes a reduction in the current along the turn and, consequently, electromagnetic asymmetry in the machine. Thus, by a combination of capacitive and inductive coupling a voltage along the shaft is generated. If this voltage is large enough the dielectric strength of the lubricant will be exceeded and current may circulate around the stator frame-bearing-shaft-bearing loop. However, due to the prevalence of rotor-fed generators in WTs, the focus of this chapter is upon EDM due to capacitive coupling.

## 8.4   Types of Bearing Currents

Rolling element bearings provide complex variable reactances that may exhibit behaviour that is purely ohmic, purely capacitive or a combination depending upon the operating conditions and the state of the bearing and the lubricant:

1. *Ohmic bearing currents.* Under certain conditions the bearing may behave as an ohmic resistor. This would happen if there is metal-metal contact, which is probable at low speeds or if the bearing is damaged and the grease contains many debris particles. Also, ohmic conduction has been reported if the bearing temperature becomes too high [114]. This is due to the reduced viscosity of the lubricant at high temperatures, which in turn results in a reduced lubricant film thickness. However, these bearing currents tend to be quite small (maximum amplitude $< 200 \; mA$)[115].

2. *Capacitive bearing currents.*

   (a) *dV/dt currents.* The high slew rate of the common-mode signal from the power electronic converter means that significant capacitive currents may flow

in the bearing. It should be noted that insulation of the bearing is not always sufficient to eliminate these currents.

(b) *Electrostatic Discharge Machining (EDM).* When the fluid film is intact, such that the surfaces are separated, the bearing behaves as a capacitor with the lubricant acting as the dielectric. However if the dielectric strength of the lubricant is exceeded the film breaks down resulting in discharge. The threshold voltage has been reported in the literature to be approximately 5-30 *V* [114]. This large range of threshold voltages is observed because it would be more appropriate to consider the electric stress to which the lubricant is subjected, rather than simply the voltage. EDM is potentially very harmful because it can result in very large current densities at the bearing contact area. This mechanism is the focus of the current chapter.

## 8.5   Test Rig

Although the greater part of this work was carried out by means of computational simulations, a small test rig was built in order to gain an empirical insight into the parasitic circuit. The purpose of the rig was to represent, on a laboratory scale, the interaction between the power electronic converter and the wound rotor induction generator.

The rig was composed of two 300 *W* identical wound rotor induction machines connected by a jaw coupling. All four (ball) bearings on the rig were insulated. This was done by removing the endplates of the motor-generators, machining out 3 mm of around the bearings, and inserting a plastic ring between the bearing and the housing before reassembling. Four slip rings were located on the rig, adjacent to the bearings, see Figure 8.5. These were used to measure the bearing current (though it should be noted that this arrangement is not identical to the real case, where charge builds and then discharges across the bearing as with EDM) by connecting the brushes to the bedplate, which was earthed, and using a clamp on high frequency current transducer to measure the current through that grounding wire. The jaw coupling had an electrically insulative rubber ele-

ment between the two plates. The machines were mounted to the earthed bedplate. One machine was operated as a motor, with stator windings fed by a three phase sinusoidal PWM switched supply from an inverter drive (the switching frequency of the inverter could be varied between 1 $kHz$ and 8 $kHz$). The other machine was generating, with a resistor bank providing the load. A schematic diagram of the rig is shown in Figure 8.5, and a photograph in Figure 8.6.
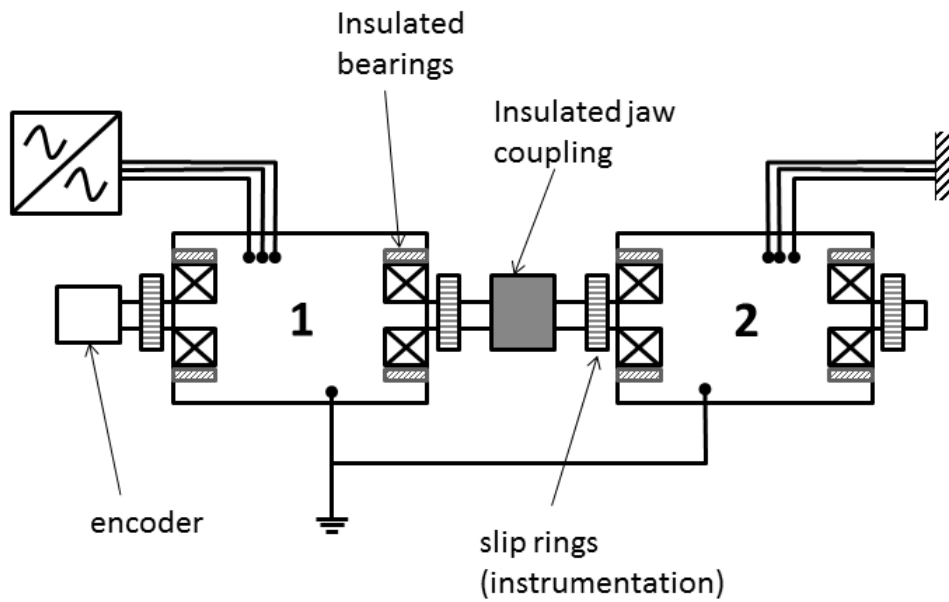
Figure 8.5: Schematic diagram of the bearing current test rig

Low amplitude currents, very rich in harmonic content, were measured flowing through the slip rings. The inverter drive was quite noisy and the same noise was visible in these ground currents. Ground current readings were taken for a range of shaft speeds and switching frequencies, but the essential characteristics of the ground current remained the same. Figure 8.7 shows the low amplitude parasitic currents measured.

The rig was run only with the inverter feeding the stator windings. Unfortunately it was not possible to operate the motor with the inverter drive feeding the rotor windings. It was considered that the motor was not suitable for this operation and would be prone to overheating dangerously.

Having seen that these parasitic currents could be replicated in the laboratory numerical simulations were carried out to investigate the likelihood of significant bearing currents

Figure 8.6: Photograph of the bearing current test rig

being found in multi-$MW$ WT generators.

## 8.6   Computational Case Study

The parasitic capacitive coupling, by which HF leakage gives rise to bearing currents, has been investigated and the general principles are now quite well understood. A range of coupling models has been proposed in the literature [108, 110, 114, 115], but all incorporate a very simplified model of the bearing. An improved model of the bearing capacitance is presented here by using both Hertzian contact mechanics and the Hamrock-Dowson film thickness equation.

By considering a typical 2 $MW$ DFIG the capacitances of the HF stray circuit were calculated from representative machine geometry (see Table 8.1) and a range of simulations, including sensitivity studies, was undertaken. Using the capacitive divider circuit proposed by Muetze $et\ al.$[111] as a starting point the circuit shown in Figure 8.8 was derived. The main difference is the inclusion of resistors in parallel with the bearing
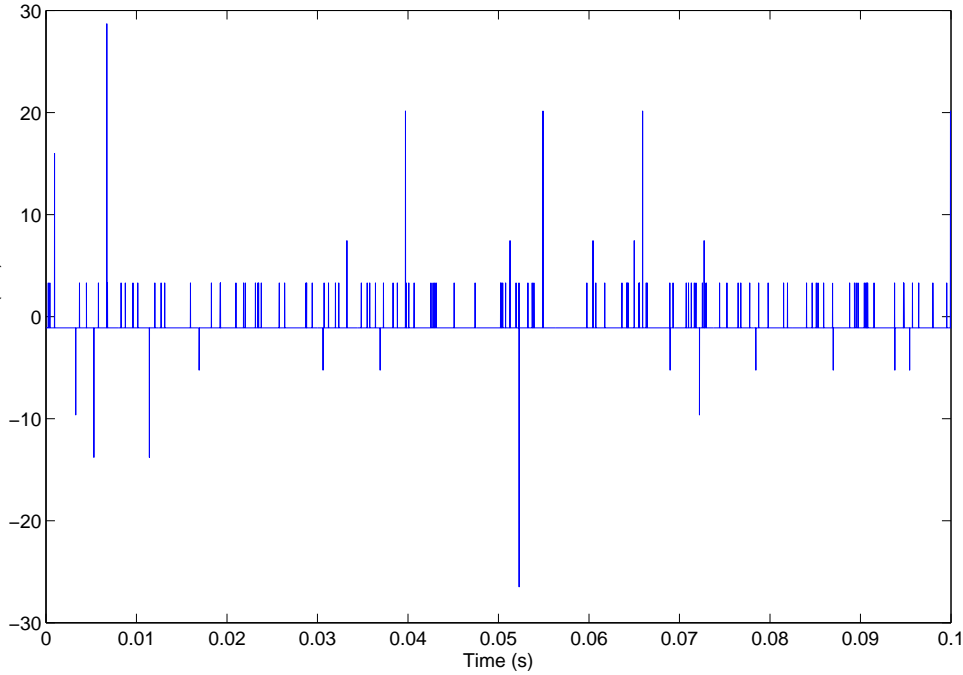
Figure 8.7: Ground current (in $mA$) measured on the small bearing current test rig

capacitances; this is a simple measure to allow for the simulation of EDM. When the dielectric strength of the lubricant is exceeded the bearing switches close, allowing discharge through the resistor.

The enclosed areas indicated on Figure 8.8 show the bearing representation. The bearing capacitance is calculated by assuming that it is the contact area which dominates and, therefore, the bearing can be modelled as a parallel plate capacitor. The plate areas are calculated using Hertzian contact mechanics [58], and the film separation is calculated using the Hamrock-Dowson minimum film thickness equation [80].

When the dielectric strength of the grease lubricant is exceeded the switches, S1 and S2, close allowing the capacitor to discharge. This represents the momentary ohmic behaviour of the bearing as the lubricant is punctured by the accumulated charge.As a result the electrical stress across the lubricant falls back within the accepted range for the grease, and the switch opens simulating the return of the bearing to capacitive behaviour.

The winding-rotor capacitance, $C_{wr}$, and the rotor-stator frame capacitance, $C_{rf}$, were calculated from the machine geometry.

Figure 8.8: Stray capacitive circuit used in computational study ($V_{cm}$ is the common-mode voltage input, $C_{wr}$ is the winding-rotor capacitance, $C_{rf}$ is the rotor-frame capacitance, $C_{b1}$ and $C_{b2}$ are the bearing capacitances, $R_1$ is the motor frame resistance, and $L_l$ is the grounding line inductance

## 8.6.1   Calculating the Stray Capacitances

**Coupling Capacitances**

**Winding-rotor capacitance.**   For a rotor-fed generator, as commonly found in wind turbines, the winding-rotor capacitance may be found by

$$C_{wr} = \frac{\epsilon_0 \epsilon_g A_{wr}}{t_g} \tag{8.5}$$

where $\epsilon_0$ is permittivity of air, $\epsilon_g$ is the groundwall insulation relative permittivity, $t_g$ is the groundwall insulation thickness, and $A_{wr}$, the capacitor plate area, is given by

$$A_{wr} = N\left(2d + b\right) l_{fe} \tag{8.6}$$

where $N$ is the number of rotor bars with depth $d$ and breadth $b$.

For a stator–fed generator the winding-rotor capacitance is given by the following

| Parameter | Symbol | Value | Units |
|-----------|--------|-------|-------|
| Permittivity of air | $\epsilon_0$ | $8.85 \times 10^{-12}$ | $F/m$ |
| Relative permittivity of groundwall insulation | $\epsilon_g$ | 3 | - |
| Carter's coefficient | $k_c$ | 1.2 | - |
| Core length | $l_{fe}$ | 1 | $m$ |
| Rotor outer diameter | $d_{re}$ | 0.5 | $m$ |
| Air gap | $\delta$ | 2 | $mm$ |
| Rotor bar depth | $d$ | 36.85 | $mm$ |
| Rotor bar breadth | $b$ | 5.6 | $mm$ |
| Rotor groundwall insulation thickness | $t_g$ | 1 | $mm$ |
| Number of rotor bars | $N$ | 84 | - |

Table 8.1: Representative data for a 2 $MW$ wind turbine generator used to compute the stray capacitances

expression [111]

$$C_{wr} = \frac{1}{\frac{1}{C_{wr0}} + \frac{1}{C_{wr1}}} \tag{8.7}$$

where

$$C_{wr0} = N_s \epsilon_0 b_0 \frac{l_{Fe}}{\delta + h_0} \tag{8.8}$$

and

$$C_{wr1} = N_s 3 \epsilon_0 b_0 \frac{l_{Fe}}{h_{wedge+ins}} \tag{8.9}$$

where $C_{wr0}$ is the stator winding-rotor capacitance for the air gap and slot opening part, $C_{wr1}$ is the stator winding-rotor capacitance for the slot wedge and slot insulation part, $N_s$ is the number of stator slots, $b_0$ is the slot opening width, $\delta$ is the air gap, $h_0$ is the height of the slot opening and $_{wedge+ins}$ is the combined thickness of the slot wedge and slot insulation.

By comparing Equation 8.5 with Equation 8.7 it may be seen that the winding-rotor capacitance is expected to be much larger for the rotor-fed machine than for the stator–fed. This is mostly because (a) the plate separation is so much smaller in the rotor case, with only a thin layer of insulation separating the rotor bars from the rotor, and (b) the

permittivity of the insulation is 3 times that of air. This has significant implications for the vulnerability of the bearings of DFIGs to EDM compared with those of stator–fed machines.

**Winding-frame capacitance.**   The winding-frame capacitance for stator–fed machines is of the same form as Equation 8.5

$$C_{wf} = \frac{\epsilon_0 \epsilon_g A_{wf}}{t_g} \tag{8.10}$$

where $A_{wf}$ is the capacitor plate area.

For the rotor-fed case it is of the same form as Equation 8.7

$$C_{wf} = \frac{1}{\frac{1}{C_{wf0}} + \frac{1}{C_{wf1}}} \tag{8.11}$$

.

**Rotor-frame capacitance.**   The rotor-frame capacitance may be found by considering the stator and rotor as cylindrical capacitors. However, because $d_{re} \gg \delta$ the problem may be linearised with negligible error to give

$$C_{rf} = \epsilon_0 l_{fe} \frac{\pi d_{re}}{k_c \delta} \tag{8.12}$$

where Carter's coefficient, $k_c$, corrects for the effect of the slot openings on the air-gap flux density and is defined as

$$k_c = \frac{\delta_e}{\delta} \tag{8.13}$$

where $\delta_e$ is the equivalent air gap including the effect of slotting and $\delta$ is the actual, or mechanical, air gap [111].

**Bearing Capacitance**

Wind turbine generators typically utilise two grease lubricated single row ball bearings. In these ball bearings the raceway-ball tribological interfaces, separated by grease, act as

| External Details | |
| --- | --- |
| Type | Radial ball |
| Rows | 1 |
| Outer diameter ($mm$) | 320 |
| Bore ($mm$) | 150 |
| Dynamic load rating ($kN$) | 275 |
| Static load rating ($kN$) | 284 |
| Mass ($kg$) | 26.2 |
| Outer raceway Young's modulus ($GPa$) | 200 |
| Inner raceway Young's modulus ($GPa$) | 200 |
| Element Young's modulus ($GPa$) | 200 |
| Outer raceway Poisson's ratio | 0.3 |
| Inner raceway Poisson's ratio | 0.3 |
| Element Poisson's ratio | 0.3 |
| Internal Details | |
| Number of balls | 10 |
| Ball pitch circle diameter ($mm$) | 257 |
| Ball diameter ($mm$) | 44 |

Table 8.2: Deep Groove Ball Bearing (designation 6330) specification

capacitors. By considering the bearing kinematics, contact mechanics and film hydrodynamics, it is possible to estimate the capacitance of the bearing.

For a 2 $MW$ WT deep groove ball bearings (designation 6330) may typically be used. The relevant bearing data are shown in Table 8.2.

In the load zone the film thickness is orders of magnitude smaller than in the unloaded region. Therefore, it is assumed that the capacitance is dominated by the loaded elements. Each loaded ball undergoes deformation in the region of the contact, and therefore the computation of the capacitance may be simplified by considering the ball and the raceway to be parallel conducting surfaces separated by the dieletric lubricant. Thus the bearing capacitance is given by

$$C_b = 0.5 \frac{\epsilon_0 \epsilon_r A}{d} \tag{8.14}$$

where $C_b$ is the capacitance, $\epsilon_0$ is the permittivity of air, $\epsilon_r$ is the relative permittivity of the dieletric (in this case, the lubricant), $A$ is the plate area, and $d$ is the plate separation. If the raceway and the ball are considered to be in non-conforming contact, and the

| Parameter | Symbol | Value | Units |
|-----------|--------|-------|-------|
| Kinematic viscosity | $\nu_0$ | 20 | $\mu m^2/s$ |
| Density | $\rho$ | 900 | $kg/m^3$ |
| Dynamic viscosity | $\eta$ | 18 | $mNs/m^2$ |
| Asymptotic isoviscous pressure | $p_{iv,as}$ | 50 | $MPa$ |
| Dielectric strength | $\epsilon_{lb}$ | 15 | $kV/mm$ |

Table 8.3: Lubricant properties (typical for a grease lubricated ball bearing such as 6330)

| Parameter | Symbol | Value | Units |
|-----------|--------|-------|-------|
| Winding-rotor capacitance (rotor–fed) | $C_{wrr}$ | 177 | $nF$ |
| Winding-rotor capacitance (stator–fed) | $C_{wrs}$ | 0.81 | $nF$ |
| Rotor-frame capacitance | $C_{rf}$ | 5.79 | $nF$ |
| Bearing capacitance | $C_b$ | 37-208 | $pF$ |
| Bearing resistance (ohmic mode) | $R_b$ | 10 | $\Omega$ |
| Cabling inductance | $L_l$ | - | - |
| Machine resistance | $R_m$ | 10 | $\Omega$ |

Table 8.4: Electrical parameters used in 2 $MW$ DFIG simulation

surface roughnesses are neglected, Hertzian theory of elastic contact may be used to find the bearing capacitance plate area, $A$ (see Equations 6.1 – 6.3).

The bearing lubricant acts as a dielectric between the balls and the raceways. Therefore Elastohydrodynamic (EHL) theory is invoked to estimate the film thickness in the contact region in order to compute the bearing capacitance. The full EHL solution involves a complicated coupling of the Reynolds equations with those of elasticity. However, for the present purposes the Hamrock-Dowson equation for the minimum film thickness for fully flooded, isothermal, elastohydrodynamic point contacts [80] may be used (Equation 6.33). See Section 6.6 for more details.

The lubricant properties used in the numerical simulations are outlined in Table 8.3; the electrical parameters are in Table 8.4. Figure 8.9 shows that these calculated capacitances compare favourably with published data. Although the winding-rotor capacitance for the rotor–fed case has not been verified it may be expected from a consideration of the machine geometry (see Equations 8.5 and 8.7) that it will be much larger than the other capacitances.
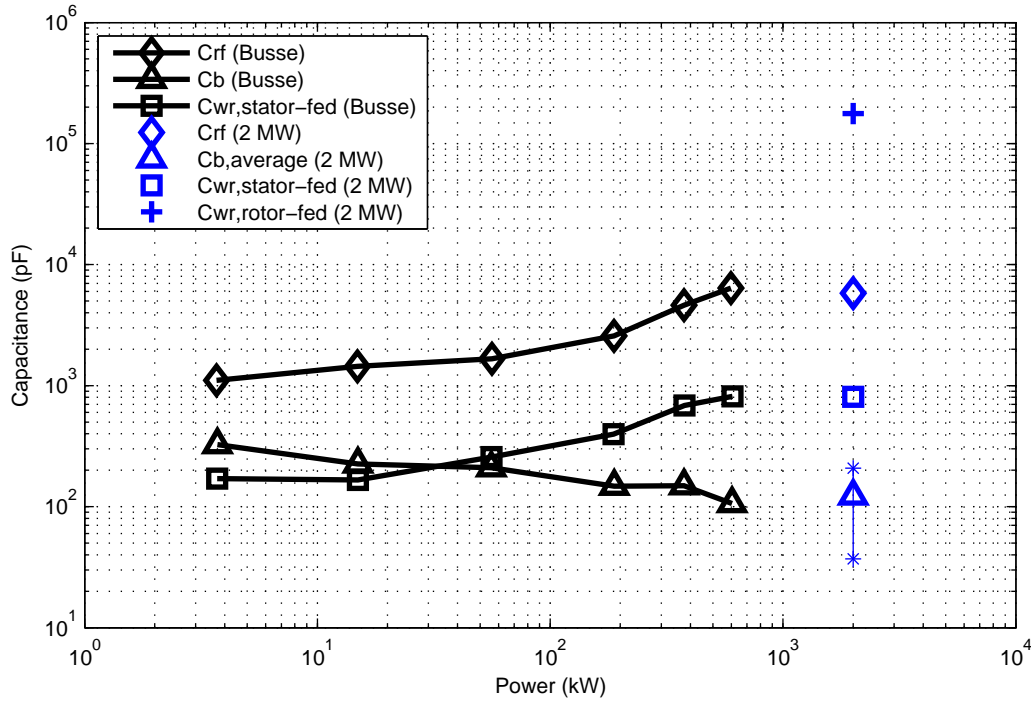
Figure 8.9: Calculated machine capacitances: comparing values from Busse *et al.* [22] with the present 2 *MW* study. (A range is given for the 2 *MW* bearing capacitance as this parameters is a function of speed and load and, therefore, varies depending upon the operation of the turbine. The upper and lower limits of the bearing capacitance are denoted by ∗)

## 8.7   Results

The simulation of the WT generator parasitic circuit indicates, as shown in Figure 8.10, that the dielectric strength of the bearing lubricant was routinely exceeded resulting in EDM of the bearing. Peak currents of approximately 3.7 *A* were found for the 2 *MW* DFIG simulated. Using the Hertzian contact area the apparent current density, $J_b$, may be calculated according to

$$J_b = \frac{i}{A_{Hz}} \tag{8.15}$$

where $i$ is the bearing current, and $A_{Hz}$ is the Hertzian contact area. In this case a peak current of 3.7 *A* yields $J_b \approx 1.05 A/mm^2$. In the literature, empirical data show that $J_b > 0.8 A/mm^2$ can significantly endanger bearings [22]. This suggests that WT

DFIG bearings are likely to be highly vulnerable to EDM and consequently may fail before reaching their $L_{10}$ life due to electrical stress, rather than mechanical stress, if stray currents are not mitigated.

The model was used to compare rotor–fed machines with stator–fed machines. It is also seen that rotor–fed WTs will suffer more from bearing currents than stator–fed WTs. This is because the coupling capacitance, $C_{wr}$, is much greater for rotor–fed WTs (see Table 8.4). The effect of this increased coupling capacitance is apparent in Figure 8.11, which shows the bearing currents when the WT is operating at rated load ($\omega = 1500rpm$, $P = 9kN$). For the rotor–fed machine (such as a DFIG) $J_b \approx 1.05A/mm^2$ with the turbine operating at rated power. However, with the converter feeding the stator windings $J_b \approx 0.05A/mm^2$. It is clear that whereas the rotor–fed case is highly vulnerable to premature bearing failure caused by electrical stress, the stator–fed case is not.
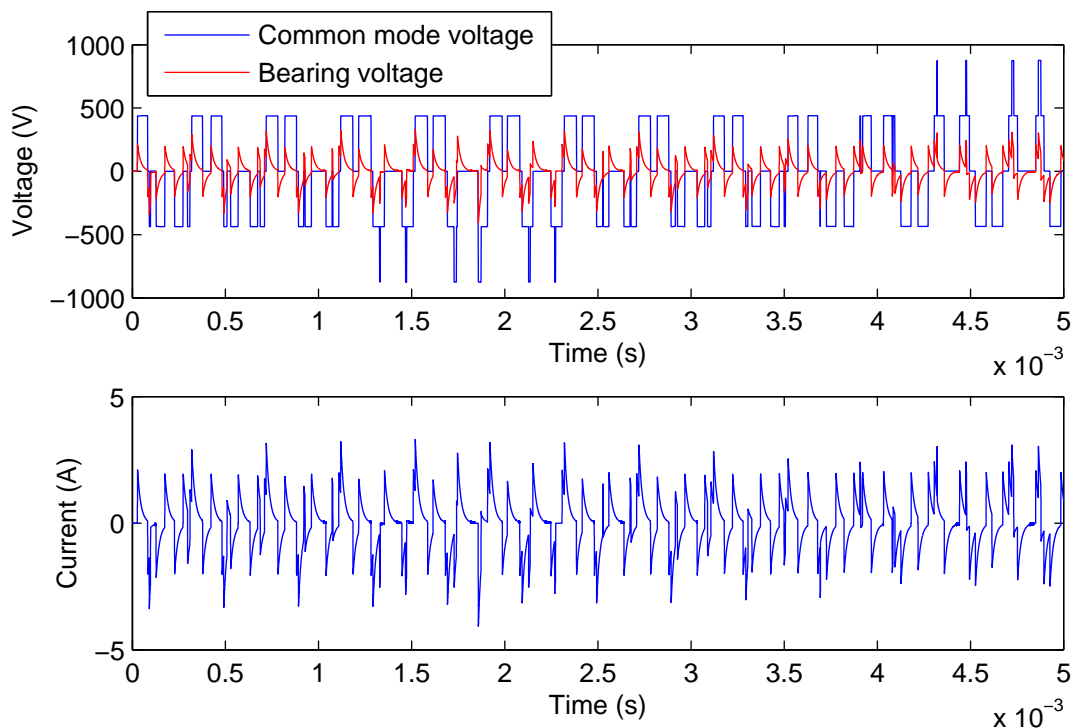


Figure 8.10: Simulation results showing EDM

## 8.7.1    Sensitivity Analyses

Sensitivity analyses were carried out for the following reasons:
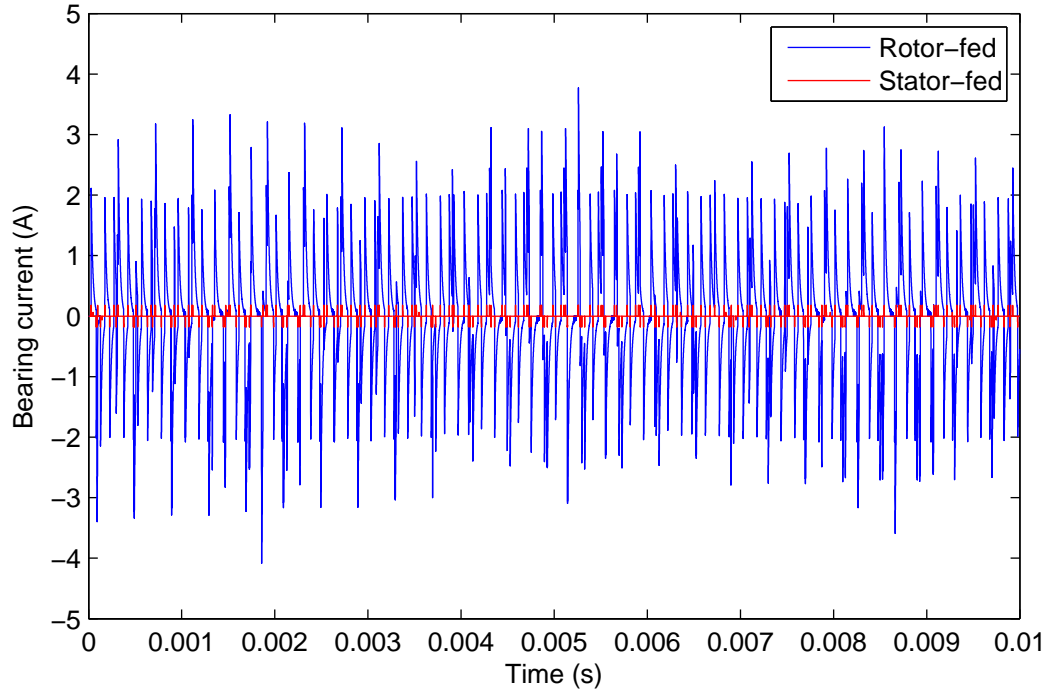
Figure 8.11: Comparing rotor-fed and stator-fed topologies susceptibility to bearing currents

- The wind speed is highly variable and, consequently, WTs rarely operate at the nameplate rated power. Therefore, it is important to consider whether variations in load, $P$, and speed, $\omega$ are likely to have a significant influence on the stray capacitive circuit.

- The phenomenon of stray HF currents is complex. Assumptions have been made regarding the geometry of the system and its material properties.

- The bearing contact area has been calculated by modelling the raceway as a flat surface. In reality there is some degree of conformity between the balls and the raceway and, therefore, some error in the calculated contact area. The sensitivity analyses are, therefore, important in order to assess how robust is the methodology.

The bearing capacitance for the 2 $MW$ machine simulated is small (37-208 $pF$, see Figure 8.12) but variable. The capacitance is a function of the generator bearing load, which itself is likely to vary due to flexibility in the drivetrain and the fluctuating nature

of the wind [116], because the contact area changes with load. Computational mechanical simulations in [116] have shown that for a typical 2 $MW$ drivetrain the generator bearing load may vary between 2 and 16 $kN$. Also important is the speed, because the film thickness is sensitive to this parameter. The speed was considered over the range 1200 to 1600 $rpm$, which is typical for a multi-$MW$ variable speed WT. Figure 8.12 shows the bearing capacitance plotted as a function of these two operational parameters. It may be seen that, in the case simulated, the dominant factor is the load. It was, however, found that for the rotor–fed case the apparent bearing current density was not sensitive to the bearing capacitance. This is because the bearing capacitance is small compared to other capacitances, particularly the winding-rotor capacitance. In the stator–fed case the apparent bearing current density was more sensitive to the bearing capacitance, but here the magnitude of the bearing current is unlikely to reduce the bearing life.
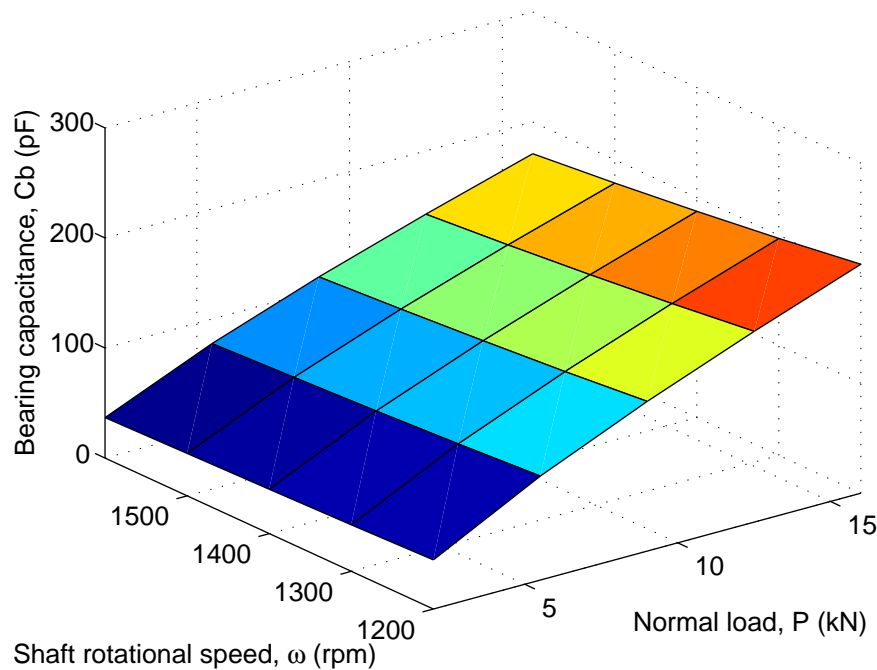


Figure 8.12: Bearing capacitance is dependent upon the applied normal force and speed

The apparent bearing current density was found to be sensitive to the bearing load, but not the speed (see Figure 8.13). At low load the apparent bearing current density was 2.5 to 2.9 $A/mm^2$ for the rotor–fed machine. As the load reduces the Hertzian contact

area becomes very small and so the current density becomes very large. Changes in the speed made very little difference with the rotor-fed machine because the voltage across the bearings was always sufficient to puncture the lubricant, even with the lubricant film at its thickest.
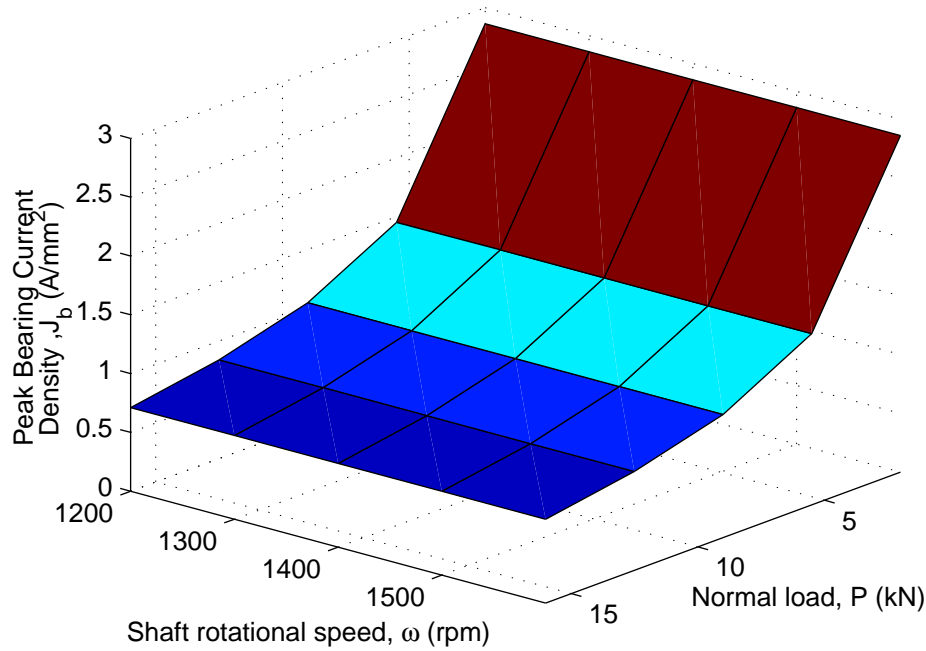


Figure 8.13: Sensitivity of peak bearing current density to speed and force (rotor-fed WT)

Although there was some error in the calculation of the contact area, introduced by considering the raceway as a flat surface, the sensitivity analyses show that it does not significantly affect the conclusion. The stator-fed WT is very unlikely to suffer from EDM, whereas the rotor-fed case is highly prone to it. For the rotor-fed WT even with the bearing heavily overloaded (and therefore with a larger contact area) the apparent bearing current density is found to exceed the criterion established by Busse *et al.*[22].

The winding-rotor and the rotor-frame capacitances were varied ±50% to assess the robustness of the methodology. Figure 8.14 shows the the apparent bearing current density sensitivity to changes in these capacitances at rated operation of the WT. Though the bearing current density does change, particularly with the winding-rotor capacitance, the overall conclusion remains unaltered.
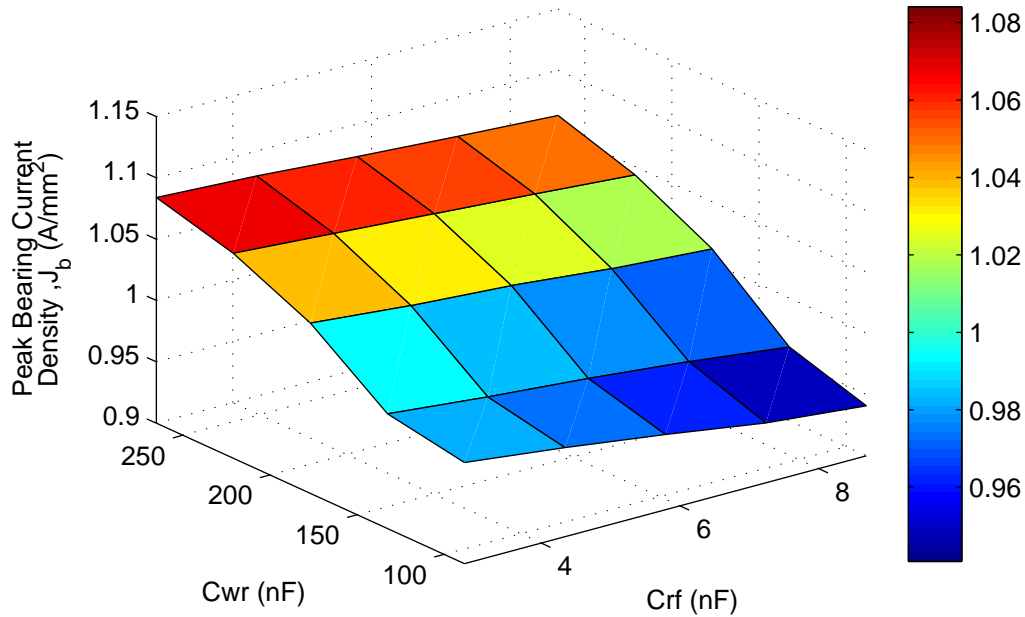
Figure 8.14: Sensitivity of peak bearing current density to the winding-rotor and the rotor-frame capacitances (rotor-fed)

## 8.8    Conclusions

A typical 2 *MW* WT generator was numerically modelled to investigate its vulnerability to bearing current damage. It was found that the dielectric strength of the grease lubricant was exceeded upon each switch of the converter, resulting in EDM of the bearing balls and raceway. Because the converter switching frequency is in the *kHz* range this results in a very large number of current discharge events taking place. Furthermore, the apparent current density was found to be in the range expected to cause significant damage to the bearing according to the criterion of Busse *et al.*[22].

The winding-rotor coupling capacitance was two orders of magnitude greater when the converter fed the rotor (as in a DFIG), rather than the stator. Therefore, for rotor-fed machines (very common in WTs) the bearing voltages are much greater, leading to an increased probability of EDM.

In this chapter the importance of mitigating stray currents in converter fed WTs, particularly DFIGs, has been demonstrated. Such mitigation is achieved by the correct arrangement of bearing insulation and shaft grounding. It should be recognised, however,

that insulating the bearings may not be sufficient to prevent EDM; bearing insulation may even increase the capacitive divider effect and, therefore, exacerbate the problem.

Shaft grounding arrangements should be checked at regular inspections and it may be advisable to incorporate the shaft grounding into the condition monitoring system. A relatively simple approach may be to monitor the current through the shaft grounding arrangement. If there is a significant change in the shaft ground current it may indicate that the brushes need to be replaced or that an alternative low impedance path to ground has been created by the ingress of dirt or debris elsewhere.

# Chapter 9

# Conclusions and Recommendations

It is clear that wind energy has an important role in providing sustainable energy. But the technology is not yet reliable enough, and this is hampering the growth of the industry. For many European countries, including the UK, offshore holds great potential but the economic model for offshore wind development is fragile. This is because the ambient conditions are particularly harsh, access for O&M is difficult and costly and the plant is not sufficiently reliable. In fiscal terms this poor reliability equates to risk and, in many situations, current risks are unacceptably high.

High level reliability surveys have usefully highlighted areas for research and development. One of the conclusions of these reliability surveys is that the reliability of electrical machines in the wind industry is poor compared to that of other industries. The technology is mature, but the application is new and combines a number of acute challenges for the plant reliability. These 'top down' statistical studies may now be usefully complemented by 'bottom up' computational analyses, in order to understand the root causes and failure modes which are driving the observed reliability data.

It has been the purpose of the present work to demonstrate the value of models which may help to explain some of the failure modes of wind turbine generators (and their root causes). The work has considered two potential root causes of wind turbine generator failure:

1. Gearbox-generator misalignment caused by deflection of the compliant drivetrain

under loading

2. EDM of the generator bearings due to the common-mode voltage caused by PWM
   of the power electronics

The numerical simulations showed that significant misalignment between the gearbox and generator is possible, and that it can result in a reduction of the generator DE bearing fatigue life. It is less likely to affect the gearbox HSS bearings as these must be rated for the larger gear mesh loads. A nominal offset is proposed to mitigate the operational gearbox-generator misalignment thereby reducing the impact upon the bearing fatigue lives. For the present purpose the system was solved quasi-statically. It is recommended that future research should explore the importance of dynamic effects upon the misaligned gearbox-generator system.

The simulation of bearing currents found that typical multi-$MW$ wind turbine generators bearings may suffer reduced useful life because of EDM. Particularly vulnerable are DFIGs because the rotor is fed by the power electronic converter. A variety of mitigation strategies exist, but some are expensive (such as using ceramic rolling elements), whilst others introduce other challenges (such as using a constrained PWM switching regime). It is quite common to apply a thin insulative coating to the outer raceway of the bearings in order to mitigate bearing currents. However, as discussed in Chapter 8, this may not prevent EDM; rather, it can increase the damage caused by EDM by increasing the capacitive divider effect. A review of the available mitigation strategies and an assessment of their relative merits may be prove useful to the wind industry. However, it is recommended that more fundamental tribological research be conducted to understand the mechanism by which electrical discharge causes bearing damage. There is clearly a gap in the understanding; approximate empirical rules are still relied upon. Improved understanding of the fundamental science could lead to much more elegant solutions than those currently available.

It is interesting to note that there exists a harmful interaction effect between misalignment and the parasitic effect which gives rise to bearing currents. Because the Hertzian

contact area is sensitive to the radial load, which is altered by gearbox-generator misalignment, there exists the possibility that misalignment unloads the bearing. Such a load reduction would reduce the contact area resulting in a very high current density, which will cause electrical damage to the tribological surface. In this case it is the interaction between the gearbox-generator misalignment and the parasitic circuit of the generator which is the root of the problem. This demonstrates the importance of systems analysis which considers the ways in which the different electro-mechanical assemblies in the system interact.

This research has focussed upon typical multi-$MW$ DFIG technology as this accounts for the majority of current installed wind energy plant worldwide. For larger turbines designed for the offshore market ( $> 5\ MW$) medium speed integrated designs are likely to occupy significant market share. The conclusions drawn in this research may not be applied directly to this new generation of large integrated drivetrains because the designs are fundamentally different. Similar analyses to those presented here should be of value. The stray electrical circuit in the new generation of integrated drivetrain designs will be very different, and it will be important to ensure that the gearbox bearings remain isolated from harmful stray currents.

The published reliability data for generators in wind turbines provided the motivation for this research, but with limited data available from manufacturers the wind industry has been left to speculate about the root causes for these failures. The research here presented provides some of the groundwork required to establish an understanding of the root causes of generator bearing failure in wind turbines. In particular it has highlighted a link between gearbox-generator misalignment and bearing currents in which there may be a harmful synergy. However this research has shown that stator fed machines are unlikely to suffer significantly from bearing currents. Further research is required to understand the different failures modes for stator fed machines.

## 9.1   Recommendations for further work

- The development of general guidelines for the mitigation of misalignment between the gearbox and the generator in wind turbines would be of practical value to industry.

- With increased computing power, dynamic analyses of complete multi-$MW$ drivetrains are now possible. As turbines get larger the natural frequencies may move into the range where significant excitation forces exist. The possibility exists to build upon the quasi-static numerical simulations of Chapter 7 with a dynamic analysis. Such an approach may be able to elucidate the effect of wakes in large wind farms upon drivetrain reliability.

- More fundamental tribological research into the mechanisms by which electrical currents cause damage to bearings is required. At present industry relies on approximate empirical rules, but a powerful predictive framework is lacking.

- Numerous alternatives drivetrain concepts exist including a variety of continuously variable transmissions (some using hydraulics, but some with differential stage gearboxes). Many of these claim improved reliability, but often the evidence base for these claims is insufficient. There is scope for a thorough analysis, beginning with a FMEA and followed by numerical simulations, of these different drivetrain concepts. A thorough evaluation of the reliability of the technologies would be valuable because even a small improvement in reliability, or maintainability, could yield significant COE savings offshore.

# References

[1] www.poullacour.dk. Accessed 11/10/2010. Poul la cour museum [online].

[2] S. Sorrell, J. Speirs, R. Bentley, A. Brandt, and R. Miller. Global oil depletion: A review of the evidence. *Energy Policy*, 38(9):5290 – 5295, 2010.

[3] S. Krohn, P.E. Morthorst, and S. Awerbuch. The economics of wind energy. Technical report, EWEA, 2009.

[4] GWEC. Global cumulative installed wind capacity 1996-2012. Online, May 2013.

[5] J. Coultate. Understanding costs for large wind-turbine drivetrains. *Wind Power Engineering and Development*, 2012.

[6] P.E Morthorst and S. Awerbuch. The economics of wind energy. Technical report, European Wind Energy Association, 2009.

[7] T. Ackermann, editor. *Wind Power in Power Systems*. John Wiley and Sons, 2005.

[8] T. Burton, D. Sharpe, N. Jenkins, and E. Bossanyi. *Wind Energy Handbook*. John Wiley & Sons, Ltd., 2001.

[9] M Whittle. Wind turbine drivetrain technology and cost drivers. In *Proceedings of FRENS 2012*, 2012.

[10] J Coultate. Wind turbine gearbox durabilty. *Wind Systems Magazine*, pages 42–45, 2009.

[11] B. M. Bird, K.G. King, and D. A. G. Pedder. *An Introduction to Power Electronics.* John Wiley & Sons, 1993.

[12] M. Wilkinson and B. Hendriks. Reliability focused research on optimizing wind energy systems design, operation and maintenance: tools, proof of concepts, guidelines & methodologies for a new generation. Technical report, Reliawind, 2011.

[13] S. Faulstich, B. Hahn, P. Lyding, and P.J. Tavner. Reliability of offshore turbines - identifying risks by onshore experience. In *Proceedings of Offshore 2009*, Stockholm, 14-16 September 2009. EWEA.

[14] S. Faulstich, B. Hahn, and P.J. Tavner. Wind turbine downtime and its importance for offshore deployment. *Wind Energy*, 14:327337, 2011.

[15] P.J. Tavner, L Ran, J. Penman, and H. Sedding. *Condition Monitoring of Rotating Electrical Machines.* IET, 2008.

[16] G.C. Stone, E.A Boulter, I. Culbert, and H. Dhirani. *Electrical Insulation for Rotating Machines: Design, Evaluation, Aging, Testing and Repair.* IEEE Press, Piscataway, 2004.

[17] K. Alewine and W. Chen. Wind turbine generator failure modes analysis and occurrence. Dallas, May 24-26 2010. WindPower 2010.

[18] T. Zika, I. C. Gebeshuber, F. Buschbeck, G. Preisinger, and M. Groeschl. Surface analysis on rolling bearings after exposure to defined electric stress. *Proceedings of the IMechE Part J- Journal of Engineering Tribology*, 223:787–797, 2009.

[19] L. Dueas-Osorio and B. Basu. Unavailability of wind turbines due to wind-induced accelerations. *Engineering Structures*, 30(4):885 – 893, 2008.

[20] I. Howard. A review of rolling element bearing vibration "detection, diagnosis and prognosis". Technical report, Aeronautical and Maritime Research Laboratory Airframes and Engines Division, 1994.

[21] NREL. Advanced wind turbine drivetrain concepts: Workshop report. Technical report, 2010.

[22] D. Busse, J. Erdman, R. Kerkman, D. Schlegel, and G. Skibinski. System electrical parameters and their influence effect on bearing currents. *IEEE Transactions on Industrial Applications*, 33(2):577–584, 1997.

[23] *BS EN 60085:2008 Electrical insulation - Thermal evaluation and designation.* British Standards Institute, London, 2008.

[24] Report of large motor reliability survey of industrial and commercial installations, part i. *Industry Applications, IEEE Transactions on*, IA-21(4):853 –864, July 1985.

[25] Report of large motor reliability survey of industrial and commercial installations, part ii. *Industry Applications, IEEE Transactions on*, IA-21(4):865 –872, July 1985.

[26] *Recommended practice for design of reliable industrial and commercial power systems.* IEEE, 1990.

[27] Enercon E32/E33 data. Online, 2012.

[28] Economic Affairs - Fourth Report : The Economics of Renewable Energy. Technical report, House of Lords, 2008.

[29] UK 2050 energy plan: Making our commitment a reality. Technical report, Institution of Mechanical Engineers, 2009.

[30] Ji. Kang, Z. Zhang, and Y. Lang. Development and trend of wind power in China. pages 330–335, Oct. 2007.

[31] F. Spinato, P.J. Tavner, G.J.W. van Bussel, and E. Koutoulakos. Reliability of wind turbine subassemblies. *Renewable Power Generation, IET*, 3:387–401, December 2009.

[32] P.J. Tavner, G.J.W. van Bussel, and F. Spinato. Machine and converter reliabilities in wind turbines. 2006. IEE 2nd International Conference on Power Electronics, Machines & Drives, Dublin, April 2006.

[33] S. Faulstich, B. Hahn, and K. Rohrig. Windenergie report deutschland. Technical report, Institut fur solare Energieversorgungstechnik:, Kassel, 2008.

[34] J Coultate. Technology trends and outlook for large wind turbine drivetrains. In *Proceedings of EWEA 2012*, 2012.

[35] N. Vatheuer J. Schmitz. Hydrostatic drive train in wind energy plants. In *Proceedings of EWEA 2011*, Brussels, 2011.

[36] G. Hehenberger and C. Pilgram. DSgen-set 3.0 MW electro mechanical differential drive from set. In *EWEA 2012*, 2012.

[37] IEC 61400-4 design requirements for wind turbine gearboxes.

[38] A. Heege, J. Hemmelmann, L. Bastard, J.L. Sanchez, L. Lens, and M. Omiciuolo. Matching experimental and numerical data of dynamic wind turbine loads by modelling of defects. ewec 2009. In *Proceedings of EWEC 2009*, Marseille, March 2009.

[39] J. Helsen, F. Vanhollebeke, B. Marrant, D. Vandepitte, and W. Desmet. Multibody modelling of varying complexity for modal behaviour analysis of wind turbine gearboxes. *Renewable Energy*, 36:3098–3113, 2011.

[40] J. Helsen, F. Vanhollebeke, F. De Coninck, D. Vandepitte, and W. Desmet. Insights in wind turbine drive train dynamics gathered by validating advanced models on a newly developed 13.2 MW dynamically controlled test-rig. *Mechatronics*, 21(4):737 – 752, 2011.

[41] R. Byars. Power system architecture: What is the best generator type for a 5mw wind turbine? In *Proceedings of AWEA Offshore 2011*, 2011.

[42] C. Kong, J. Bang, and Y. Sugiyama. Structural investigation of composite wind turbine blade considering various load cases and fatigue life. *Energy*, 30(1112):2101 – 2114, 2005. ¡ce:title¿International Symposium on {CO2} Fixation and Efficient Utilization of Energy (CandE 2002) and the International World Energy System Conference (WESC-2002)¡/ce:title¿.

[43] R.R. Pedersen, S.R.K. Nielsen, and P. Thoft-Christensen. Stochastic analysis of the influence of tower shadow on fatigue life of wind turbine blade. *Structural Safety*, 35(0):63 – 71, 2012.

[44] Changduk Kong, Taekhyun Kim, Dongju Han, and Yoshihiko Sugiyama. Investigation of fatigue life for a medium scale composite wind turbine blade. *International Journal of Fatigue*, 28(10):1382 – 1388, 2006. ¡ce:title¿The Third International Conference on Fatigue of Composites¡/ce:title¿ ¡xocs:full-name¿The Third International Conference on Fatigue of Composites¡/xocs:full-name¿.

[45] JC Marín, A Barroso, F París, and J Canas. Study of fatigue damage in wind turbine blades. *Engineering failure analysis*, 16(2):656–668, 2009.

[46] Landwirtschaftskammer Windenergie. Online.

[47] P.J. Tavner, C. Edwards, A. Brinkman, and F. Spinato. Influence of wind speed on wind turbine reliability. *Wind Engineering*, 30(1):55–72, 2006.

[48] H. Arabian-Hoseynabadi, H. Oraee, and P.J. Tavner. Wind turbine productivity considering electrical subassembly reliability. *Renewable Energy*, 35(1):190 – 197, 2010.

[49] P. J. Tavner, J. Xiang, and F. Spinato. Reliability analysis for wind turbines. *Wind Energy*, 10(1):1–18, JAN-FEB 2007.

[50] P. Wyllie, P.J. Tavner, and L. Ran. Visit to converteam, UK (4th and 5th August 2009). Technical report, University of Durham, 2009.

[51] H.W. van der Broeck and H.C. Skudelny. Analytical analysis of the harmonic effects of a pwm ac drive. *Power Electronics, IEEE Transactions on*, 3(2):216–223, 1988.

[52] D. J. Johns. *Thermal Stress Analyses*. Pergamon Press, Oxford, 1965.

[53] B. Stone G. Culbert, I. Lloyd. Stator insulation problems caused by variable speed drives. In *PCIC Europe, 2009. Conference Record*, 2009.

[54] F. Schemmel, K. Bauer, and M. Kaufhold. Reliability and statistical lifetime- prognosis of motor winding insulation in low-voltage power drive systems. *Electrical Insulation Magazine, IEEE*, 25(4):6 –13, Jul-Aug. 2009.

[55] J.F. Calvert. Forces in turbine generator stator windings. *Trans. of AIEE*, pages 178–196, 1931.

[56] I. van der Hoven. Power spectrum of horizontal wind speed in the frequency range from 0.0007 to 900 cycles per hour. *American Journal of Meteorology*, 14:160–164, 1957.

[57] M. Hodowanec. Satisfactory motor bearing service life: A review of often overlooked design considerations. In *Conference Record of 1995 Annual Pulp and Paper Industry Technical Conference*, pages 170–177, 345 E 47th St., New York, NY 10017, 1995. IEEE Ind Applicat Soc, Proc Ind Dept, Pulp & Paper Ind Comm, I E E E. 1995 Annual Pulp and Paper Industry Technical Conference, Vancouver, Canada, Jun 12-16, 1995.

[58] K.L. Johnson. *Contact Mechanics*. Cambridge University Press, 1987.

[59] N. Raje and F. Sadeghi. Statistical numerical modelling of sub-surface initiated spalling in bearing contacts. *Proceedings of the Institution of Mechanical Engineers, Part J: Journal of Engineering Tribology*, 223(6):849–858, 2009.

[60] N. Raje, F. Sadeghi, and R.G. Rateick. A statistical damage mechanics model for subsurface initiated spalling in rolling contacts. *Journal of Tribology*, 130, 2008.

[61] G. K. Nikas and R. S. Sayles. Surface coatings and finite-element analysis of layered fretting contacts. *Proceedings of the Institution of Mechanical Engineers, Part J: Journal of Engineering Tribology*, 223(J2):159–181, Mar 2009.

[62] JA Wensing and GC van Nijen. The dynamic behaviour of a system that includes a rolling bearing. *Proceedings of the Institution of Mechanical Engineers, Part J: Journal of Engineering Tribology*, 215(J6):509–518, 2001.

[63] N.K Arakere, N. Branch, G. Levesque, V. Svendsen, and N.H. Forster. Rolling contact fatigue life and spall propagation characteristics of aisi m50, m50 nil, and aisi 52100. part 2. stress modeling (preprint). Technical report, Air Force Research Lab Wright-Patterson AFB OH Propulsion Directorate, 2009.

[64] F. Sadeghi, B. Jalalahmadi, T.S. Slack, N. Raje, and N.K. Arakere. A review of rolling contact fatigue. *Journal of Tribology*, 131, 2009.

[65] B. Drury. *The Control Techniques: Drives and Control Handbook.* Iet Power and Energy Series. Institution of Engineering and Technology, 2009.

[66] D. Dahl, D. Sosnowski, D. Schlegel, R.J. Kerkman, and M. Pennings. Field experience identifying electrically induced bearing failures. In *IEEE Conference Record of 2007 Annual Pulp and Paper Industry Technical Conference*, pages 155–163, 345 E 47th St., New York, NY 10017 USA, 2007. IEEE Ind Applicat Soc; Proc Ind Dept; Pulp & Paper Ind Comm, IEEE. 53rd Annual Pulp and Paper Industry Technical Conference, Williamsburg, VA, Jun 24-29, 2007.

[67] S. Bell, T.J. Cookson, S.A. Cope, R.A. Epperly, A. Fischer, D.W. Schlegel, and G.L. Skibinski. Experience with variable-frequency drives and motor bearing reliability. *IEEE Transactions on Industry Applications*, 37(5):1438–1446, Sep - Oct 2001. 1998 IEEE Petroleum and Chemical Industry Technical Conference, Indianapolis, Indiana, Sep 28-30, 1998.

[68] A.M. Garcia, D.G. Holmes, and T.A. Lipo. Reduction of bearing currents in doubly fed induction generators. 1:84–89, Oct. 2006.

[69] H. Prashad. *Solving tribology problems in rotating machines*. CRC Press, 2006.

[70] N. T. Liao and J. F. Lin. Ball bearing skidding under radial and axial loads. *Mechanism and Machine Theory*, 37:91–113, 2002.

[71] M Neale. Learning from rotating machinery failures around the world. *IMechE - The President's Choice*, 2006.

[72] A.H. Bonnett. Cause and analysis of bearing failures in electrical motors. In *Industry Applications Society: 39th Annual Petroleum and Chemical Industry Conference - Record of Conference Papers*, Record of Conference Papers - Petroleum and Chemical Industry Conference, pages 87–95. IEEE, Ind. App. Soc., IEEE, Sep 28-30 1992.

[73] American Society for Metals. *ASM Handbook: Volume 18: Friction, Lubrication, and Wear Technology*. ASM International, 1992.

[74] M. Shokrieh and R. Rafiee. Simulation of fatigue failure in a full composite wind turbine blade. *Composite Structures*, 74(3):332 – 342, 2006.

[75] M. Whittle. Thermal modelling of a wind turbine generator. Master's thesis, University of Durham, 2009.

[76] V.A. Riziotis and S.G. Voutsinas. Fatigue loads on wind turbines of different control strategies operating in complex strategies operating in complex terrain. *Journal of Wind Engineering and Industrial Aerodynamics*, 85:211–240, 2000.

[77] K.A.Porter and A.S. Kiremidjian. Assembly-based vulnerability of buildings and its uses in seismic performance evaluation and risk management decision-making. Technical Report 139, Stanford University, 2001.

[78] P.J. Tavner. Personal communication. February 2010.

[79] W. Weibull. *A Statistical Theory of the Strength of Materials.* Ingeniörsvetenskapsakademiens handlingar. Generalstabens litografiska anstalts förlag, 1939.

[80] B.J. Hamrock and D. Dowson. Isothermal elastohydrodynamic lubrication of point contact, part iii fully flooded results. *Journal of Lubrication Technology*, 99(2):246–276, 1977.

[81] S. Faulstich, B. Hahn, and P. J. Tavner. Wind turbine downtime and its importance for offshore deployment. *Wind Energy*, 14(3):327–337, 2011.

[82] Y. Feng, P.J. Tavner, and H. Long. Early experiences with UK round 1 offshore wind farms. *Proceedings of the Institution of Civil Engineers : Energy*, 163:167–181, 2010.

[83] S. Faulstich. Windenergie report deutschland. Technical report, Kassel: Institut fur solare Energieversorgungstechnik, 2008.

[84] J. Ribrant and L.M. Bertling. Survey of failures in wind power systems with focus on Swedish wind power plants during 1997-2005. *Energy Conversion, IEEE Transactions on*, 22(1):167 –173, March 2007.

[85] EWEA. Upwind: Design limits and solutions for very large wind turbines. Technical report, 2011.

[86] V. Hariharan and P. Srinivasan. Vibration analysis of misaligned shaft ball bearing system. *Indian Journal of Science and Technology*, 2:45–50, 2009.

[87] J. van Dam B. McNiff, W. LaCava. Nrel - doe gearbox reliability collaborative: Experimental data analysis. In *EWEA 2011*, 2011.

[88] M. Whittle, W. Shin, J. Trevelyan, and J. Wu. A parametric study of the effect of generator misalignment on bearing fatigue life in wind turbine generators. In *Proceedings of EWEA 2011*, pages 24–27, Brussels, 16-19 April 2011.

[89] F. Oyague. Gearbox Reliability Collaborative (GRC) description and loading. Technical report, NREL, 2011.

[90] H. Long, J. Wu, F. Matthew, and P.J. Tavner. Fatigue analysis of wind turbine gearbox bearings using scada data miner's rule. In *Proceedings of EWEA 2011*, pages 334–337, Brussels, 14-17 March 2011.

[91] H. Long, J. Wu, and P.J. Tavner. Analysis of statistical loading conditions of wind turbine gearboxes based on scada data. In *Proceedings of EWEA 2012*, Copenhagen, 16-19 April 2012.

[92] J. Brändlein. *Ball and roller bearings: theory, design, and application*. John Wiley, 1999.

[93] ISO 281:2007 rolling bearings - dynamic load ratings and rating life.

[94] G. Lundberg and A. Palmgren. Dynamic capacity of rolling bearings. *Acta Polytechnica Mechanical Engineering Series*, 1, 1947.

[95] G. Lundberg and A. Palmgren. Dynamic capacity of rolling bearings. *Acta Polytechnica Mechanical Engineering Series*, 2, 1952.

[96] Romaxwind, 2012. Software.

[97] C. Halse Z. Wright and A. Crowther. Validation of romaxwind modeldel vs. dynamometer measurement camaign for nrel grc gearbox. In *NREL GRC*, 2012.

[98] GH bladed, 2012. Software.

[99] Jan Helsen, Frederik Vanhollebeke, Ben Marrant, Dirk Vandepitte, and Wim Desmet. Multibody modelling of varying complexity for modal behaviour analysis of wind turbine gearboxes. *Renewable Energy*, 36(11):3098 – 3113, 2011.

[100] Centa Power Transmission. Centalink product catalogue. [Online], 2012.

[101] T.A. Harris. An analytical method to predict skidding in high speed roller bearings. *ASLE Transactions*, 9:229–241, 1966.

[102] N.T. Liao and J.F. Lin. Ball bearing skidding under radial and axial loads. *Mechanism and Machine Theory*, 37(1):91 – 113, 2002.

[103] SKF. Single row deep groove ball bearings: minimum load. Online, 2012.

[104] FAG. Deep groove ball bearings generation C. Online, 2012.

[105] CW. Minimum load requirements. Online, 2012.

[106] A. Heege, J. Hemmelmann, L. Bastard, J.L. Sanchez, L. Lens, and M. Omiciuolo. Matching experimental and numerical data of dynamic wind turbine loads by modelling of defects. In *Proceedings of EWEC 2009*, pages 16–19 March, Marseille, 2009.

[107] A. Munoz Garcia, D.G. Holmes, and T.A. Lipo. Reduction of bearing currents in doubly fed induction generators. *Industry Applications Conference, 2006. 41st IAS Annual Meeting. Conference Record of the 2006 IEEE*, 1:84–89, 2006.

[108] S. Ogasawara and H. Akagi. Modeling and damping of high-frequency leakage currents in pwm inverter-fed ac motor drive systems. *IEEE Transactions on Industry Applications*, 32:1105–1114, 1996.

[109] S. Chen and T. A. Lipo. Source of induction motor bearing currents caused by pwm inverters. *IEEE Transactions on Energy Conversion*, 11(1):25–32, 1996.

[110] S. Chen, T. A. Lipo, and D. Fitzgerald. Modeling of motor bearing currents in pwm inverter drives. *IEEE Transactions on Industry Applications*, 32(5):1365–1370, 1996.

[111] A. Muetze and A. Binder. Calculation of motor capacitances for prediction of the voltage across the bearings in machines of inverter-based drive systems. *IEEE Transactions on Industry Applications*, 43(3):665–672, 2007.

[112] D. Busse, J. Erdman, R. Kerkman, D. Schlegel, and G. Skibinski. Characteristics of shaft voltage and bearing currents. *IEEE Industry Applications Magazine*, 3(6):21–32, 1997.

[113] S. Chen and T. A. Lipo. Circulating type motor bearing current in inverter drives. *IEEE Industry Applications Magazine*, (4)1:32–38, 1998.

[114] A. Muetze and A. Binder. Practical rules for assessment of inverter-induced bearing currents in inverter-fed ac motors up to 500 kw. *IEEE Transactions on Industrial Electronics*, 54:1614–1622, 2007.

[115] V. Hausberg and H.O. Seinsch. Kapazitive lagerspannungen undstroeme bei umrichtergespeisten induktionsmachinen. *Electrical Engineeering*, 82:153–162, 2000.

[116] M. Whittle, J. Trevelyan, W. Shin, and P.J. Tavner. Improving wind turbine drivetrain bearing reliability through pre-misalignment. *Wind Energy*, 2013.